



The Carnegie Supernova Project. I. Third Photometry Data Release of Low-redshift Type Ia Supernovae and Other White Dwarf Explosions

Kevin Krisciunas¹ , Carlos Contreras^{2,3}, Christopher R. Burns⁴ , M. M. Phillips² , Maximilian D. Stritzinger^{2,3} , Nidia Morrell² , Mario Hamuy⁵, Jorge Anais², Luis Boldt², Luis Busta² , Abdo Campillay², Sergio Castellón², Gastón Folatelli^{2,6}, Wendy L. Freedman^{4,7}, Consuelo González², Eric Y. Hsiao^{2,3,8} , Wojtek Krzeminski^{2,17}, Sven Eric Persson⁴ , Miguel Roth^{2,9}, Francisco Salgado^{2,10} , Jacqueline Serón^{2,11}, Nicholas B. Suntzeff¹, Simón Torres^{2,12}, Alexei V. Filippenko^{13,14} , Weidong Li^{13,17}, Barry F. Madore^{4,15} , D. L. DePoy¹, Jennifer L. Marshall¹ , Jean-Philippe Rheault¹, and Steven Villanueva^{1,16}

¹ George P. and Cynthia Woods Mitchell Institute for Fundamental Physics and Astronomy, Department of Physics and Astronomy, Texas A&M University, College Station, TX 77843, USA; krisciunas@physics.tamu.edu

² Carnegie Observatories, Las Campanas Observatory, Casilla 601, La Serena, Chile

³ Department of Physics and Astronomy, Aarhus University, Ny Munkegade 120, DK-8000 Aarhus C, Denmark

⁴ Observatories of the Carnegie Institution for Science, 813 Santa Barbara Street, Pasadena, CA 91101, USA

⁵ Departamento de Astronomía, Universidad de Chile, Casilla 36-D, Santiago, Chile

⁶ Facultad de Ciencias Astronómicas y Geofísicas, Universidad Nacional de La Plata, Instituto de Astrofísica de La Plata (IALP), CONICET, Paseo del Bosque S/N, B1900FWA La Plata, Argentina

⁷ Department of Astronomy and Astrophysics, University of Chicago, 5640 South Ellis Avenue, Chicago, IL 60637, USA

⁸ Department of Physics, Florida State University, Tallahassee, FL 32306, USA

⁹ GMTO Corporation, Avenida Presidente Riesco 5335, Suite 501, Las Condes, Santiago, Chile

¹⁰ Leiden Observatory, Leiden University, P.O. Box 9513, NL-2300 RA Leiden, The Netherlands

¹¹ Cerro Tololo Inter-American Observatory, Casilla 603, La Serena, Chile

¹² SOAR Telescope, Casilla 603, La Serena, Chile

¹³ Department of Astronomy, University of California, Berkeley, CA 94720-3411, USA

¹⁴ Miller Senior Fellow, Miller Institute for Basic Research in Science, University of California, Berkeley, CA 94720, USA

¹⁵ Infrared Processing and Analysis Center, Caltech/Jet Propulsion Laboratory, Pasadena, CA 91125, USA

¹⁶ Department of Astronomy, Ohio State University, Columbus, OH 43210, USA

Received 2017 July 20; revised 2017 September 12; accepted 2017 September 12; published 2017 November 6

Abstract

We present final natural-system optical (*ugriBV*) and near-infrared (*YJH*) photometry of 134 supernovae (SNe) with probable white dwarf progenitors that were observed in 2004–2009 as part of the first stage of the Carnegie Supernova Project (CSP-I). The sample consists of 123 Type Ia SNe, 5 Type Iax SNe, 2 super-Chandrasekhar SN candidates, 2 Type Ia SNe interacting with circumstellar matter, and 2 SN 2006bt-like events. The redshifts of the objects range from $z = 0.0037$ to 0.0835 ; the median redshift is 0.0241 . For 120 (90%) of these SNe, near-infrared photometry was obtained. Average optical extinction coefficients and color terms are derived and demonstrated to be stable during the five CSP-I observing campaigns. Measurements of the CSP-I near-infrared bandpasses are also described, and near-infrared color terms are estimated through synthetic photometry of stellar atmosphere models. Optical and near-infrared magnitudes of local sequences of tertiary standard stars for each supernova are given, and a new calibration of *Y*-band magnitudes of the Persson et al. standards in the CSP-I natural system is presented.

Key words: instrumentation: photometers – supernovae: general – surveys – techniques: photometric

Supporting material: figure sets, machine-readable tables

1. Introduction

Type Ia supernovae (SNe) are generally agreed to be the result of a carbon–oxygen white dwarf that undergoes a thermonuclear runaway (Hoyle & Fowler 1960) owing to mass accretion in a binary system (Wheeler & Hansen 1971). The mechanism for the ignition of the degenerate material is thought to be tied to the interplay between the exploding white dwarf and its companion star. Potential progenitor systems are broadly categorized as “single-degenerate,” where the companion star is a main sequence, red giant, or helium star, or

“double-degenerate,” where the system consists of two white dwarfs. Within this scheme, several triggering mechanisms have been proposed. The thermonuclear explosion can be triggered by the heat created during the dynamical merger of two white dwarfs after expelling angular momentum via gravitational radiation (e.g., Iben & Tutukov 1984; Webbink 1984). The explosion can also be triggered by compressional heating as the white dwarf accretes material from a degenerate or nondegenerate companion to close to the Chandrasekhar limit (e.g., Whelan & Iben 1973). A third mechanism involves the explosion of a sub-Chandrasekhar-mass white dwarf triggered by detonating a thin surface helium layer, which, in turn, triggers a central detonation front (e.g., Nomoto 1982). A fourth mechanism might be a collision of two C–O white dwarfs in a triple-star system (Kushnir et al. 2013).

Currently, it is unclear whether the observed SN Ia population results from a combination of these explosion mechanisms or is largely dominated by one. The power-law

¹⁷ Deceased.



dependence of the delay time between the birth of the progenitor system and the explosion as an SN Ia (the “delay-time distribution”; Maoz et al. 2010) and the unsuccessful search for evidence of the companions to normal Type Ia SNe (see, e.g., Li et al. 2011; Schaefer & Pagnotta 2012; Olling et al. 2015) would seem to favor the double-degenerate model, but some events, such as SN 2012cg (Marion et al. 2016) and SN 2017cbv (Hosseinzadeh et al. 2017) show a blue excess in their early-time light curves, indicative of nondegenerate companions. The rare SNe Ia that interact with circumstellar matter (CSM), such as SNe 2002ic (Hamuy et al. 2003) and PTF 11kx (Dilday et al. 2012), also favor a single-degenerate system.

Type Ia SNe are important for their role in the chemical enrichment of the universe (e.g., Nomoto et al. 2013, and references therein). They also play a fundamental role in observational cosmology as luminous standardizable candles in the optical bands (e.g., Phillips 1993; Hamuy et al. 1996; Riess et al. 1996; Phillips et al. 1999) and as (essentially) standard candles at maximum light in the near-infrared (NIR; Krisciunas et al. 2004; Krisciunas 2012; Phillips 2012, and references therein). The most precise current estimates for the value of the Hubble constant are based on SNe Ia (Riess et al. 2016, and references therein); moreover, Riess et al. (1998) and Perlmutter et al. (1999) used them to find that the universe is currently expanding at an accelerating rate.

In this age of precision cosmology, observations of SNe Ia continue to play a crucial role (see, e.g., Sullivan et al. 2011). Ironically, we are still faced with the situation that many more events have well-observed light curves at high redshifts ($z > 0.1$) than at low redshifts (Betoule et al. 2014). Since the SN Ia results are derived from a comparison of the peak magnitudes of distant and nearby events, the relatively heterogeneous quality of the low-redshift data directly affects the precision with which we are able to determine the nature of dark energy. Moreover, there are still legitimate concerns about systematic errors arising from the conversion of instrumental magnitudes into a uniform photometric system, calibration errors, the treatment of host-galaxy dust reddening corrections, and evolutionary effects caused by differing ages or metallicities (Wood-Vasey et al. 2007; Freedman et al. 2009; Conley et al. 2011).

The Carnegie Supernova Project I (CSP-I; Hamuy et al. 2006) was initiated to address these problems by creating a new data set of low-redshift optical/NIR light curves of SNe Ia in a well-understood and stable photometric system. The use of NIR data provides several major advantages over optical wavelengths alone. First, color corrections caused by dust and any systematic errors associated with these are up to a factor of five smaller than at optical wavelengths (Krisciunas et al. 2000; Freedman et al. 2009). The combination of optical and NIR photometry also provides invaluable information on the shape of the host-galaxy dust reddening curve (Folatelli et al. 2010; Mandel et al. 2011; Burns et al. 2014). Finally, both theory and observations indicate that the rest-frame peak NIR magnitudes of SNe Ia exhibit a smaller intrinsic scatter (Kasen 2006; Mandel et al. 2009; Kattner et al. 2012) and require only minimal luminosity versus decline-rate corrections.

The CSP-I was a 5 yr (2004–2009) project funded by the National Science Foundation (NSF). It consisted of low-redshift ($z \lesssim 0.08$) and high-redshift ($0.1 < z < 0.7$) components. Hamuy et al. (2006) presented an overview of the goals of the low-redshift portion of the project, the facilities at Las Campanas Observatory (LCO), and details of photometric calibration. It

should be noted that the CSP-I also obtained observations of more than 100 low-redshift core-collapse SNe.

Contreras et al. (2010, hereafter Paper I) presented CSP-I photometry of 35 low-redshift SNe Ia, 25 of which were observed in the NIR. Analysis of the photometry of these objects is given by Folatelli et al. (2010). Stritzinger et al. (2011, hereafter Paper II) presented CSP-I photometry of 50 more low-redshift SNe Ia, 45 of which were observed in the NIR. This sample included two super-Chandrasekhar candidates (Howell et al. 2006) and two SN 2006bt-like objects (Foley et al. 2010). The high-redshift objects observed by the CSP-I in the rest-frame i band are discussed by Freedman et al. (2009).

In this paper, we present optical and NIR photometry of the final 49 SNe in the CSP-I low-redshift sample, including five members of the SN 2002cx-like subclass, also referred to as Type Iax SNe (see Foley et al. 2013), and two examples of the Type Ia-CSM subtype (Silverman et al. 2013). We provide updated optical and NIR photometry of the 85 previously published low-redshift SNe in the CSP-I sample since, in several cases, we have eliminated bad data points, improved the photometric calibrations, and obtained better host-galaxy reference images. This combined data set represents the definitive version of the CSP-I photometry for low-redshift white dwarf SNe and supersedes the light curves published in Papers I and II, as well as those published for a few individual objects by Prieto et al. (2007), Phillips et al. (2007), Schweizer et al. (2008), Stritzinger et al. (2010), Taddia et al. (2012), Stritzinger et al. (2014), and Gall et al. (2017). Other useful optical and near-IR observations of Type Ia SNe include the photometry obtained by the Center for Astrophysics group (Hicken et al. 2009, 2012; Friedman et al. 2015).

2. Supernova Sample

In Figure 1 we present finder charts for the 134 SNe Ia composing the low-redshift CSP-I white dwarf SN sample, indicating the positions of the SN and the local sequence of tertiary standard stars in each field (see Section 5.2). General properties of each SN and host galaxy are provided in Table 1. Two “targeted” searches, the Lick Observatory SN Search (LOSS; Filippenko et al. 2001; Leaman et al. 2011; Li et al. 2011) with the 0.76 m Katzman Automatic Imaging Telescope (KAIT) and the Chilean Automatic Supernova Search (Pignata et al. 2009), accounted for 55% of the SNe selected for follow-up observations. Another 36% of the SNe in the sample were discovered by amateur astronomers, and the remaining 19% were drawn from two “untargeted” (sometimes referred to as “blind”) searches: the Robotic Optical Transient Search Experiment (ROTSE-III; Akerlof et al. 2003) and the Sloan Digital Sky Survey II Supernova Survey (SDSS-II; Frieman et al. 2008).

Note that the host galaxies of five SNe in the sample are somewhat ambiguous:

1. The field of SN 2006bt lies at large angular distances from any potential hosts in a field rich in galaxies. Redshift measurements taken from the NASA/IPAC Extragalactic Database (NED) show that the majority of the galaxies within $10'$ of the SN are members of a cluster at $z_{\text{helio}} = 0.0482 \pm 0.0026$. The closest galaxy to the SN, 2MASX J15562803+2002482, is $35''$ distant and has $z_{\text{helio}} = 0.0463$. However, the second-closest galaxy, CGCG 108–013, which lies $50''$ from the SN and has

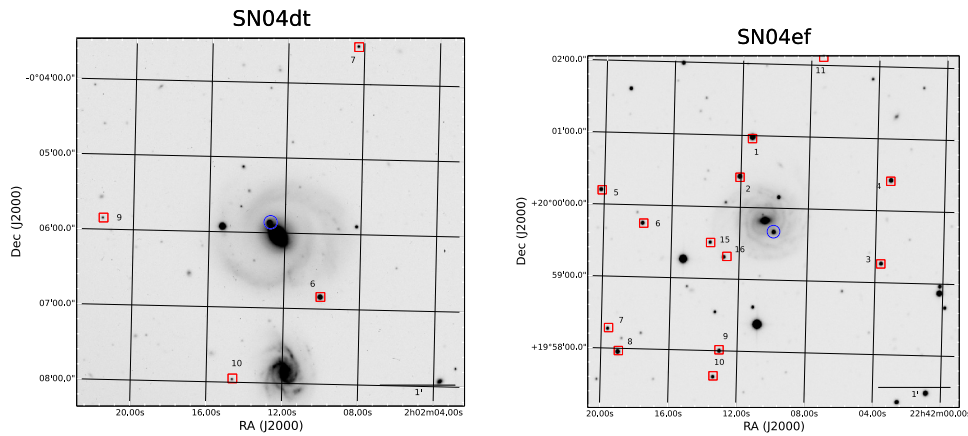


Figure 1. Mosaic of V -band CCD images of 134 Type Ia SNe observed by CSP-I. The location of each SN is indicated by a blue circle. The positions of secondary standards used for calibrating the optical photometry are indicated by red squares. For uniformity, each finder chart is $5' \times 5'$ in size. In some cases, a few of the local standard stars are outside the boundaries of the chart. All 134 finder charts are in the Figure Set.

(The complete figure set (134 images) is available.)

$z_{\text{helio}} = 0.0322$, was determined by Foley et al. (2010) to be the most likely host using the SuperNova IDentification code (SNID; Blondin & Tonry 2007). As discussed by these authors, SN 2006bt displayed unusual photometric and spectroscopic properties compared to typical SNe Ia. By chance, another object with very similar characteristics whose host galaxy is unambiguous, SN 2006ot (see Figure 1), was discovered in the CSP-I sample by Stritzinger et al. (2014). After de-redshifting our spectra of SN 2006ot, we used them as templates to determine at what redshift they best matched spectra of SN 2006bt taken at comparable epochs. We derive $z_{\text{helio}} = 0.0325 \pm 0.0005$ for SN 2006bt, confirming that CGCG 108-013 is the likely host.

2. SN 2007mm exploded in the midst of a compact group of galaxies, five of whose members are within $33''$ of the SN position. The redshift listed in Table 1 corresponds to the average of these five galaxies.
3. SN 2008bf appeared between three galaxies in the NGC 4065 group, the closest being 2MASX J12040495 +2014489, which has $z_{\text{helio}} = 0.0224$. However, any of the three galaxies could be the host, and so we adopt the NGC 4065 group redshift of $z_{\text{helio}} = 0.0235$. A pre-SN image by the Sloan Digital Sky Survey (SDSS) shows an unresolved source at the position of the SN. Host-galaxy reference images obtained by the CSP-I after the SN faded show the same unresolved source. The colors of this object are most consistent with a star, and so we assume that it is unrelated to the SN.
4. SN 2008ff is $32''$ from 2MASX J20135726–4420540, whose redshift is $z_{\text{helio}} = 0.0194$, and is $40''$ from ESO 284–G032, which has $z_{\text{helio}} = 0.0192$. We assume the average of these redshifts for the SN.
5. NGC 3425 (also known as NGC 3388), the supposed host of SN 2009al at $z_{\text{helio}} = 0.0221$, is $66''$ distant from the SN. Although a second galaxy (SDSS J105124.64 +083326.7) with $z_{\text{helio}} = 0.0232$ is located $85''$ from the SN, we adopt $z_{\text{helio}} = 0.0221$.

The top panel of Figure 2 shows a histogram of the heliocentric radial velocities of the host galaxies of the 134 SNe in our sample. The redshifts range from $z = 0.0037$

(for SN 2010ae) to 0.0835 (for SN 2006fw). The median redshift is 0.0241, corresponding to a distance of 100 Mpc for a Hubble constant of $72 \text{ km s}^{-1} \text{ Mpc}^{-1}$ (Freedman et al. 2001).

Table 2 summarizes spectroscopic classifications for the sample. The spectral subtype is listed, along with the epoch of the spectrum (relative to the time of B -band maximum) used to determine the spectral subtype. Also given are classifications in the Branch et al. (2006) and Wang et al. (2009) schemes using the same criteria as Folatelli et al. (2013). Photometric parameters for the subset of 123 SNe Ia are provided in Table 3. See Section 7.1 for details.

3. Imaging

Between 2004 and 2010, five 9-month CSP-I observing campaigns were carried out, each running from approximately September through May. During these campaigns, the vast majority of the optical imaging in the $ugriBV$ bandpasses was obtained with the SITE3 CCD camera attached to the LCO Swope 1 m telescope. A limited amount of optical imaging was also taken with the Tek5 CCD camera on the LCO 2.5 m du Pont telescope.

NIR imaging of the CSP-I SNe during the first observing campaign was obtained exclusively with the Wide-Field IR Camera (WIRC) on the du Pont 2.5 m telescope (Persson et al. 2002), and some additional WIRC observations were carried out during campaigns 2–5. However, beginning with the second CSP-I campaign, a new imager built especially for the CSP-I, RetroCam, went into use on the Swope 1 m telescope and became the workhorse NIR camera for the remaining four campaigns.

Basic reductions of the optical and NIR images are discussed in detail in Paper I. For the optical data, these consisted of electronic bias subtraction, flat-fielding, application of a linearity correction appropriate for the CCD, and an exposure-time correction that corrects for a shutter time delay. The individual dithered NIR images were corrected for electronic bias, detector linearity, pixel-to-pixel variations of the detector sensitivity, and sky background and were then aligned and stacked to produce a final image.

Host-galaxy reference images were obtained a year or more after the last follow-up image. As described in Paper I, most of

Table 1
General Properties of 134 Type Ia Supernovae

SN Name	SN α (2000)	SN δ (2000)	Host Galaxy	Morphology ^a	z_{helio} ^a	Discovery Reference	Discovery Indiv/Group ^b
2004dt	02:02:12.77	-00:05:51.5	NGC 799	(R')SB(s)a	0.0197	IAUC 8386	LOSS
2004ef	22:42:10.02	+19:59:40.4	UGC 12158	Sb	0.0310	IAUC 8399	Boles/Armstrong
2004eo	20:32:54.19	+09:55:42.7	NGC 6928	SB(s)ab	0.0157	IAUC 8406	Itagaki
2004ey	21:49:07.81	+00:26:39.2	UGC 11816	SB(rs)c	0.0158	IAUC 8419	Tenagra-II
2004gc	05:21:49.95	+06:40:33.7	ARP 327 NED04	...	0.0321	IAUC 8442	del Olmo/Tenagra-II
2004gs	08:38:23.18	+17:37:39.8	MCG +03-22-020	S0?	0.0267	IAUC 8453	LOSS
2004gu	12:46:24.72	+11:56:56.1	FGC 175A	...	0.0459	IAUC 8454	ROTSE-III
2005A	02:30:43.25	-02:56:19.8	NGC 958	SB(rs)c	0.0191	IAUC 8459	LOSS
2005M	09:37:32.36	+23:12:02.7	NGC 2930	S?	0.0220	IAUC 8470	Puckett
2005W	01:50:45.77	+21:45:35.4	NGC 691	SA(rs)bc	0.0089	IAUC 8475	Hirose
2005ag	14:56:43.65	+09:19:42.5	J14564322+0919361	...	0.0797	IAUC 8484	LOSS
2005al	13:50:00.33	-30:34:34.2	NGC 5304	E+ pec	0.0124	IAUC 8488	BRASS
2005am	09:16:12.47	-16:18:16.0	NGC 2811	SB(rs)a	0.0079	IAUC 8490	Perth
2005be	14:59:32.72	+16:40:11.6	J14593310+1640070	...	0.0350	IAUC 8506	Puckett
2005bg	12:17:17.18	+16:22:17.6	MCG +03-31-93	Sab	0.0231	CBET 133	ROTSE-III
2005bl	12:04:12.26	+20:24:24.8	NGC 4059	E	0.0241	IAUC 8512	LOSS/Puckett
2005bo	12:49:41.03	-11:05:47.3	NGC 4708	SA(r)ab pec?	0.0139	CBET 141	Puckett
2005el	05:11:48.72	+05:11:39.4	NGC 1819	SB0	0.0149	CBET 233	LOSS
2005eq	03:08:49.31	-07:01:59.7	MCG -01-09-006	SB(rs)cd?	0.0290	IAUC 8608	LOSS
2005gj	03:01:11.95	-00:33:13.9	SDSS J030111.99-003313.5	...	0.0616 ^c	CBET 247	SDSS-II
2005hc	01:56:47.94	-00:12:49.4	MCG +00-06-003	...	0.0459	CBET 259	SDSS-II
2005hj	01:26:48.27	-01:14:16.8	SDSS J012648.45-011417.3	...	0.0574	CBET 266	ROTSE-III
2005hk	00:27:50.87	-01:14:16.8	UGC 272	SAB(s)d?	0.0130	IAUC 8625	SDSS-II/LOSS
2005iq	23:58:32.50	-18:42:33.0	MCG -03-01-008	Sa	0.0340	IAUC 8628	LOSS
2005ir	01:16:43.76	+00:47:40.4	SDSS J011643.87+004736.9	...	0.0763	CBET 277	SDSS-II
2005kc	22:34:07.34	+05:34:06.3	NGC 7311	Sab	0.0151	IAUC 8629	Puckett
2005ke	03:35:04.35	-24:56:38.8	NGC 1371	(R')SAB(r'l)a	0.0049	IAUC 8630	LOSS
2005ki	10:40:28.22	+09:12:08.4	NGC 3332	(R)SA0	0.0192	IAUC 8632	LOSS
2005ku	22:59:42.61	+00:00:49.3	2MASX J2259426500	...	0.0454	CBET 304	SDSS-II
2005lu	02:36:03.71	-17:15:50.0	ESO 545-G038	S.../Irr?	0.0320	IAUC 8645	LOSS
2005mc	08:27:06.36	+21:38:45.6	UGC 04414	S0a	0.0252	CBET 331	THCA
2005na	07:01:36.62	+14:07:59.7	UGC 3634	SB(r)a	0.0263	CBET 350	Puckett
2006D	12:52:33.94	-09:46:30.8	MCG -01-33-34	SAB(s)ab pec? HII	0.0085	CBET 362	BRASS
2006X	12:22:53.99	+15:48:33.1	NGC 4321	SAB(s)bc	0.0052	IAUC 8667	Suzuki/CROSS
2006ax	11:24:03.46	-12:17:29.2	NGC 3663	SA(rs)bc pec	0.0167	CBET 435	LOSS
2006bd	11:38:28.46	+20:31:34.4	UGC 6609	E	0.0257	CBET 448	Puckett
2006bh	22:40:16.10	-66:29:06.3	NGC 7329	SB(r)b	0.0109	CBET 457	Monard
2006br	13:30:01.80	+13:24:56.8	NGC 5185	Sb	0.0246	CBET 482	Puckett
2006bt	15:56:30.53	+20:02:45.3	CGCG 108-013 ^d	SA0/a	0.0322	CBET 485	LOSS
2006dd	03:22:41.62	-37:12:13.0	NGC 1316 (Fornax A)	SAB0 ^(s) pec	0.0059	IAUC 8723	Monard
2006ef	02:04:19.51	-08:43:42.2	NGC 809	(R)S0	0.0179	CBET 597	LOSS
2006ej	00:38:59.77	-09:00:56.6	NGC 191A	S0 pec sp	0.0205	CBET 603	LOSS
2006eq	21:28:37.13	+01:13:41.5	2MASX J21283758+0113490	...	0.0495	CBET 611	SDSS-II
2006et	00:42:45.82	-23:33:30.4	NGC 232	SB(r)a? pec	0.0226	CBET 616	Itagaki
2006ev	21:30:59.26	+13:59:21.2	UGC 11758	Sbc	0.0287	IAUC 8747	Ory
2006fw	01:47:10.34	-00:08:49.2	GALEXASC J014710.29-000848.3	...	0.0835	CBET 627	SDSS-II
2006gj	03:17:35.80	-01:41:30.2	UGC 2650	Sab	0.0284	CBET 631	Puckett
2006gt	00:56:17.30	-01:37:46.0	2MASX J00561810-0137327	...	0.0448	CBET 641	ROTSE-III
2006hb	05:02:01.28	-21:07:55.1	MCG-041234	E?	0.0153	CBET 649	LOSS
2006hx	01:13:57.31	+00:22:18.0	2MASX J01135716+0022	S0	0.0455	CBET 656	SDSS-II
2006is	05:17:34.37	-23:46:54.2	GALEXASC J051734.53-234659.1	...	0.0310 ^c	CBET 659	LOSS
2006kf	03:41:50.48	+08:09:25.0	UGC 2829	S0	0.0213	CBET 686	LOSS
2006lu	09:15:17.63	-25:36:00.3	2MASX J09151727-2536001	...	0.0534 ^c	IAUC 8770	LOSS
2006mr	03:22:43.04	-37:12:29.6	NGC 1316 (Fornax A)	SAB	0.0059	CBET 723	Monard
2006ob	01:51:48.11	+00:15:48.3	UGC 1333	Sb	0.0592	CBET 745	LOSS/SDSS-II
2006os	02:55:01.10	+16:00:34.8	UGC 2384	S	0.0328	IAUC 8779	ROTSE-III/LOSS
2006ot	02:15:04.84	-20:45:58.2	ESO 544G31	Sa	0.0531	IAUC 8779	Puckett/LOSS
2006py	22:41:42.05	-00:08:12.9	SDSS J224142.04-000812.9	...	0.0579	CBET 762	SDSS-II
2007A	00:25:16.66	+12:53:12.5	NGC 105	Sab	0.0177	CBET 795	Puckett/LOSS

Table 1
(Continued)

SN Name	SN α (2000)	SN δ (2000)	Host Galaxy	Morphology ^a	z_{helio} ^a	Discovery Reference	Discovery Indiv/Group ^b
2007N	12:49:01.25	-09:27:10.2	MCG 0133012	SA(s)a	0.0129	CBET 818	LOSS
2007S	10:00:31.26	+04:24:26.2	UGC 5378	Sb	0.0139	CBET 825	Puckett
2007af	14:22:21.03	-00:23:37.6	NGC 5584	SAB(rs)cd	0.0055	CBET 863	Itagaki
2007ai	16:12:53.74	-21:37:48.7	MCG 0438004	Sc	0.0317	CBET 870	LOSS
2007al	09:59:18.48	-19:28:25.8	2MASX J09591870-1928233	...	0.0122	IAUC 8822	LOSS
2007as	09:27:36.01	-80:10:39.2	ESO 18G18	SB(rs)c	0.0176	CBET 888	Tengra-II
2007ax	08:22:43.26	+22:33:16.9	NGC 2577	S0	0.0069	CBET 904	Arbour/Itagaki
2007ba	15:16:42.63	+07:23:47.8	UGC 9798	S0/a	0.0385	CBET 911	LOSS
2007bc	11:19:14.57	+20:48:32.5	UGC 6332	(R)SBa	0.0208	CBET 913	LOSS
2007bd	08:31:33.28	-01:11:58.0	UGC 4455	SB(r)a	0.0309	CBET 914	LOSS
2007bm	11:25:02.30	-09:47:53.8	NGC 3672	SA(s)c	0.0062	CBET 936	Perth
2007ca	13:31:05.81	-15:06:06.6	MCG 023461	Sc pec sp	0.0141	CBET 945	LOSS
2007cg	13:25:33.58	-24:39:08.1	ESO 508-G75	Sc	0.0332	IAUC 8843	LOSS
2007hj	23:01:47.89	+15:35:11.4	NGC 7461	SB0	0.0141	IAUC 8874	LOSS
2007hx	02:06:27.08	-00:53:58.3	SDSS J020627.93005353.1	...	0.0794	CBET 1057	SDSS-II
2007if	01:10:51.37	+15:27:39.9	SNF 20070825-001 HOST	...	0.0742	CBET 1059	ROTSE-IIIb/SN Factory
2007jd	02:59:53.37	+01:09:38.6	SDSS J025953.65+010936.1	...	0.0726	CBET 1076	SDSS-II
2007jg	03:29:50.82	+00:03:24.6	SDSS J032950.83+000316.0	...	0.0371	CBET 1076	SDSS-II
2007jh	03:36:01.54	+01:06:12.2	CGCG 391014	...	0.0408	CBET 1076	SDSS-II
2007le	23:38:48.41	-06:31:21.3	NGC 7721	SA(s)c	0.0067	CBET 1100	Monard
2007mm	01:05:46.67	-00:45:31.8	ambiguous ^f	...	0.0664	CBET 1102	SDSS-II
2007nq	00:57:33.57	-01:23:19.0	UGC 595	E	0.0450	CBET 1106	ROTSE-IIIb
2007ol	01:37:23.70	-00:18:43.2	2MASX J01372378-0018422	...	0.0559	CBET 1117	SDSS-II
2007on	03:38:50.90	-35:34:30.0	NGC 1404	E1	0.0065	CBET 1121	TAROT
2007so	02:47:43.13	+13:15:14.8	NGC 1109	compact	0.0297	CBET 1168	LOSS
2007 sr	12:01:52.80	-18:58:21.7	NGC 4038 (The Antennae)	SB(s)m pec	0.0055	CBET 1172	CSS
2007st	01:48:42.47	-48:38:57.8	NGC 692	(R')SB(r)bc?	0.0212	CBET 1177	Monard
2007ux	10:09:19.98	+14:59:32.8	2MASX J10091969+1459268	...	0.0309	CBET 1187	LOSS
2008C	06:57:11.53	+20:26:13.7	UGC 3611	S0/a	0.0166	CBET 1195	Puckett
2008J	02:34:24.20	-10:50:38.5	MCG -02-7-33	SBbc?	0.0159	CBET 1211	LOSS
2008O	06:57:34.46	-45:48:44.3	ESO 256-G11	SA0 ^{0(s)?}	0.0389	CBET 1220	CHASE
2008R	03:03:53.70	-11:59:39.4	NGC 1200	SA(s)0	0.0135	CBET 1230	Itagaki
2008ae	09:56:03.20	+10:29:58.8	IC 577	S?	0.0300	CBET 1247	Sostero/Puckett
2008ar	12:24:37.92	+10:50:17.4	IC 3284	Sab	0.0261	CBET 1273	ROTSE-III
2008bc	09:38:31.23	-63:58:25.6	KK 1524	S	0.0151	CBET 1301	CHASE
2008bd	10:18:23.32	-13:06:11.2	MCG -02-26-42	(R')SAB ^{(s)?}	0.0301	CBET 1301	CHASE
2008bf	12:04:02.90	+20:14:42.6	ambiguous ^f	E?	0.0235	CBET 1307	LOSS
2008bi	08:35:53.39	+00:42:23.1	NGC 2618	(R')SA(rs)ab	0.0134	CBET 1312	CHASE
2008bq	06:41:02.51	-38:02:19.0	ESO 308G25	Sa	0.0340	CBET 1328	Tengra-II
2008bt	10:50:16.88	-12:06:32.0	NGC 3404	SBab? edge-on	0.0154	CBET 1336	LOSS/Itagaki
2008bz	12:38:57.74	+11:07:46.2	2MASX J12385810+1107502	...	0.0603	CBET 1353	ROTSE-III
2008cc	21:03:29.62	-67:11:01.1	ESO 107-G4	E1?	0.0104	CBET 1356	CHASE
2008cd	13:15:01.75	-15:57:06.8	NGC 5038	S0? edge-on	0.0074	CBET 1360	LOSS
2008cf	14:07:32.56	-26:33:06.6	J140732.38-263305.6	...	0.0460	CBET 1365	LOSS
2008ff	20:13:59.96	-44:21:07.8	ambiguous ^f	...	0.0193	CBET 1488	Tan
2008fl	19:36:44.84	-37:33:04.5	NGC 6805	E1	0.0199	CBET 1498	CHASE
2008fp	07:16:32.60	-29:19:31.8	ESO 428G014	SAB(r)0 pec	0.0057	CBET 1506	CHASE
2008fr	01:11:49.14	+14:38:27.0	SDSS J011149.19+143826.5	...	0.0397 ^c	CBET 1513	ROTSE-III
2008fu	03:02:28.50	-24:27:21.5	ESO 480-IG21	...	0.0520	CBET 1517	LOSS
2008fw	10:28:55.97	-44:39:55.6	NGC 3261	SB(rs)b	0.0085	CBET 1521	Monard
2008gg	01:25:23.04	-18:10:20.8	NGC 539	SB(rs)c	0.0320	CBET 1538	CSS
2008gl	01:20:54.82	+04:48:19.1	UGC 881	E	0.0340	CBET 1545	CHASE
2008go	22:10:44.83	-20:47:17.2	2MASX J22104396-2047256	...	0.0623	CBET 1553	LOSS
2008gp	03:23:00.73	+01:21:42.8	MCG +00-9-74	(R)SAB(r)a	0.0334	CBET 1555	LOSS
2008 ha	23:38:27.52	+18:13:35.4	UGC 12682	Im	0.0046	CBET 1567	Puckett
2008hj	00:04:01.91	-11:10:07.5	MCG -02-1-14	SB(rs)c?	0.0379	CBET 1579	Puckett
2008hu	08:09:14.76	-18:39:13.1	ESO 561-G18	Sc	0.0497	CBET 1600	LOSS
2008hv	09:07:34.06	+03:23:32.1	NGC 2765	S0	0.0126	CBET 1601	CHASE
2008ia	08:50:35.15	-61:16:40.6	ESO 125-G 006	S0	0.0219	CBET 1612	CHASE

Table 1
(Continued)

SN Name	SN α (2000)	SN δ (2000)	Host Galaxy	Morphology ^a	z_{helio} ^a	Discovery Reference	Discovery Indiv/Group ^b
2009D	03:54:22.83	-19:10:54.2	MCG -03-10-52	Sb	0.0250	CBET 1647	LOSS
2009F	04:59:23.56	-11:07:50.1	NGC 1725	S0	0.0130	CBET 1650	CHASE
2009I	02:45:10.40	-04:42:49.4	NGC 1080	SAB(s)c?	0.0262	CBET 1660	CHASE
2009J	05:55:21.13	-76:55:20.8	IC 2160	(R')SB(s)c pec?	0.0158	CBET 1661	CHASE
2009P	11:20:38.78	-03:32:46.3	CGCG 011-065	...	0.0251	CBET 1674	Puckett
2009Y	14:42:23.85	-17:14:48.4	NGC 5728	SAB(r)a?	0.0094	CBET 1684	Perth/LOSS
2009aa	11:23:42.28	-22:16:14.5	ESO 570-G20	Sc	0.0273	CBET 1685	LOSS
2009ab	04:16:36.39	+02:45:51.0	UGC 2998	SB(rs)b	0.0112	CBET 1690	LOSS
2009ad	05:03:33.38	+06:39:35.7	UGC 3236	Sbc	0.0284	CBET 1694	Puckett
2009ag	07:11:40.81	-26:41:06.3	ESO 492-2	SAB(rs)b pec	0.0086	CBET 1698	Puckett
2009al	10:51:22.07	+08:34:42.7	NGC 3425 ^f	S0	0.0221	CBET 1705	CSS
2009cz	09:15:00.02	+29:44:07.1	NGC 2789	S0/a	0.0211	CBET 1759	LOSS
2009dc	15:51:12.12	+25:42:28.0	UGC 10064	S0	0.0214	CBET 1762	Puckett
2009ds	11:49:04.11	-09:43:44.9	NGC 3905	SB(rs)c	0.0193	CBET 1784	Itagaki
2009le	02:09:17.14	-23:24:44.8	ESO 478-6	Sbc	0.0178	CBET 2022	CHASE
2010ae	07:15:54.65	-57:20:36.9	ESO 162-17	SB? pec edge-on	0.0037	CBET 2184	CHASE

Notes.

^a Host-galaxy morphology and heliocentric redshift are from the NASA/IPAC Extragalactic Database (NED) or SDSS unless otherwise indicated.

^b References/URLs: CHASE (<http://www.das.uchile.cl/proyectoCHASE/>); CSS (<http://www.lpl.arizona.edu/css/>); LOSS (Filippenko et al. 2001; Filippenko 2005; Leaman et al. 2011); Perth (Williams 1997); ROTSE-III (Quimby 2006); Puckett (<http://www.cometwatch.com>); Tenagra-II (<http://www.tenagraobservatories.com/>); SDSS-II (Frieman et al. 2008).

^c Host-galaxy redshift of SN 2005gj from Prieto et al. (2007). Note that Aldering et al. (2006) give $z = 0.0667$.

^d Most likely host according to Foley et al. (2010b). See text for further details.

^e The host of SN 2006is was observed with the Magellan Baade Telescope and IMACS; the hosts of SN 2006lu and SN 2008fr were observed with the du Pont 2.5 m and WFCCD. Emission/absorption lines for radial velocity determination were weighted according to their equivalent widths.

^f Ambiguous host. See text for further details.

the optical *ugriBV* reference images were obtained with the du Pont telescope and the Tek5 CCD camera using the same filters employed to take the original science images.¹⁸ A smaller set of reference images was also taken with the du Pont telescope using a second CCD camera, SITe2, and a few were obtained using the Swope+SITe3 camera under good seeing conditions. For a small number of objects located far outside their host galaxies, subtraction of a reference image was unnecessary.

NIR *YJH* host-galaxy reference images were obtained exclusively with WIRC on the du Pont telescope using similar filters to those in RetroCam.

4. Filters

Precision photometry requires knowledge of the filter throughputs as a function of wavelength (e.g., Bessell 1990; Stubbs & Tonry 2006), so we devised an instrument incorporating a monochromator and calibrated detectors to precisely determine the response functions (telescope+filter+instrument) of the CSP-I bandpasses (Rheault et al. 2014). Paper II provides a detailed account of the measurement of the optical bandpasses, and in Appendix A we describe the calibration of the NIR bandpasses using the same instrument and similar techniques.

Repeated scans of the CSP-I *ugriBV* bandpasses show that the relative measurement errors in transmission are $\sim 1\%$ or less. That is, the ratios as a function of wavelength of repeated scans of each individual filter fall within an envelope that is $\pm 1\%$. Repeated scans of the *YJH* bandpasses (for both the Swope+RetroCam and the du Pont+WIRC) indicate that each of these filters has been determined in a relative sense to a precision of 2%–3%. Unfortunately, the throughput of the WIRC K_s filter is highly uncertain beyond 2200 nm (2.2 μm) owing to the low power of the monochromator light source at these wavelengths and the rising thermal contamination at 2.3 μm . Nearly all of the K_s -band observations made by CSP-I were obtained during the first observing campaign and were published in Papers I and II. However, due to the uncertainty in the K_s filter response function, we have elected not to include any K_s -band observations in this final data release paper. Those wishing to employ the CSP-I photometry for precision cosmology applications are advised not to use the K_s -band measurements given in Papers I and II.

Figure 3 displays the optical and NIR bandpasses employed by the CSP-I after including atmospheric transmission typical of LCO. In constructing the optical filter bandpasses, we have assumed an airmass of 1.2, a value that corresponds to the mode of the airmasses of the standard-star observations used to calibrate the data. In Appendix B we test the validity of the final optical bandpasses by reproducing the measured color terms (see Section 6.1.1) via synthetic photometry performed on spectra of Landolt standards.

¹⁸ If the set of CSP-I *ugri* filters used at the Swope telescope was not available, a duplicate set produced by Asahi Spectral Company Ltd. in the same run as the Swope filters was employed. Likewise, if the *B* and/or *V* filters were not available, filters from the du Pont telescope with similar throughput curves were used.

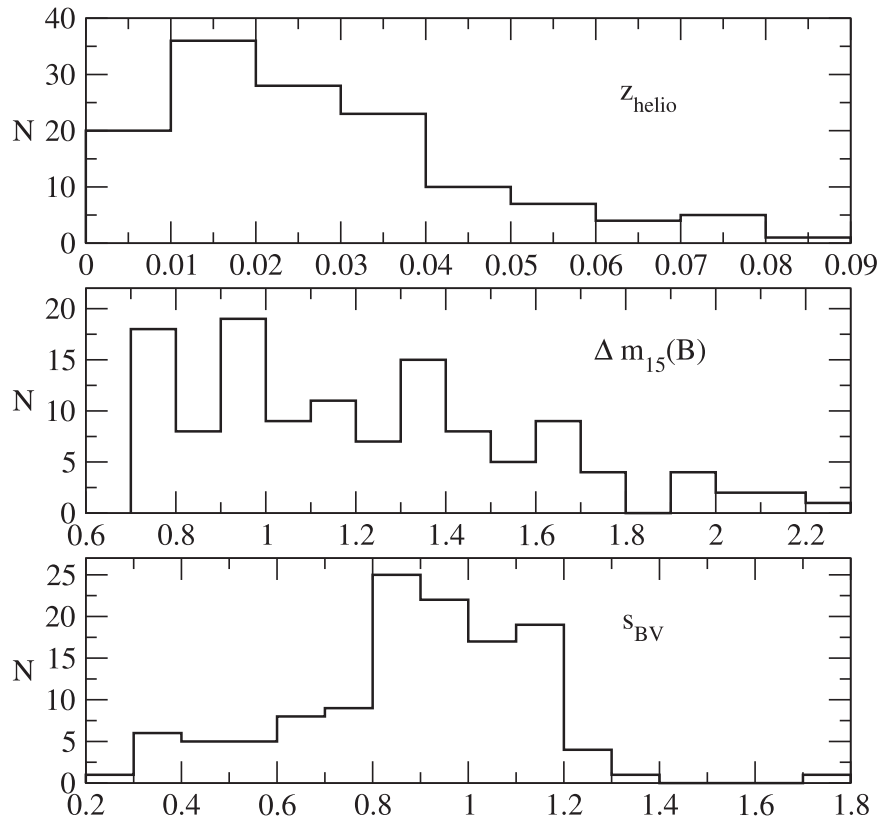


Figure 2. Top: histogram of values of heliocentric redshift of host galaxies of the 134 SNe included in this paper. Middle: histogram of values of the B -band decline rate, $\Delta m_{15}(B)$, of the SNe Ia, as determined from the template fits. Bottom: histogram of values of the color stretch parameter s_{BV} for the SNe Ia.

5. Photometric Reductions: Overview

In this and the following section we define the CSP-I natural photometric system and describe the methodology used to calibrate it. While this has been described in previous CSP-I publications, several changes have been made in our definitions and procedures. These changes affect the entire CSP-I sample, and as this is the final data release, we seek to make the procedure as clear as possible.

5.1. The CSP-I Natural System

Because of differences in instrument throughputs, photometry measured by different facilities will not agree. These differences are a strong function of color of the object and can therefore be taken into account through the use of color terms (see, e.g., Harris et al. 1981). These color terms are typically measured empirically by observing a set of standard stars with a large range in color and allow the observer to transform their instrumental photometry into the system in which the standards were measured.

The primary difficulty in dealing with *supernova* photometry is the fact that their spectral energy distributions (SEDs) are significantly different than those of the stars we use to calibrate. Supernova spectra also evolve significantly with time. Consequently, the color terms cannot be used on the SN magnitudes to transform them to a standard system. Instead, we adopt a *natural* system, in which the standard-star magnitudes are transformed to what we would measure through our own telescopes/instruments. There are several advantages to working in the natural system, as follows:

1. If the system is stable (i.e., color terms do not vary significantly with time), nightly calibration of each filter does not rely on other filters to measure colors. This can be advantageous if time is short.
2. Working in the natural system requires fewer standard-star measurements to obtain the nightly zero-points, as the equations have one fewer unknown. In fact, the equations can be reduced to only one unknown, the nightly zero-point (see Section 6).
3. Photometry in the natural system is the “purest” form of the data and, given precise bandpass response function measurements, allows the CSP-I observations to be more readily combined with photometry in other photometric systems using S -corrections (Stritzinger et al. 2002; Krisciunas et al. 2003).

To compare photometry of SNe in host galaxies at different redshifts, precision K -corrections must be calculated with the transmission functions used in the observations and not that of the standard system. Thus, one must back out the standard system color transformation to the natural system in order to do the K -correction.

Having introduced the natural system, we now proceed to describe in general terms the procedure used to measure and calibrate the photometry using standard stars.

5.2. Standard Stars

Observations of standard stars are required in order to calibrate the SN photometry. In this paper, we adopt the following nomenclature in referring to the different types of standard stars used by the CSP-I:

Table 2
Photometric and Spectroscopic Properties of the Supernovae

SN Name	$\Delta m_{15}(B)^a$ (mag)	Subtype ^b	Wang Subtype ^c	Branch Subtype ^d	N_{opt}^e	N_{IR}^f	t_{sp}^g (days)
2004dt	1.067(081)	normal	HV	BL	49	0	23.6
2004ef	1.371(060)	normal	HV	BL	49	4	-1.8
2004eo	1.339(060)	normal	N	CL	42	9	-10.3
2004ey	0.950(061)	normal	N	CN	32	8	-0.8
2004gc	1.103(084)	normal	29	0	11.1
2004gs	1.587(060)	normal	N	CL	54	9	-3.4
2004gu	0.796(067)	06gz-like	91T	SS	31	3	-3.1
2005A	0.977(072)	normal	HV	BL	36	9	25.4
2005M	0.796(061)	91T-like	91T	SS	59	13	-0.1
2005W	1.196(061)	...	N	BL	22	0	...
2005ag	0.917(062)	normal	N	BL	46	4	0.4
2005al	1.302(062)	normal	35	5	14.0
2005am	1.491(061)	normal	HV	BL	38	6	7.7
2005be	1.418(071)	normal	13	0	7.2
2005bg	0.922(075)	normal	N	SS	17	0	2.0
2005bl	2.000(063)	91bg-like	91bg	CL	12	0	-4.6
2005bo	1.237(069)	normal	N	CN	10	0	-1.0
2005el	1.354(061)	normal	N	CN	25	22	-6.4
2005eq	0.796(063)	91T-like	91T	SS	27	15	-5.4
2005gj	...	Ia-CSM	23	25	66.0
2005hc	0.834(061)	normal	N	CN	25	13	-5.4
2005hj	0.796(078)	normal	N	SS	17	7	-4
2005hk	...	Iax	24	22	...
2005iq	1.254(061)	normal	N	CN	20	12	...
2005ir	0.796(085)	14	0	...
2005kc	1.191(063)	normal	N	CN	13	9	0.8
2005ke	1.736(061)	91bg-like	91bg	CL	39	27	-1.4
2005ki	1.334(062)	normal	N	CN	47	15	-5.8
2005ku	0.990(081)	normal	HV	CN	7	3	-1.0
2005lu	0.796(098)	normal	17	4	12.7
2005mc	1.528(104)	normal	N	CN	17	0	-2.2
2005na	1.033(063)	normal	N	CN	27	9	11.7
2006D	1.364(060)	normal	N	CN	43	14	-6.1
2006X	1.095(066)	normal	HV	BL	36	33	-6.3
2006ax	0.976(061)	normal	N	CN	25	19	-10.6
2006bd	2.256(105)	91bg-like	91bg	CL	8	4	...7.0
2006bh	1.410(060)	normal	25	12	8.2
2006br	0.886(094)	normal	HV	BL	10	5	0.0
2006bt	...	06bt-like	11	5	...
2006dd	...	normal	41	1	...
2006ef	1.406(077)	normal	HV	BL	10	0	37.0
2006ej	1.367(070)	normal	HV	BL	13	3	30.0
2006eq	1.448(081)	normal	N	CL	18	10	26.4
2006et	0.837(061)	normal	N	CN	27	21	9.0
2006ev	1.326(077)	normal	N	BL	12	14	...
2006fw	1.132(198)	normal	N	CN	6	0	2.0
2006gj	1.555(064)	normal	N	CL	19	11	4.0
2006gt	1.641(064)	91bg-like	91bg	CL	14	10	-0.3
2006hb	1.460(071)	86G-like	91bg	...	28	10	6.0
2006hx	0.987(074)	normal	N	SS	12	4	-3.0
2006is	0.796(078)	normal	HV	CN	28	9	4.0
2006kf	1.503(062)	normal	N	CL	21	17	30.0
2006lu	0.938(074)	normal	29	4	8.0
2006mr	1.929(079)	91bg-like	91bg	CL	31	24	-2.3
2006ob	1.467(072)	normal	N	CN	13	7	1
2006os	1.172(112)	normal	N	CL	16	10	-2.0
2006ot	...	06bt-like	HV	BL	17	14	17.0
2006py	1.177(107)	normal	HV	SS	7	0	16.0
2007A	0.853(071)	normal	N	CN	10	9	-1.0
2007N	2.121(083)	91bg-like	91bg	CL	23	15	12.0

Table 2
(Continued)

SN Name	$\Delta m_{15}(B)^a$ (mag)	Subtype ^b	Wang Subtype ^c	Branch Subtype ^d	N_{opt}^e	N_{IR}^f	t_{sp}^g (days)
2007S	0.795(064)	91T-like	91T	SS	20	17	-2.0
2007af	1.193(061)	normal	N	BL	28	26	-11.0
2007ai	0.796(119)	91T-like	91T	SS	17	5	-2.0
2007al	1.782(082)	91bg-like	91bg	CL	16	10	...
2007as	1.120(076)	normal	HV	BL	19	11	-2.0
2007ax	2.036(066)	91bg-like	91bg	CL	13	8	-2.0
2007ba	1.668(062)	91bg-like	91bg	CL	18	14	6.0
2007bc	1.331(061)	normal	N	CL	15	12	3.0
2007bd	1.241(063)	normal	HV	BL	12	12	-4.0
2007bm	1.157(064)	normal	N	CN	10	8	-4.0
2007ca	0.853(062)	normal	N	CN	12	10	-4.0
2007cg	0.811(052)	8	5	...
2007hj	1.630(062)	...	N	CL	28	24	...
2007hx	0.905(057)	normal	12	8	...
2007if	...	SC	N	SS	18	8	-2.0
2007jd	1.330(091)	normal	HV	BL	14	4	0
2007jg	1.242(066)	normal	HV	BL	20	9	10.0
2007jh	1.700(069)	86G-like	91bg	...	13	2	14.0
2007le	0.931(061)	normal	HV	BL	25	17	-9.0
2007mm	2.142(095)	86G-like	9	0	...
2007nq	1.507(064)	normal	HV	BL	26	19	-4.0
2007ol	1.357(140)	normal	N	CN	7	0	-3.6
2007on	1.648(061)	normal	N	CL	38	29	-4.0
2007so	1.071(129)	normal	8	7	23.0
2007sr	0.978(073)	normal	30	27	13.0
2007st	1.638(077)	normal	14	15	8.0
2007ux	1.660(062)	86G-like	N	CL	22	15	...
2008C	1.192(106)	normal	N	SS	22	12	5.0
2008J	...	Ia-CSM	10	7	...
2008O	1.655(062)	normal	HV	...	25	10	0.4
2008R	1.600(073)	normal	91bg	CL	13	9	4.0
2008ae	...	lax	18	13	-0.7
2008ar	1.001(061)	normal	N	CN	18	13	-0.7
2008bc	0.873(060)	normal	N	CN	31	12	-10.0
2008bd	1.929(104)	91bg-like	91bg	...	18	5	7.9
2008bf	0.905(060)	normal	N	CN	27	7	0.7
2008bi	2.092(094)	91bg-like	91bg	...	18	6	9.9
2008bq	0.895(062)	normal	N	CN	17	4	0.0
2008bt	1.743(063)	91bg-like	91bg	CL	14	3	1
2008bz	0.984(093)	normal	N	CN	14	1	2.2
2008cc	1.380(073)	normal	21	10	9.4
2008cd	1.071(158)	normal	5	0	12.3
2008cf	0.796(084)	normal	N	SS	13	9	2.7
2008ff	0.903(062)	normal	24	19	19.7
2008fl	1.354(071)	normal	N	CN	23	20	3.2
2008fp	0.756(061)	normal	N	CN	30	23	-4.0
2008fr	0.933(074)	normal	N	CN	21	16	3.8
2008fu	1.620(140)	normal	N	SS	21	10	4.5
2008fw	0.794(072)	91T-like	91T	SS	25	7	5.6
2008gg	0.796(077)	normal	HV	BL	26	13	4.8
2008gl	1.320(062)	normal	N	BL	22	11	...
2008go	1.105(136)	normal	6	4	-0.6
2008gp	1.031(061)	normal	21	11	-6.0
2008ha	...	lax	18	5	7.1
2008hj	0.946(061)	normal	HV	CN	16	11	-7.4
2008hu	1.413(067)	normal	HV	BL	17	8	...
2008hv	1.305(061)	normal	N	CN	24	18	-6.0
2008ia	1.297(063)	normal	N	BL	20	15	-2.0
2009D	0.905(062)	normal	N	CN	21	10	...
2009F	1.973(061)	91bg-like	91bg	CL	18	10	-5.0

Table 2
(Continued)

SN Name	$\Delta m_{15}(B)^a$ (mag)	Subtype ^b	Wang Subtype ^c	Branch Subtype ^d	N_{opt}^e	N_{IR}^f	t_{sp}^g (days)
2009I	0.796(115)	normal	N	CN	5	5	-3.3
2009J	...	Iax	7	4	...
2009P	0.796(091)	normal	HV	SS	15	7	1.8
2009Y	0.969(063)	normal	HV	BL	32	19	...
2009aa	1.212(061)	normal	N	CN	22	19	...
2009ab	1.279(061)	normal	N	CN	10	7	...
2009ad	0.961(061)	normal	N	SS	12	12	...
2009ag	1.046(066)	normal	N	BL	19	18	...
2009al	0.734(087)	normal	16	8	13.1
2009cz	0.762(065)	normal	N	CN	11	7	-5.1
2009dc	...	SC	N	SS	10	10	-8.5
2009ds	0.796(075)	normal	HV	SS	12	7	-9.9
2009le	1.023(036)	normal	N	BL	9	2	-4.7
2010ae	...	Iax	2	9	16.0

Notes.

^a Values of $\Delta m_{15}(B)$ were determined from the template fits. In parentheses are the 1σ uncertainties in units of 0.001 mag.

^b Type Ia subtypes from SNID (Blondin & Tonry 2007). Members of Type Iax and Ia+CSM subtypes are listed as “Iax” and “Ia+CSM,” respectively; super-Chandrasekhar candidates are denoted by “SC”; SN 2006bt-like objects are listed as “06bt-like.”

^c Wang et al. (2009) classification. N = normal; HV = high velocity; 91bg = SN 1991bg-like.

^d CN = core normal; CL = cool; SS = shallow silicon; BL = broad line (Branch et al. 2006).

^e Number of nights with optical photometry.

^f Number of nights with near-IR photometry.

^g Epoch of the spectrum, in days, with respect to $T(B_{\text{max}})$ used to determine spectral subtype. If no epoch is given, the spectral classification was taken from the literature.

1. *Primary standards.* We use this term to refer to Vega (α Lyr), the F subdwarf BD +17°4708, and the two CALSPEC (Bohlin et al. 2014) solar-analog standards P177D and P330E.
2. *Secondary standards.* We employed observations of Landolt (1992) and Smith et al. (2002) standard stars to provide the fundamental calibration of the CSP-I optical photometry. The Landolt and Smith et al. stars are considered “secondary standards” since they were calibrated with respect to the primary standards Vega and BD +17°4708, respectively. In the NIR, the CSP-I photometry is calibrated with respect to the Persson et al. (1998, hereafter P98) secondary standards, which are tied to Vega.
3. *Tertiary standards.* A “local sequence” of stars was established in each SN field in order to allow relative photometry of the SN to be measured. We refer to the local sequence stars as “tertiary standards” because they were calibrated via observations of secondary standards.

5.3. Supernova Photometry and Calibration

In order to measure photometry of the SNe accurately, the underlying host-galaxy light is first subtracted from each SN image using the host-galaxy reference images obtained after the SN has disappeared. The details of this procedure are discussed in Papers I and II. DAOPhot (Stetson 1987) is then used to measure counts in our CCD frames for both the SN and the local sequence of tertiary standards using point-spread-function (PSF) photometry. For each tertiary standard, i , we measure a

differential magnitude with respect to the SN,

$$\Delta m_{\text{SN},i} = -2.5 \log_{10} \left(\frac{e_{\text{SN}}^-}{e_i^-} \right), \quad (1)$$

where e_{SN}^- and e_i^- are the photoelectrons measured for the SN and tertiary standards, respectively. The uncertainty $\sigma(\Delta m_{\text{SN},i})$ is computed assuming Poisson statistics.

Once the tertiary standards have been calibrated to the natural system, the final magnitude of the SN can be computed as a weighted average,

$$m_{\text{SN}} = \frac{\sum_i (\Delta m_{\text{SN},i} + m_i) w_i}{\sum_i w_i}, \quad (2)$$

where m_i are the calibrated magnitudes of the tertiary standards and the weights w_i are the inverse variance

$$w_i = [\sigma^2(\Delta m_{\text{SN},i}) + \sigma^2(m_i)]^{-1}. \quad (3)$$

The uncertainty in the SN photometry is therefore

$$\sigma(m_{\text{SN}}) = \left[\sum_i (\sigma^2(\Delta m_{\text{SN},i}) + \sigma^2(m_i))^{-1} \right]^{-1/2}, \quad (4)$$

which contains a variance term for the statistical uncertainty from photon counts, as well as a systematic variance term that describes the uncertainty in each tertiary standard’s absolute flux. This procedure is applied for each SN field in each filter. The remainder of this section deals with the determination of the calibrated magnitudes of the tertiary standard stars, m_i .

Table 3
Supernova Light-curve Parameters

SN Name	$T_{\max}(B)^a$	$T_{\max}(\text{template})^b$	$\Delta m_{15}(B)^c$ (mag)	$\Delta m_{15}(\text{template})^d$ (mag)	s_{BV}^e	$s_{BV}(\text{template})^f$
2004dt	...	53,234.72 (0.73)	...	1.067 (0.081)	...	1.189 (0.061)
2004ef	53,263.77 (0.12)	53,264.38 (0.77)	1.353 (0.014)	1.371 (0.060)	0.846 (0.007)	0.816 (0.060)
2004eo	53,278.24 (0.08)	53,278.53 (0.60)	1.389 (0.010)	1.339 (0.060)	0.835 (0.010)	0.824 (0.060)
2004ey	53,303.73 (0.13)	53,304.18 (0.60)	0.954 (0.040)	0.950 (0.061)	1.088 (0.008)	1.010 (0.060)
2004gc	...	53,324.78 (0.98)	...	1.098 (0.084)	...	0.923 (0.064)
2004gs	53,355.93 (0.12)	53,356.41 (0.78)	1.628 (0.025)	1.587 (0.060)	0.730 (0.008)	0.702 (0.060)
2004gu	53,362.97 (1.05)	53,361.76 (0.66)	0.853 (0.091)	0.796 (0.067)	...	1.248 (0.061)
2005A	53,379.72 (0.85)	53,379.67 (0.88)	1.115 (0.111)	0.977 (0.072)	...	0.964 (0.061)
2005M	53,405.50 (0.19)	53,405.74 (0.60)	0.871 (0.021)	0.796 (0.061)	1.123 (0.011)	1.210 (0.060)
2005W	53,411.33 (0.25)	53,412.08 (0.60)	1.121 (0.034)	1.196 (0.061)	...	0.923 (0.061)
2005ag	53,414.24 (0.48)	53,413.43 (0.81)	0.980 (0.060)	0.917 (0.062)	1.022 (0.016)	1.184 (0.060)
2005al	53,430.10 (0.29)	53,430.42 (0.81)	1.193 (0.036)	1.302 (0.062)	0.918 (0.007)	0.860 (0.060)
2005am	53,436.50 (0.21)	53,437.14 (0.61)	1.524 (0.029)	1.491 (0.061)	0.794 (0.006)	0.730 (0.060)
2005be	...	53,461.17 (0.86)	...	1.418 (0.071)	...	0.760 (0.063)
2005bg	...	53,469.63 (0.91)	...	0.922 (0.075)	...	1.002 (0.066)
2005bl	53,481.95 (0.15)	53,482.60 (0.61)	...	2.000 (0.063)	...	0.387 (0.061)
2005bo	...	53,478.93 (0.61)	...	1.237 (0.069)	...	0.850 (0.060)
2005el	53,646.76 (0.39)	53,646.70 (0.78)	1.299 (0.064)	1.354 (0.061)	0.863 (0.006)	0.840 (0.060)
2005eq	53,655.34 (0.71)	53,654.52 (0.60)	0.835 (0.060)	0.796 (0.063)	1.165 (0.011)	1.125 (0.061)
2005gj
2005hc	53,666.53 (0.26)	53,667.16 (0.60)	0.848 (0.037)	0.834 (0.061)	1.117 (0.013)	1.193 (0.060)
2005hj	53,674.46 (0.91)	53,673.67 (0.64)	0.827 (0.097)	0.796 (0.078)	1.096 (0.016)	1.280 (0.062)
2005hk	53,684.62 (0.10)	...	1.610 (0.018)
2005iq	53,687.25 (0.08)	53,687.59 (0.60)	1.207 (0.014)	1.254 (0.061)	0.887 (0.015)	0.871 (0.060)
2005ir	53,685.14 (0.66)	53,684.58 (0.62)	0.883 (0.068)	0.796 (0.085)	...	1.121 (0.063)
2005kc	53,697.61 (0.16)	53,697.76 (0.60)	1.222 (0.027)	1.191 (0.063)	...	0.899 (0.060)
2005ke	53,698.54 (0.09)	53,698.97 (0.61)	1.764 (0.011)	1.736 (0.061)	0.384 (0.007)	0.419 (0.060)
2005ki	53,704.75 (0.14)	53,705.33 (0.61)	1.246 (0.019)	1.334 (0.061)	0.868 (0.007)	0.825 (0.060)
2005ku	...	53,699.05 (1.06)	...	0.990 (0.081)	...	0.950 (0.072)
2005lu	...	53,711.55 (0.90)	...	0.796 (0.098)	...	1.130 (0.069)
2005mc	...	53,734.37 (0.88)	...	1.528 (0.104)	...	0.640 (0.065)
2005na	53,739.85 (0.57)	53,740.27 (0.62)	0.980 (0.065)	1.033 (0.063)	1.029 (0.009)	0.957 (0.060)
2006D	53,757.35 (0.14)	53,757.54 (0.61)	1.414 (0.025)	1.364 (0.060)	0.830 (0.010)	0.815 (0.060)
2006X	...	53,786.39 (0.60)	...	1.095 (0.066)	...	0.968 (0.060)
2006ax	53,827.11 (0.25)	53,827.11 (0.77)	1.038 (0.036)	0.976 (0.061)	1.020 (0.011)	0.987 (0.060)
2006bd	...	53,824.47 (0.62)	...	2.256 (0.105)	...	0.377 (0.061)
2006bh	53,833.31 (0.10)	53,833.46 (0.77)	1.426 (0.015)	1.410 (0.060)	0.848 (0.008)	0.802 (0.060)
2006br	...	53,850.65 (0.99)	...	0.886 (0.094)	...	0.908 (0.067)
2006bt
2006dd
2006ef	...	53,969.24 (0.95)	...	1.406 (0.077)	...	0.837 (0.063)
2006ej	...	53,975.97 (0.64)	...	1.367 (0.070)	...	0.829 (0.063)
2006eq	...	53,979.13 (0.60)	...	1.448 (0.081)	...	0.624 (0.064)
2006et	53,993.16 (0.17)	53,993.84 (0.61)	0.881 (0.018)	0.837 (0.061)	1.145 (0.010)	1.093 (0.060)
2006ev	...	53,989.68 (0.64)	...	1.326 (0.073)	...	0.845 (0.063)
2006fw	...	54,003.57 (0.90)	...	1.132 (0.198)	...	0.888 (0.078)
2006gj	54,000.03 (0.19)	54,000.40 (0.62)	1.679 (0.081)	1.555 (0.064)	0.771 (0.016)	0.656 (0.060)
2006gt	54,003.01 (0.21)	54,003.55 (0.81)	1.886 (0.074)	1.641 (0.064)	0.637 (0.012)	0.562 (0.061)
2006hb	...	54,003.02 (0.81)	...	1.460 (0.071)	...	0.673 (0.063)
2006hx	54,023.85 (0.72)	54,021.74 (0.62)	1.187 (0.071)	0.987 (0.074)	...	0.993 (0.063)
2006is	...	54,005.17 (0.98)	...	0.796 (0.078)	...	1.327 (0.065)
2006kf	54,041.03 (0.16)	54,041.31 (0.60)	1.581 (0.029)	1.503 (0.062)	0.734 (0.011)	0.735 (0.060)
2006lu	...	54,034.38 (0.65)	...	0.938 (0.074)	...	1.050 (0.064)
2006mr	54,050.54 (0.06)	54,050.77 (0.62)	1.817 (0.022)	1.929 (0.079)	0.301 (0.012)	0.239 (0.060)
2006ob	54,062.95 (0.20)	54,063.52 (0.85)	1.558 (0.031)	1.467 (0.072)	...	0.720 (0.061)
2006os	...	54,064.66 (0.93)	...	1.172 (0.112)	...	0.913 (0.065)
2006ot
2006py	...	54,070.87 (0.66)	...	1.177 (0.107)	...	0.950 (0.065)
2007A	54,113.37 (0.60)	54,112.96 (0.60)	0.971 (0.074)	0.853 (0.071)	...	1.012 (0.061)
2007N	54,123.46 (0.24)	54,123.53 (0.83)	1.752 (0.064)	2.121 (0.083)	0.328 (0.014)	0.312 (0.061)
2007S	54,143.55 (0.86)	54,144.36 (0.60)	0.833 (0.089)	0.795 (0.064)	1.138 (0.011)	1.115 (0.061)
2007af	54,174.07 (0.24)	54,174.40 (0.60)	1.183 (0.037)	1.193 (0.061)	0.937 (0.008)	0.926 (0.060)
2007ai	...	54,173.03 (0.64)	...	0.796 (0.119)	1.188 (0.016)	1.229 (0.061)

Table 3
(Continued)

SN Name	$T_{\max}(B)^a$	$T_{\max}(\text{template})^b$	$\Delta m_{15}(B)^c$ (mag)	$\Delta m_{15}(\text{template})^d$ (mag)	s_{BV}^e	$s_{BV}(\text{template})^f$
2007al	...	54,170.26 (0.83)	...	1.782 (0.082)	0.366 (0.012)	0.336 (0.064)
2007as	...	54,181.60 (0.62)	...	1.120 (0.076)	0.913 (0.011)	0.886 (0.060)
2007ax	54,187.75 (0.11)	54,187.94 (0.62)	1.868 (0.055)	2.036 (0.066)	0.336 (0.012)	0.355 (0.061)
2007ba	54,196.65 (0.13)	54,197.57 (0.61)	1.827 (0.029)	1.668 (0.062)	0.608 (0.014)	0.546 (0.060)
2007bc	54,200.03 (0.19)	54,200.22 (0.62)	1.350 (0.117)	1.331 (0.061)	...	0.876 (0.060)
2007bd	54,206.27 (0.37)	54,206.80 (0.61)	1.165 (0.036)	1.241 (0.063)	0.914 (0.013)	0.880 (0.060)
2007bm	...	54,224.62 (0.64)	...	1.157 (0.064)	0.879 (0.014)	0.900 (0.061)
2007ca	54,226.95 (0.25)	54,227.38 (0.60)	0.882 (0.025)	0.853 (0.062)	...	1.061 (0.060)
2007cg	...	54,227.35 (0.78)	...	0.811 (0.052)	...	1.103 (0.077)
2007hj	54,349.49 (0.14)	54,349.86 (0.61)	1.763 (0.020)	1.630 (0.062)	0.678 (0.010)	0.603 (0.060)
2007hx	...	54,353.65 (1.06)	...	0.905 (0.057)	...	1.053 (0.074)
2007if	54,415.41 (2.71)	...	0.278 (0.127)
2007jd	...	54,361.79 (1.20)	...	1.330 (0.091)	...	0.877 (0.069)
2007jg	54,366.31 (0.32)	54,366.34 (0.61)	1.221 (0.042)	1.242 (0.066)	0.897 (0.015)	0.925 (0.060)
2007jh	54,365.38 (0.65)	54,366.33 (0.63)	1.723 (0.175)	1.700 (0.069)	...	0.584 (0.063)
2007le	54,398.40 (0.36)	54,399.07 (0.61)	0.953 (0.038)	0.931 (0.061)	1.021 (0.038)	1.028 (0.060)
2007mm	54,392.19 (0.47)	54,392.26 (0.62)	1.993 (0.098)	2.098 (0.090)	...	0.501 (0.063)
2007nq	54,398.37 (0.55)	54,398.90 (0.62)	1.487 (0.081)	1.507 (0.064)	0.843 (0.013)	0.750 (0.060)
2007ol	...	54,412.86 (0.63)	...	1.357 (0.140)	...	0.696 (0.069)
2007on	54,420.16 (0.09)	54,419.79 (0.78)	1.989 (0.036)	1.648 (0.061)	0.416 (0.008)	0.570 (0.060)
2007so	...	54,427.93 (0.83)	...	1.071 (0.129)	...	0.853 (0.061)
2007 sr	...	54,448.51 (0.80)	...	0.978 (0.073)	...	0.988 (0.062)
2007st	...	54,455.39 (0.91)	...	1.638 (0.077)	...	0.742 (0.064)
2007ux	...	54,466.85 (0.61)	...	1.660 (0.062)	...	0.600 (0.060)
2008C	...	54,465.86 (0.71)	...	1.192 (0.106)	...	0.953 (0.065)
2008J	...	54,494.53 (0.86)	1.761 (0.088)
2008O	54,490.92 (0.38)	54,491.71 (0.84)	1.646 (0.063)	1.655 (0.062)	0.559 (0.016)	0.656 (0.061)
2008R	54,494.34 (0.09)	54,494.65 (0.79)	1.822 (0.020)	1.600 (0.073)	0.623 (0.010)	0.591 (0.060)
2008ae	54,508.63 (0.60)	...	1.648 (0.078)
2008ar	...	54,534.61 (0.61)	...	1.001 (0.061)	...	0.970 (0.060)
2008bc	54,548.83 (0.17)	54,549.58 (0.60)	0.843 (0.019)	0.873 (0.060)	1.052 (0.009)	1.048 (0.060)
2008bd	...	54,531.21 (0.77)	...	1.929 (0.104)	...	0.415 (0.061)
2008bf	54,554.46 (0.22)	54,554.64 (0.60)	0.954 (0.026)	0.905 (0.060)	1.058 (0.012)	1.024 (0.060)
2008bi	...	54,543.16 (1.11)	...	2.092 (0.094)	...	0.485 (0.066)
2008bq	...	54,562.46 (0.80)	...	0.895 (0.062)	1.056 (0.014)	1.157 (0.061)
2008bt	54,571.98 (0.20)	54,572.30 (0.62)	1.878 (0.026)	1.743 (0.063)	0.525 (0.014)	0.470(0.061)
2008bz	...	54,578.99 (0.65)	...	0.984 (0.095)	...	0.927 (0.064)
2008cc	...	54,573.02 (0.63)	...	1.380 (0.073)	...	0.789 (0.062)
2008cd	...	54,578.89 (1.24)	...	1.071 (0.158)	...	1.012 (0.100)
2008cf	...	54,594.53 (0.92)	...	0.796 (0.084)	...	1.121 (0.070)
2008ff	...	54,704.21 (0.63)	...	0.903 (0.062)	...	1.132 (0.061)
2008fl	...	54,720.79 (0.86)	...	1.354 (0.071)	...	0.856 (0.063)
2008fp	54,729.53 (0.29)	54,730.26 (0.60)	0.811 (0.035)	0.756 (0.061)	1.057 (0.005)	1.077 (0.060)
2008fr	...	54,732.80 (0.65)	...	0.933 (0.074)	...	1.059 (0.064)
2008fu	...	54,732.47 (0.72)	...	1.620 (0.140)	...	0.822 (0.064)
2008fw	...	54,731.72 (0.62)	...	0.794 (0.072)	...	1.114 (0.064)
2008gg	...	54,749.21 (0.85)	...	0.796 (0.077)	...	1.112 (0.066)
2008gl	54,767.75 (0.18)	54,768.16 (0.60)	1.268 (0.033)	1.320 (0.062)	0.823 (0.012)	0.850 (0.060)
2008go	...	54,766.09 (0.63)	...	1.105 (0.136)	...	0.912 (0.064)
2008gp	54,778.82 (0.24)	54,778.99 (0.60)	1.024 (0.031)	1.031 (0.061)	1.014 (0.013)	0.973 (0.060)
2008 ha	54,781.89 (0.37)	...	1.969 (0.049)
2008hj	54,800.83 (0.14)	54,801.50 (0.78)	0.869 (0.025)	0.946 (0.061)	1.005 (0.013)	1.011 (0.060)
2008hu	...	54,806.56 (0.62)	...	1.413 (0.067)	...	0.786 (0.060)
2008hv	54,816.50 (0.27)	54,817.06 (0.61)	1.217 (0.035)	1.305 (0.061)	0.876 (0.006)	0.846 (0.060)
2008ia	54,812.42 (0.21)	54,813.00 (0.61)	1.236 (0.036)	1.297 (0.063)	0.905 (0.015)	0.843 (0.060)
2009D	54,840.88 (0.21)	54,840.80 (0.78)	0.987 (0.025)	0.905 (0.062)	...	1.185 (0.060)
2009F	54,841.87 (0.11)	54,842.03 (0.81)	1.934 (0.019)	1.973 (0.061)	...	0.325 (0.061)
2009I	...	54,851.90 (0.61)	...	0.796 (0.115)	...	1.064 (0.063)
2009J
2009P	...	54,868.40 (0.66)	...	0.796 (0.091)	...	1.093 (0.067)
2009Y	54,875.37 (0.20)	54,876.08 (0.60)	0.980 (0.027)	0.969 (0.063)	0.956 (0.006)	1.189 (0.061)
2009aa	54,877.86 (0.59)	54,878.23 (0.60)	1.206 (0.073)	1.212 (0.061)	0.950 (0.014)	0.906 (0.060)
2009ab	54,882.94 (0.19)	54,883.26 (0.60)	1.237 (0.030)	1.279 (0.061)	...	0.874 (0.060)

Table 3
(Continued)

SN Name	$T_{\max}(B)^a$	$T_{\max}(\text{template})^b$	$\Delta m_{15}(B)^c$ (mag)	$\Delta m_{15}(\text{template})^d$ (mag)	s_{BV}^e	$s_{BV}(\text{template})^f$
2009ad	54,885.59 (0.16)	54,886.27 (0.60)	0.913 (0.026)	0.961 (0.061)	...	1.015 (0.060)
2009ag	54,888.85 (0.93)	54,889.55 (0.61)	1.093 (0.109)	1.046 (0.066)	0.982 (0.007)	0.961 (0.060)
2009al	...	54,893.53 (0.98)	...	0.734 (0.087)	...	1.174 (0.072)
2009cz	54,942.31 (0.18)	54,943.14 (0.60)	0.825 (0.025)	0.762 (0.065)	...	1.189 (0.061)
2009dc	54,946.87 (0.49)	...	0.785 (0.042)
2009ds	54,960.03 (0.16)	54,961.04 (0.81)	0.720 (0.023)	0.796 (0.075)	...	1.125 (0.063)
2009le	...	55,165.94 (0.61)	...	1.023 (0.036)	...	1.156 (0.064)
2010ae

Notes.^a Modified Julian date of B -band maximum, as derived from B -band data only.^b Modified Julian date of maximum light, as derived from data in all filters.^c As derived from the B -band data only, the number of B -band magnitudes the SN faded in the first 15 days since the time of B -band maximum.^d Assigned B -band decline rate (mag in 15 days), as derived using B -band templates. For SN 2007cg, SN 2007hx, SN 2008cd, and SN 2009le, the decline rate is derived from data in all filters.^e Stretch BV from data. See text for details.^f Stretch BV from templates. See text for details.

5.4. Tertiary Standard Calibration

In the natural system, the calibrated magnitudes of the tertiary standards are determined relative to the natural magnitudes of secondary standards observed on photometric nights. For a set of photometric nights (j), on which a set of secondary standards (k) is measured, the estimate of the magnitude of the tertiary standard (i) in a particular filter (λ) is

$$m_{i,\lambda} = \frac{\sum_{j,k} (m'_{\text{nat},k,\lambda} + \Delta m_{i,j,k,\lambda} - k_{\lambda}(X_{i,j,\lambda} - X_{j,k,\lambda})) w_{j,k,\lambda}}{\sum_{j,k} w_{j,k,\lambda}}, \quad (5)$$

where $m'_{\text{nat},k,\lambda}$ is the natural-system magnitude of the secondary standard k , $\Delta m_{i,j,k,\lambda}$ is the differential magnitude (see Equation (1)) between the tertiary standard i and the secondary standard k on night j , $X_{i,j,\lambda}$ and $X_{j,k,\lambda}$ are the respective airmasses of the tertiary and secondary standards, and k_{λ} is the extinction coefficient. The weights ($w_{j,k,\lambda}$) are the inverse variances

$$w_{j,k,\lambda} = [\sigma^2(\Delta m_{i,j,k,\lambda}) + \sigma^2(m'_{\text{nat},k,\lambda})]^{-1}, \quad (6)$$

where $\sigma(\Delta m_{i,j,k,\lambda})$ is calculated assuming Poisson errors and $\sigma(m'_{\text{nat},k,\lambda})$ is taken from the published standard photometry. The uncertainty, $\sigma(m_{i,\lambda})$, is analogous to Equation (4):

$$\sigma(m_{i,\lambda}) = \left[\sum_i (\sigma^2(\Delta m_{i,j,k,\lambda}) + \sigma^2(m'_{\text{nat},k,\lambda}))^{-1} \right]^{-1/2}. \quad (7)$$

Note that because this is a natural system, there is no color term in Equation (5) and hence no dependence on the color of the tertiary standards. The differential magnitudes, $\Delta m_{i,j,k,\lambda}$, are measured using aperture photometry, as this was found to be more robust for the secondary standard stars, which tend to be significantly brighter than the tertiary standards. In the optical we used an aperture of $7''$, while for the NIR we used an aperture of $5''$. A sky annulus of inner radius $9''$ and $2''$ width was used to estimate the sky level for both the optical and NIR.

The final ingredients are the natural-system magnitudes for the secondary standards, $m'_{\text{nat},\lambda}$. As discussed in Section 5.1,

color terms are used to transform the standard magnitudes of these stars into the natural-system magnitudes that would be measured through our telescopes. The form of these transformations is assumed to be linear with color,

$$m'_{\text{nat},\lambda} = m'_{\lambda} - \epsilon_{\lambda} \times C'_{\lambda}, \quad (8)$$

where ϵ_{λ} is the color term and C'_{λ} is the associated color based on the standard magnitudes. As an example, for $\lambda = B$, we choose $C'_{\lambda} = (B - V)$. It is important to emphasize that because these color terms are only ever used to compute $m'_{\text{nat},\lambda}$, it is the range of colors of the secondary standards used for calibration that determines their relative importance. In other words, we are forcing the zero-point of the natural system and standard system to be the same at zero color.

Technically, each telescope/instrument used by the CSP-I will have its own color terms and hence its own set of natural magnitudes for the secondary standards. In the next section, we describe each of these in detail.

6. Photometric Reductions: Details

Our natural system is defined by Equation (8). If all published secondary standards had zero color, then the definition of the natural system would be trivial. However, the published standard stars have a range of colors. To use all the published standards to define the natural system, we must calculate color terms, as given in Equation (8), which transform the published standard system into a table of the same stars with natural-system photometry.

If something goes wrong with the photometric system and the transmission functions change, then the color terms in Equation (8) will change. However, for program objects that are stars, the natural system will remain well defined because stars were used to define the standard to natural systems.

This is not true for SNe because they have different SEDs. Thus, an important sanity check on our reductions is to see whether the color terms vary over time. Provided that the transmission functions do not change, the color terms should never change. However, we must keep track of any variations of the color terms to verify that the natural system is stable.

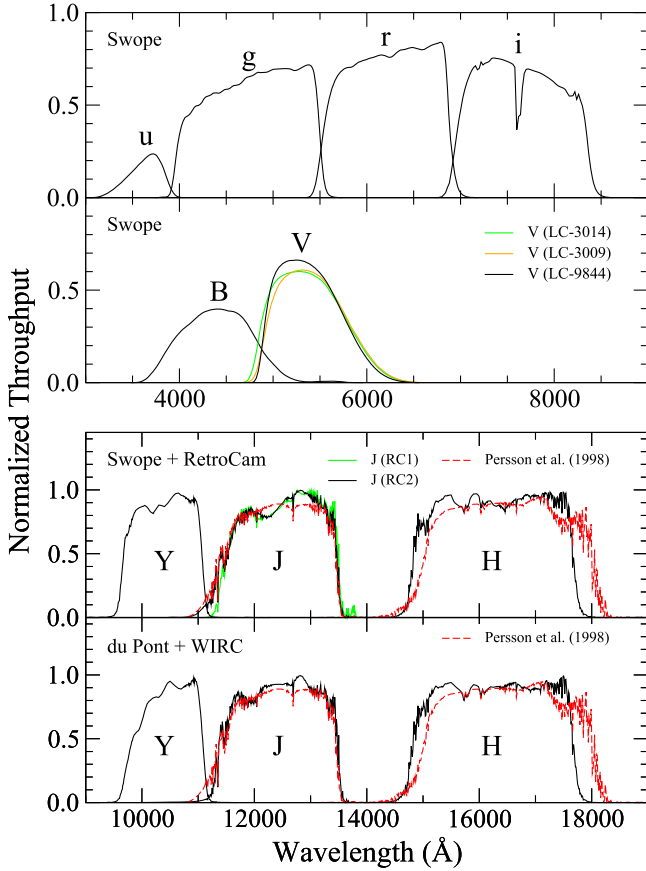


Figure 3. CSP-I optical and NIR filter response functions. The optical bandpasses shown in the upper portion of the figure were measured using a monochromator, as described in Paper II, and have then been multiplied by an atmospheric absorption and extinction spectrum typical of LCO for an airmass of 1.2. The NIR bandpasses shown in the lower half of the figure were determined with the same monochromator (see Appendix A for details) and also include atmospheric absorption appropriate for LCO. Note that three different V filters were used with the Swope telescope+SITe2 CCD camera during the course of the CSP-I (see Section 6.1.1 for details), and two J filters were utilized at the Swope with RetroCam (see Section 6.2.1). The dashed red lines show the response functions for the J and H filters employed by P98. These were derived by combining the filter transmission and detector quantum efficiency data given by these authors with two aluminum reflections and an atmospheric transmission function appropriate to LCO.

6.1. Optical Photometry

6.1.1. Swope+SITe3

We define the transformation of the instrumental $ugribv$ magnitudes into the natural system through the following equations:

$$u_{\text{nat}} = u' - \epsilon_u \times (u' - g'), \quad (9)$$

$$g_{\text{nat}} = g' - \epsilon_g \times (g' - r'), \quad (10)$$

$$r_{\text{nat}} = r' - \epsilon_r \times (r' - i'), \quad (11)$$

$$i_{\text{nat}} = i' - \epsilon_i \times (r' - i'), \quad (12)$$

$$B_{\text{nat}} = B - \epsilon_b \times (B - V), \quad \text{and} \quad (13)$$

$$V_{\text{nat}} = V - \epsilon_v \times (V - i'), \quad (14)$$

where $u'g'r'i'BV$ correspond to magnitudes in the standard system. The color terms (ϵ_λ) are measured in the manner described below. The magnitudes of the secondary photometric standards of Landolt (1992) and Smith et al. (2002) are thus used to calculate new magnitudes of these stars in the natural

photometric system of the Swope telescope using the above equations.

On photometric nights, we can solve for these color terms based on observations of the secondary standards. To do this, we fit the instrumental magnitudes with the following equations:

$$u = u' + k_u X - \epsilon_u \times (u' - g') - \zeta_u, \quad (15)$$

$$g = g' + k_g X - \epsilon_g \times (g' - r') - \zeta_g, \quad (16)$$

$$r = r' + k_r X - \epsilon_r \times (r' - i') - \zeta_r, \quad (17)$$

$$i = i' + k_i X - \epsilon_i \times (r' - i') - \zeta_i, \quad (18)$$

$$b = B + k_b X - \epsilon_b \times (B - V) - \zeta_b, \quad \text{and} \quad (19)$$

$$v = V + k_v X - \epsilon_v \times (V - i') - \zeta_v. \quad (20)$$

Note that these equations differ slightly from those defined in Equations (1)–(6) of Hamuy et al. (2006) in that the colors on the right-hand side of the equations are in the standard system and not the instrumental system.

The calibration strategy adopted by the CSP-I for the optical imaging obtained with the Swope telescope was to observe a minimum of eight secondary standard stars over a range of airmass during one photometric night every week. During the course of the CSP-I, different team members would use IRAF¹⁹ tools and procedures to fit these observations to Equations (15)–(20) to obtain the nightly extinction coefficients, color terms, and zero-points for each band. For this final data release, we have redone the nightly measurements of the extinction coefficients, color terms, and zero-points in a uniform manner using a more sophisticated, noninteractive method that accounts for outliers and provides more realistic error bars. In detail, we used a Mixture Model Markov Chain Monte Carlo (MCMC) fitting procedure (as in Hogg et al. 2010), which includes a photometric model, a Gaussian model for the outliers, an extra variance term, and a q parameter accounting for the fraction of the data points that fit the photometric model. The MCMC modeling is specified as follows:

$$f_1(k_\lambda, \epsilon_\lambda, \zeta_\lambda) = m'_\lambda + k_\lambda X - \epsilon_\lambda \times C'_\lambda - \zeta_\lambda \quad (21)$$

is the photometric model for the observed instrumental magnitudes, and

$$f_2(\mu, \sigma) = N(\mu, \sigma) \quad (22)$$

is the Gaussian normal distribution model for outliers. The seven-parameter likelihood function, $\mathcal{L}(k_\lambda, \epsilon_\lambda, \zeta_\lambda, \sigma_e^2, q, \mu, \sigma)$, is then expressed as

$$\mathcal{L} = \prod_{i=1}^N \left[q \frac{\exp(-0.5(f_1 - m_i)^2 / (\sigma_i^2 + \sigma_{\text{extra}}^2))}{\sqrt{2\pi(\sigma_i^2 + \sigma_{\text{extra}}^2)}} + (1 - q) \frac{\exp(-0.5(f_2 - m_i)^2 / (\sigma_i^2 + \sigma^2))}{\sqrt{2\pi(\sigma_i^2 + \sigma^2)}} \right], \quad (23)$$

where N is the number of standard-star observations in one photometric night in one filter.

In this model, m_i and σ_i correspond to instrumental magnitude and error bars; k_λ , ϵ_λ , and ζ_λ are the nightly extinction

¹⁹ IRAF is distributed by the National Optical Astronomy Observatory, which is operated by the Association of Universities for Research in Astronomy Inc. under cooperative agreement with the NSF.

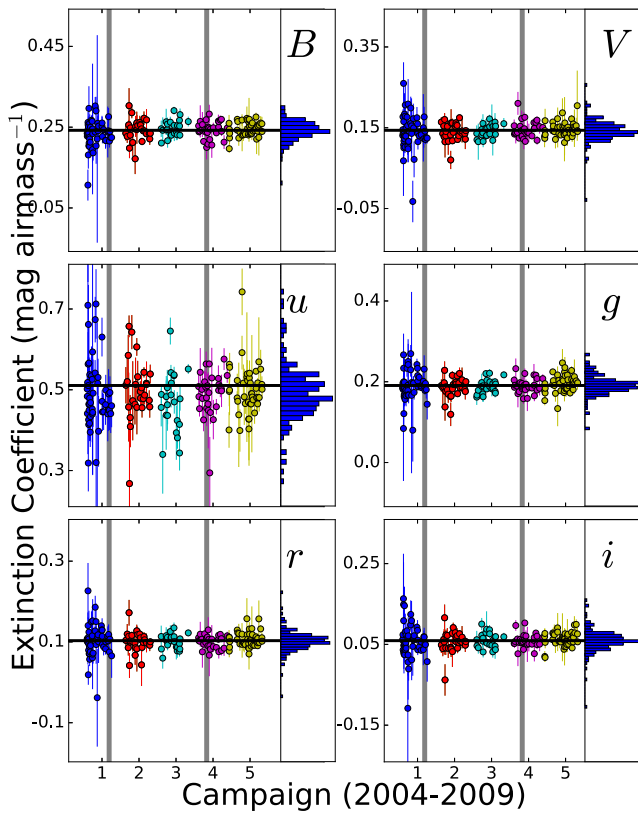


Figure 4. Optical broadband atmospheric extinction values (mag airmass^{-1}) measured at LCO from 2004 September through 2009 November. Histograms for the entire 5 yr are shown at the right of each panel.

coefficients, color terms, and zero-points (respectively) for filter λ ; C'_λ is the color associated with the color term; and σ is the standard deviation of the Gaussian error distribution (for outliers) centered on μ . The extra variance, σ_{extra}^2 , is an additional error term added to every single measurement. This is necessary because a single bright secondary standard star typically has an uncertainty due to photon statistics of only a few millimagnitudes, while the zero-point dispersion for a good night is no better than 0.01 mag. Finally, q represents the fraction of the data that fits the photometric model, while $1 - q$ is the fraction that can be considered as outliers. A handful of nights with values of $q < 0.8$ in different filters was discarded as likely to have been nonphotometric.

Figure 4 displays nightly values of the atmospheric extinction coefficients in $ugriBV$ for the Swope+SITe3 camera derived with this MCMC model over the five CSP-I campaigns. Histograms of the collected extinction-coefficient measurements are shown on the right side of each panel. Figure 5 shows a similar plot of the color terms over the five campaigns. In neither of these figures is there evidence for significant secular changes in the extinction coefficients or color terms.

The nightly photometric zero-points for the Swope+SITe3 camera are shown in Figure 6. The obvious zigzag pattern arises from the accumulation of dust and aerosols between the two washings of the primary mirror (marked by the red arrows) that occurred during the CSP-I observing campaigns. Smaller dips in sensitivity are observed around 2006 mid-February (JD 2,453,780) and 2008 mid-March (JD 2,454,540). Similar dips are visible during the summer months in the zero-points measured by Burki et al. (1995) between 1975 November and 1994 August at the neighboring La Silla Observatory, and we

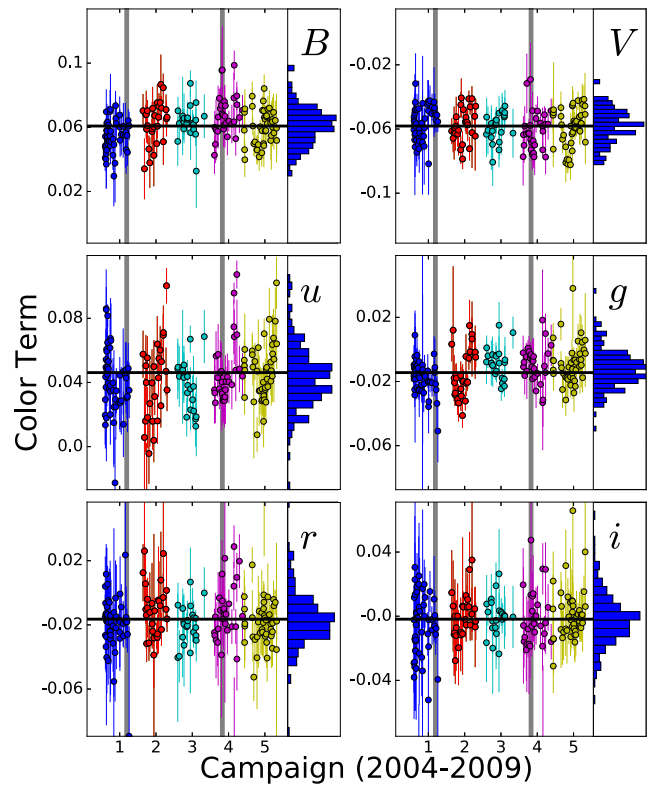


Figure 5. Optical broadband color terms from LCO 1 m photometry. Histograms for the entire 5 yr are shown on the right side of each panel.

speculate that these are associated with an increase in atmospheric haze that occurs due to the inversion layer being generally higher at that time of the year. Interestingly, these dips do not appear to be accompanied by significant changes in the extinction coefficients and color terms.

The demonstrated stability of the nightly extinction coefficients and color terms over all five CSP-I campaigns justifies adopting average color terms and extinction coefficients for the final photometric reductions. This reduces the problem to solving for nightly zero-points only. In this way, just a handful of secondary standard star observations is needed to calibrate the natural photometry for the local sequence of tertiary standards observed during the same night. The final mean extinction coefficients and color terms adopted for the five CSP-I campaigns are given in Table 4. Using these mean color terms, natural-system magnitudes for the Smith et al. (2002) and Landolt (1992) secondary standards were calculated via Equations (9)–(14). These, in turn, were used to derive magnitudes in the natural system of the local sequences of tertiary standards in each of the SN fields.

Final $u'g'r'i'BV$ magnitudes of the local sequences of tertiary standards for all 134 SNe are listed in Table 5. Note that these are given in the *standard* system (i.e., as calculated using Equations (9)–(14)) in order to facilitate their usage by others. In all cases, these magnitudes are based on observations made on at least three different photometric nights, and the accompanying uncertainties are weighted averages of the errors computed from these multiple measurements.²⁰

As discussed in Paper II, on 2006 January 14 (unless otherwise noted, UT dates are used throughout this paper;

²⁰ In this paper, in the tables of field-star magnitudes or SN photometry, any entry given as “0.000(000)” indicates missing data.

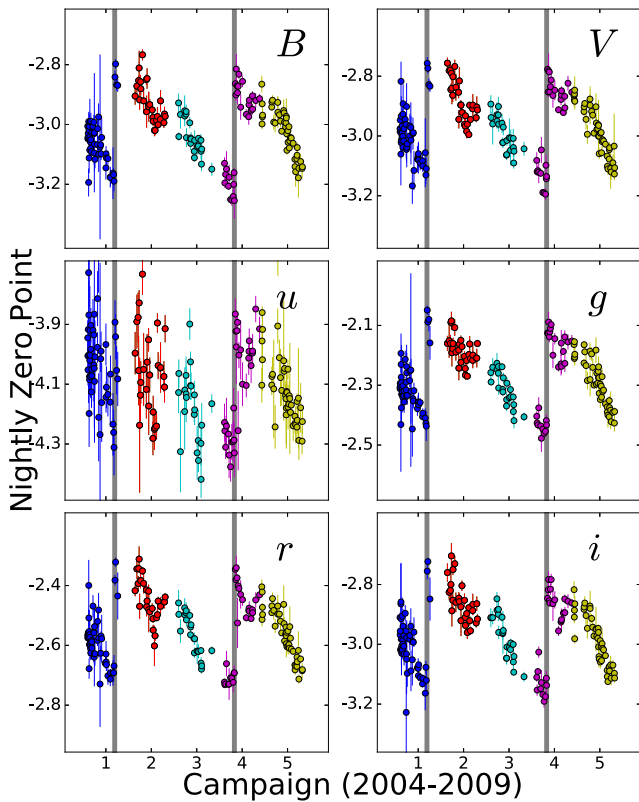


Figure 6. Nightly photometric zero-points derived from observations of secondary standard stars with the LCO Swope telescope+SITe3 camera over the course of CSP-I. The vertical gray lines indicate dates on which the primary mirror was washed.

JD 2,453,749) the original V filter (“LC-3014”) used at the Swope telescope was broken and subsequently replaced by another V filter (“LC-3009”). However, after a few nights of use, it was determined that the replacement filter had a significantly different color term compared to the original. This filter was replaced on 2006 January 25 (JD 2,453,760) with a third filter (“LC-9844”), which was used for the remainder of the CSP-I campaigns. Although the bandpass of the LC-9844 filter is slightly broader than that of the LC-3014 filter (see Figure 3), observations at the telescope, as well as synthetic photometry, showed the color terms to be the same to within ~ 0.002 . Hence, we adopted the same natural magnitudes of the local sequences of tertiary standards for observations made in both of these filters. However, the color term of the LC-3009 filter was sufficiently different that we have treated separately the reduction of the smaller number of observations obtained with this filter. Table 4 gives the mean color term for V -band transformations for the LC-3014 and LC-9844 filters, whose value is -0.058 . For the small amount of V -band photometry obtained with the LC-3009 filter, we assume the color term of -0.044 derived in Paper II.

6.1.2. du Pont+Tek5

As already mentioned, owing to its larger aperture and better delivered image quality, the 2.5 m du Pont telescope was used during the CSP-I to obtain host-galaxy reference images in $ugriBV$ using the facility Tek5 CCD camera. A small amount of SN follow-up imaging was also obtained with this telescope/instrument combination. Unfortunately, precise measurements of the filter response functions with the Tek5 camera were not

Table 4
Photometric Reduction Terms

Filter	Extinction Coefficient ^a	Color Term ^b
Swope+SITe3		
u	0.511 ± 0.057	0.046 ± 0.017
B	0.242 ± 0.022	0.061 ± 0.012
g	0.191 ± 0.021	-0.014 ± 0.011
V	0.144 ± 0.018	-0.058 ± 0.011
r	0.103 ± 0.019	-0.016 ± 0.015
i	0.059 ± 0.020	-0.002 ± 0.015
Swope+RetroCam		
Y	0.044 ± 0.012	...
J	0.076 ± 0.015	0.016^c
H	0.041 ± 0.013	-0.029^c
du Pont+WIRC		
Y	0.044 ± 0.012	-0.042^c
J	0.076 ± 0.015	0.016^c
H	0.041 ± 0.013	-0.029^c

Notes.

^a Measured in mag airmass^{-1} . All uncertainties in this table are the “standard deviations of the distributions,” not the standard deviations of the means.

^b See Equations (9)–(14) or Equations (15)–(20), for which standard colors are used in combination with these coefficients to obtain the color correction terms for the optical photometry. V -band photometry obtained with the LC-3009 filter and given in Table 9 is associated with a color term of -0.044 . See Appendix B of Paper II. As described in the text, color terms are not needed to transform the J and H magnitudes between the Swope+Retrocam and du Pont+WIRC natural systems.

^c Color terms estimated from synthetic photometry of Castelli & Kurucz (2003) stellar atmosphere models.

carried out, and this camera has since been decommissioned. Nevertheless, it is possible to estimate the color terms of this system using the local sequences of tertiary standards (established with the Swope+SITe3 camera) in the fields of the SNe observed with the du Pont+Tek5 camera.

To carry out this experiment, we chose two objects, SN 2007ab and SN 2008O, that were observed in both the Swope+SITe3 and du Pont+Tek5 systems. Both SNe are at relatively low Galactic latitudes with many foreground stars in their fields. Natural-system magnitudes in the $ugriBV$ bandpasses were measured for the 100 brightest stars in each field using all of the Swope+SITe3 images calibrated by the respective local sequence of tertiary standards. The range in $(B - V)$ colors covered by these stars was $+0.2$ to $+1.5$ mag for SN 2007ab and $+0.4$ to $+1.2$ mag for SN 2008O.

SN 2007ab was observed on one night with the du Pont+Tek5 camera, and SN 2008O on four nights. Instrumental magnitudes were measured for the same 100 field stars in each of the images taken on these nights, and differences (Δm) were calculated with respect to the Swope+SITe3 natural-system magnitudes:

$$\Delta m = m(\text{Swope SITe3})_{\text{nat}} - m(\text{du Pont Tek5})_{\text{ins}}. \quad (24)$$

If the response functions for a given filter are identical between the Swope SITe3 and du Pont Tek5 cameras, we would expect Δm to be a constant. On the other hand, if the response functions are significantly different, we would expect to detect a relative color term as well. We therefore analyzed the

Table 5
Optical Photometry of Secondary Standards^a

ID	α (2000)	δ (2000)	u'	g'	r'	i'	B	V
SN 2004dt								
1	02:02:09.95	−00:08:43.8	17.479(008)	15.477(003)	14.652(004)	14.266(004)	16.053(003)	15.100(003)
2	02:02:05.30	−00:02:03.4	16.387(007)	15.385(003)	15.185(003)	15.136(003)	15.634(003)	15.270(003)
3	02:02:04.23	−00:02:31.3	18.567(012)	16.128(002)	15.068(003)	14.621(003)	16.784(003)	15.667(003)
4	02:02:24.14	−00:08:31.2	0.000(000)	18.819(008)	17.522(005)	16.678(004)	19.291(016)	18.245(008)
5	02:02:16.90	−00:02:52.3	0.000(000)	19.484(014)	18.166(007)	16.986(005)	20.264(038)	18.929(014)
6	02:02:10.06	−00:06:50.4	18.874(014)	16.786(003)	16.021(003)	15.778(003)	17.341(004)	16.429(003)
7	02:02:08.30	−00:03:30.2	20.142(043)	19.317(012)	18.884(013)	18.723(019)	19.599(021)	19.089(016)
8	02:02:01.59	−00:05:58.1	0.000(000)	20.053(024)	18.675(011)	17.617(007)	20.637(063)	19.389(020)
9	02:02:21.58	−00:05:50.8	0.000(000)	20.275(029)	18.906(013)	18.019(010)	20.690(091)	19.636(028)
10	02:02:14.61	−00:07:56.9	0.000(000)	20.180(027)	19.110(016)	18.599(016)	20.524(081)	19.755(029)

Note.

^a All photometry is measured in magnitudes. Values in parentheses are 1σ uncertainties. This photometry of field stars is in the two standard systems, not the natural system.

(This table is available in its entirety in machine-readable form.)

observations by fitting the model

$$\Delta m_\lambda = \epsilon_\lambda \times C_\lambda + \zeta_\lambda, \quad (25)$$

Here the color C_λ is in the natural system and depends on the filters as per Equations (15)–(20). For example, $\Delta B = \epsilon_b (B - V) + \zeta_b$ for the B band.

For the $griBV$ filters, we find that the color term is within 1σ – 2σ of zero. The color term for the u filter is also consistent with zero to $\sim 2\sigma$, but these results are of lower confidence since this filter was utilized only one night for each SN.

Based on these results, it is justified to assume that the SN photometry obtained in the $griBV$ filters with the du Pont+Tek5 camera is on the same natural system as the Swope+SITe3 camera. It also seems likely that any difference between the u bandpasses is small. We have therefore opted to calibrate the SN photometry obtained with the du Pont+Tek5 camera using the natural-system tertiary standard star magnitudes, mean extinction coefficients, and mean color terms measured with the Swope+SITe3 camera.

6.2. NIR Photometry

6.2.1. Swope+RetroCam

The Swope+RetroCam YJH bandpasses are shown in Figure 3. On the night of 2008 December 8 (JD 2,454,808), the observer detected a change in the J -band dome flat-field images, suggesting either contamination or that the filter might be starting to delaminate. The decision was taken to replace the suspect filter, and this was accomplished approximately a month later. The last observations made with the original filter, which we will refer to as “ J_{RC1} ,” were obtained on 2009 January 2 (JD 2,454,833). Observations with the replacement filter, which we call “ J_{RC2} ,” began on 2009 January 15 (JD 2,454,846). It was eventually determined that the change in the J_{RC1} filter was due to contamination, and this problem affected the J_{RC1} observations obtained between JD 2,454,808 and 2,454,833. Although we have no evidence that the contamination significantly changed the bandpass of the J_{RC1} filter and have therefore included these observations in this paper, we caution the reader that the reliability of these observations is less certain than that of the other J -band photometry published in this paper.

In Papers I and II, we neglected any color terms that might exist in transforming J and H measurements made by the CSP-I to the P98 photometric system. In order to check this assumption, we have reproduced the P98 bandpasses by combining the filter transmission data and typical NICMOS3 quantum efficiency curve given by these authors with two aluminum reflectivity curves (one for the primary and another for the secondary mirror) and an atmospheric transmission spectrum typical of LCO. The resulting response functions are plotted in red in Figure 3.

The $(J - H)$ colors of the P98 secondary standard stars used by the CSP-I to calibrate both the Swope and du Pont NIR observations range from only +0.19 to +0.35 mag. This is too small of a color range to measure the NIR color terms, and so we must resort to synthetic photometry of model atmospheres to estimate these. We downloaded the Castelli & Kurucz (2003) atmosphere models for a range of stellar parameters. For each model spectrum, we then computed synthetic photometry for a range of reddenings ($E(B - V) = 0.0$ to 2.5 mag) and plotted the differences between the P98 magnitudes and the RetroCam and WIRC J and H magnitudes as a function of the $(J - H)_{P98}$ color (see Figure 7). Linear fits to these data yield the following:

$$J_{P98} = J_{RC1} + 0.039 \times (J - H)_{P98} + \zeta_j, \quad (26)$$

$$J_{P98} = J_{RC2} + 0.016 \times (J - H)_{P98} + \zeta_j, \quad \text{and} \quad (27)$$

$$H_{P98} = H_{RC} - 0.029 \times (J - H)_{P98} + \zeta_h. \quad (28)$$

In Appendix C, we present du Pont+RetroCam observations of P98 standards covering a much wider range of colors that validate the accuracy of this procedure.

Although the effect of the color terms in Equations (26)–(28) is less than 0.01 mag over the small range of color of the P98 standards, it is a systematic effect, and so we use them to transform the P98 magnitudes to the natural system.

The Y photometric band was introduced by Hillenbrand et al. (2002). Hamuy et al. (2006) calculated synthetic $(Y - K_s)$ and $(J - K_s)$ colors from Kurucz model atmosphere spectra using the estimated filter response functions for the Magellan 6.5 m Baade telescope “PANIC” NIR imager. These values were fitted with a fifth-order polynomial with the requirement that $(Y - K_s) = 0.0$ when $(J - K_s) = 0.0$ mag, consistent with the

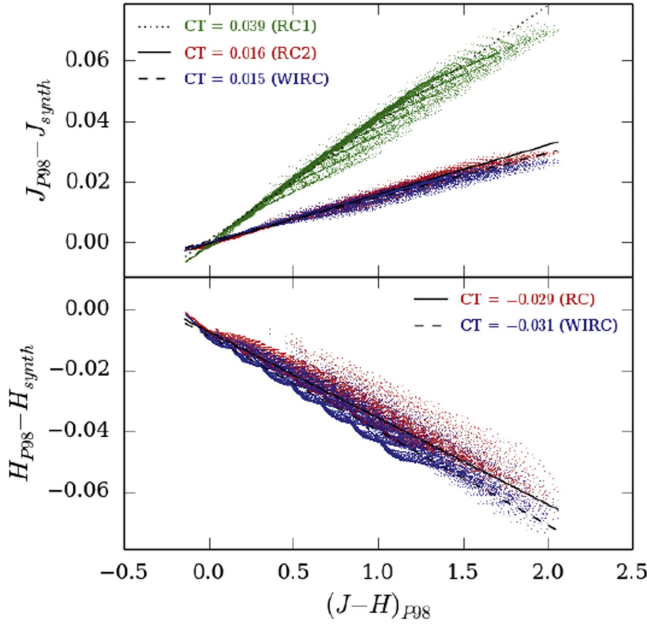


Figure 7. Top: differences between synthetic photometry in the natural systems of the two Swope+RetroCam filters, J_{RC1} and J_{RC2} , and the P98 J bandpass vs. the $(J - H)_{P98}$ color (green and red points, respectively). The differences between synthetic photometry in the natural system of the du Pont+WIRC J filter and the P98 J bandpass are also shown (blue points). The slopes give the J -band color terms (CT) for the Swope+RetroCam and the du Pont+WIRC systems using synthetic photometry derived from Castelli & Kurucz (2003) atmosphere models covering a range of stellar parameters and reddening ($E(B - V) = 0.0$ to 2.5 mag). Bottom: same as top panel, but for H -band magnitude differences vs. $(J - H)_{P98}$ color. The slopes of the solid and dashed lines give the H -band color terms derived for the Swope+RetroCam and du Pont+WIRC H filters.

definition that α Lyr (Vega) has magnitudes of zero at all NIR wavelengths (Elias et al. 1982). This relation was then used to compute Y -band magnitudes from J and K_s for all of the P98 secondary standards. In Appendix D, we repeat this exercise using the *measured* Swope+RetroCam Y -band response function along with the J and K_s filter response functions we have derived for the P98 standards.

6.2.2. du Pont+WIRC

Color terms for the du Pont+WIRC system were calculated from synthetic photometry of the Castelli & Kurucz (2003) stellar atmosphere models in the manner described previously for the Swope+RetroCam. We find

$$J_{P98} = J_{WIRC} + 0.015 \times (J - H)_{P98} + \zeta_j, \quad \text{and} \quad (29)$$

$$H_{P98} = H_{WIRC} - 0.031 \times (J - H)_{P98} + \zeta_h. \quad (30)$$

We note that these color terms are nearly identical to those for the J_{RC2} and H_{RC} filters (see Equations (27) and (28)).

Figure 3 shows that the du Pont+WIRC Y bandpass cuts off more rapidly at blue wavelengths than is the case for the Swope+RetroCam Y filter. We again employ synthetic photometry to evaluate the color term required to transform the du Pont+WIRC Y -band secondary standard star observations to the Swope+RetroCam system. This gives

$$Y_{\text{RetroCam}} = Y_{\text{WIRC}} - 0.042 \times (J - H)_{P98} + \zeta_y. \quad (31)$$

Over the range of $(J - H)$ colors of the local sequence of tertiary standards, this color term is too large to be ignored.

This means that for the Y band we must work in two different natural systems: that of the Swope+RetroCam, which we adopt as the “standard” system, and that of the du Pont+WIRC.

6.2.3. NIR Natural-system Photometry

From the above, we conclude that the color terms for the J_{RC2} and J_{WIRC} filters are sufficiently similar that we can average them and, therefore, create a single natural system for all of the tertiary standards and SNe observed. Likewise, the color terms for the H_{RC} and H_{WIRC} filters are nearly identical, and the photometry obtained with them can also be considered on the same natural system. However, the J_{RC1} color term differs considerably with respect to those of the other two J filters and therefore defines its own natural system. Likewise, the color term for the Y_{WIRC} filter compared to Y_{RC} is too large to be ignored.

We therefore adopt the following equations to transform the secondary standard star magnitudes to the natural systems in YJH for the Swope+RetroCam:

$$Y_{\text{nat,RC}} \equiv Y_{RC}, \quad (32)$$

$$J_{\text{nat,RC1}} = J_{P98} - 0.039 \times (J - H)_{P98}, \quad (33)$$

$$J_{\text{nat,RC2}} = J_{P98} - 0.015 \times (J - H)_{P98}, \quad \text{and} \quad (34)$$

$$H_{\text{nat,RC}} = H_{P98} + 0.030 \times (J - H)_{P98}. \quad (35)$$

For the du Pont+WIRC system, the transformation equations for $J_{\text{nat,WIRC}}$ and $H_{\text{nat,WIRC}}$ are identical to Equations (34) and (35), while for $Y_{\text{nat,WIRC}}$ the equation is

$$Y_{\text{nat,WIRC}} = Y_{RC} + 0.042 \times (J - H)_{P98}, \quad (36)$$

where the Y_{RC} magnitudes are taken from Appendix D and the J_{P98} and H_{P98} magnitudes are from P98.

For each photometric night where secondary standard stars were observed, the NIR photometric equations are then simplified to

$$Y_{\text{nat}} = y - k_y X + \zeta_y, \quad (37)$$

$$J_{\text{nat}} = j - k_j X + \zeta_j, \quad \text{and} \quad (38)$$

$$H_{\text{nat}} = h - k_h X + \zeta_h, \quad (39)$$

where y , j , and h correspond to the instrumental magnitudes and k_y , k_j , and k_h are extinction coefficients. Figure 8 displays nightly values of the atmospheric extinction coefficients in YJH over the five CSP-I campaigns for both the Swope+RetroCam and du Pont+WIRC systems. These were derived using the MCMC fitting procedure described in Section 6.1.1 from observations of typically 2–10 secondary standards per night. Histograms of the collected extinction-coefficient measurements are shown on the right side of each panel. No significant difference is observed between the two telescope+camera systems, so we can combine the observations. The resulting mean extinction coefficients are given in Table 4. As was found to be the case for the optical bandpasses, the stability of the extinction coefficients during the five CSP-I observing campaigns is such that these average values can be adopted, leaving only the nightly zero-points in Equations (37)–(39) to be determined.

Thirteen SN fields were not observed for the requisite minimum of three photometric nights. In order to improve the photometric calibration of the tertiary standards for these fields,

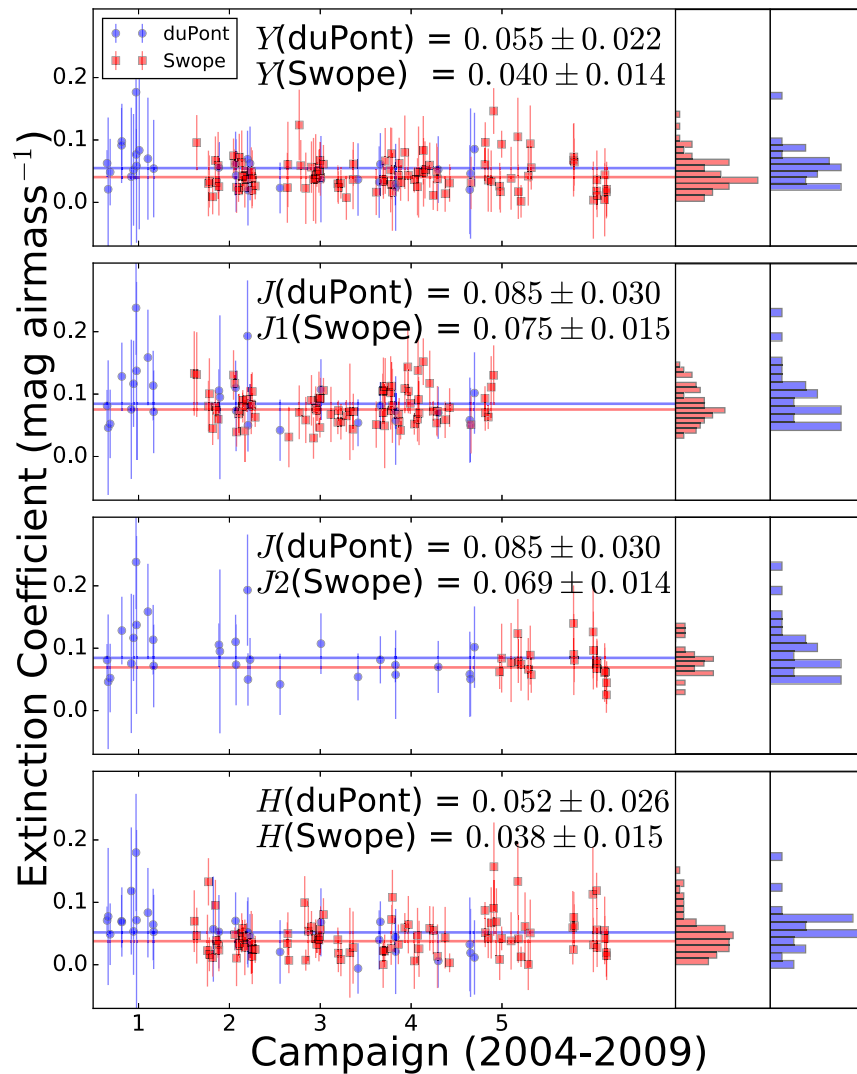


Figure 8. NIR broadband extinction values (mag airmass^{-1}) measured at LCO from 2004 September through 2009 November. Blue symbols correspond to observations made with the du Pont+WIRC, and red symbols show measurements made with the Swope+RetroCam. Histograms for the entire 5 yr are shown on the right side of each panel.

we devised a “hybrid” calibration whereby calibrated tertiary standards from one field are used to calibrate the tertiary standards in another field that is observed on the same night under photometric conditions, but when secondary standards were not observed. In this case, we use a modified version of Equation (5):

$$m_{i,\lambda} = \frac{\sum_{j,k} (m_{\text{nat},k,\lambda} + \Delta m_{i,j,k,\lambda} - k_{\lambda}(X_{i,j,\lambda} - X_{j,k,\lambda})) w_{j,k,\lambda}}{\sum_{j,k} w_{j,k,\lambda}}, \quad (40)$$

where k now refers to calibrated tertiary standards of different SN fields observed in filter λ on the same photometric night (j).

In brief, this procedure worked as follows:

1. A catalog of tertiary standard stars was produced from 126 SN fields (90 SNe Ia and 36 SNe of other types) calibrated on a minimum of four photometric nights in each of the three NIR filters.
2. This catalog of tertiary standards was then used to measure an alternative set of zero-points for each night of NIR imaging during the five CSP-I campaigns.
3. These new zero-points were then filtered to include only those nights where (1) a minimum of three SN fields with calibrated tertiary standards was observed, (2) a minimum continuous span of 3 hr of imaging was obtained, and (3) a maximum dispersion of 0.08 mag in the nightly zero-point as calculated from the observations of the tertiary standards was observed that night. This last criterion is similar to that used in filtering the photometric nights chosen for calibrating the tertiary standard stars using the P98 secondary standards, but it should be noted that the typical dispersion in zero-points for photometric nights was significantly less (0.02–0.03 mag).

In Figures 9 and 10, the zero-points calculated using only the P98 secondary standard stars are plotted as a function of time for the du Pont+WIRC and the Swope+RetroCam, respectively. Shown for comparison are the zero-points obtained

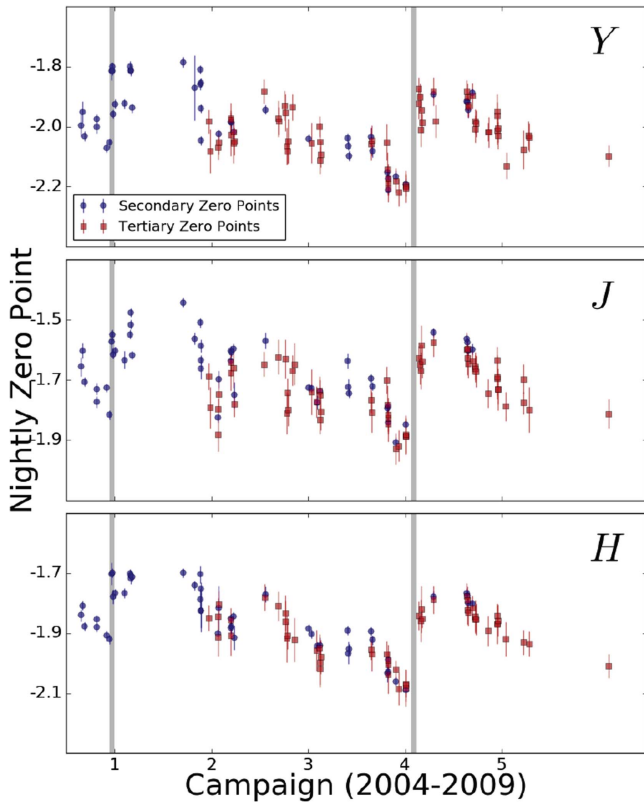


Figure 9. Nightly NIR photometric zero-points for the du Pont+WIRC derived from observations of both secondary and tertiary standard stars over the course of the CSP-I. The blue circles denote zero-points calculated from secondary standards, and the red squares indicate zero-points derived from tertiary standards. The vertical gray lines indicate dates on which the primary mirror was aluminized.

using the hybrid method described above. Note that the agreement is generally excellent, although the uncertainties in the zero-points derived in the hybrid method are generally larger since the local sequence stars are typically 3–4 mag fainter than the P98 secondary standards. The hybrid method provides potential photometric zero-points for an additional 52 nights in *Y*, 44 nights in *J*, and 40 nights in *H* for the du Pont+WIRC observations, and an additional 154 nights in *Y*, 139 nights in *J*, and 123 nights in *H* for the Swope+RetroCam data. Nevertheless, we used only those nights that allowed us to improve the calibration of the 13 SN fields.

6.2.4. Filter Contamination

Close inspection of Figure 10 reveals a faster-than-expected change in the zero-point evolution of the RetroCam *Y* and *H* filters during campaign 3, producing large breaks between the end of campaign 3 and the beginning of campaign 4. These discontinuities do not correspond to when the primary mirror was washed (indicated by the vertical gray lines in Figure 10). A similar problem is observed with the *H* band during campaign 4, where the zero-point decreases by nearly 1 mag between the washing of the primary mirror and the end of the campaign, as opposed to the much smaller changes observed for the *Y* and *J* filters over the same period. This behavior suggests slowly increasing contamination of the filters. To test this hypothesis, we plot with dashed blue lines in Figure 10 the dates that the RetroCam dewar was warmed up, pumped, and

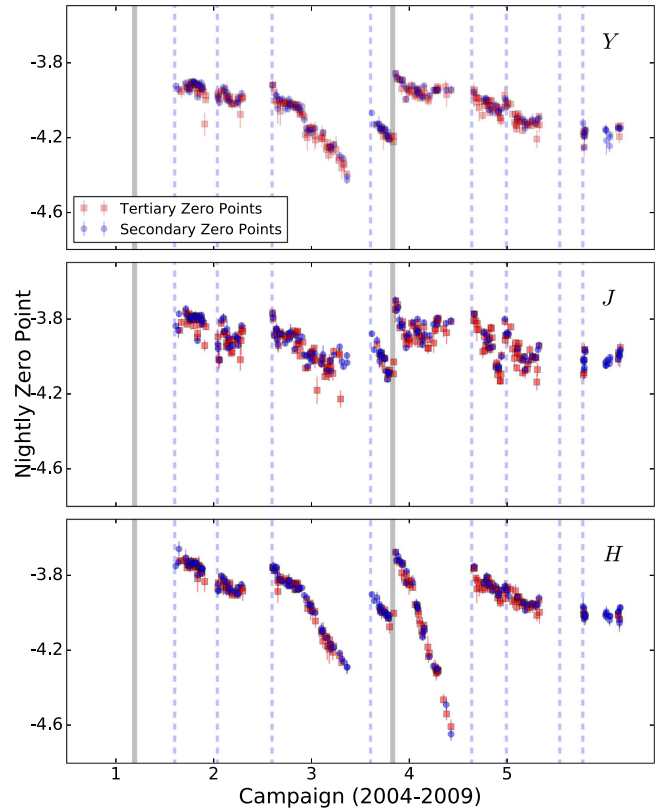


Figure 10. Nightly NIR photometric zero-points for the Swope+RetroCam derived from observations of both secondary and tertiary standard stars over the course of the CSP-I. The blue circles denote zero-points calculated from secondary standards, and the red squares indicate zero-points derived from tertiary standards. The vertical gray lines indicate dates on which the primary mirror was washed.

then cooled down again. The recovery of the *Y* and *H* zero-point values in campaign 3 and the *H* zero-point in campaign 4 is seen to coincide with when the dewar was pumped, consistent with the contamination hypothesis. Comparison of flat fields taken during campaigns 3 and 4 provides further evidence for slowly changing contamination seen as a radial pattern of increasing counts from the center to the edges of the filter that disappears when the dewar is pumped.

To examine the effect of this changing contamination on the photometry, we used observations of stars in the fields of several SNe at low Galactic latitudes. The observations of the Type IIn SN 2006jd (Stritzinger et al. 2012) from both campaigns 3 and 4 were used, supplemented by observations of the Type Ia SN 2007hj and SN 2007on and the Type II SN 2008M and SN 2008ag carried out during campaign 4. Figure 11 shows an example of the magnitude differences in the *Y*-, *J*-, and *H*-band photometry of stars in the field of SN 2008ag between images obtained on 2007 October 20 and 2008 April 5. For the *Y* and *J* bands in campaign 4, the magnitude differences are consistent with zero over the entire detector. In contrast, the *H* filter shows clear evidence of a radial gradient amounting to ~ 0.014 mag per 100 pixels as measured from the center of the detector. However, as the bottom right panel of Figure 11 shows, there is no evidence that the filter bandpass itself was changed significantly by the contamination since both blue and red stars show the same radial gradients. *Y*- and *H*-band observations in campaign 3 show a similar radial gradient effect.

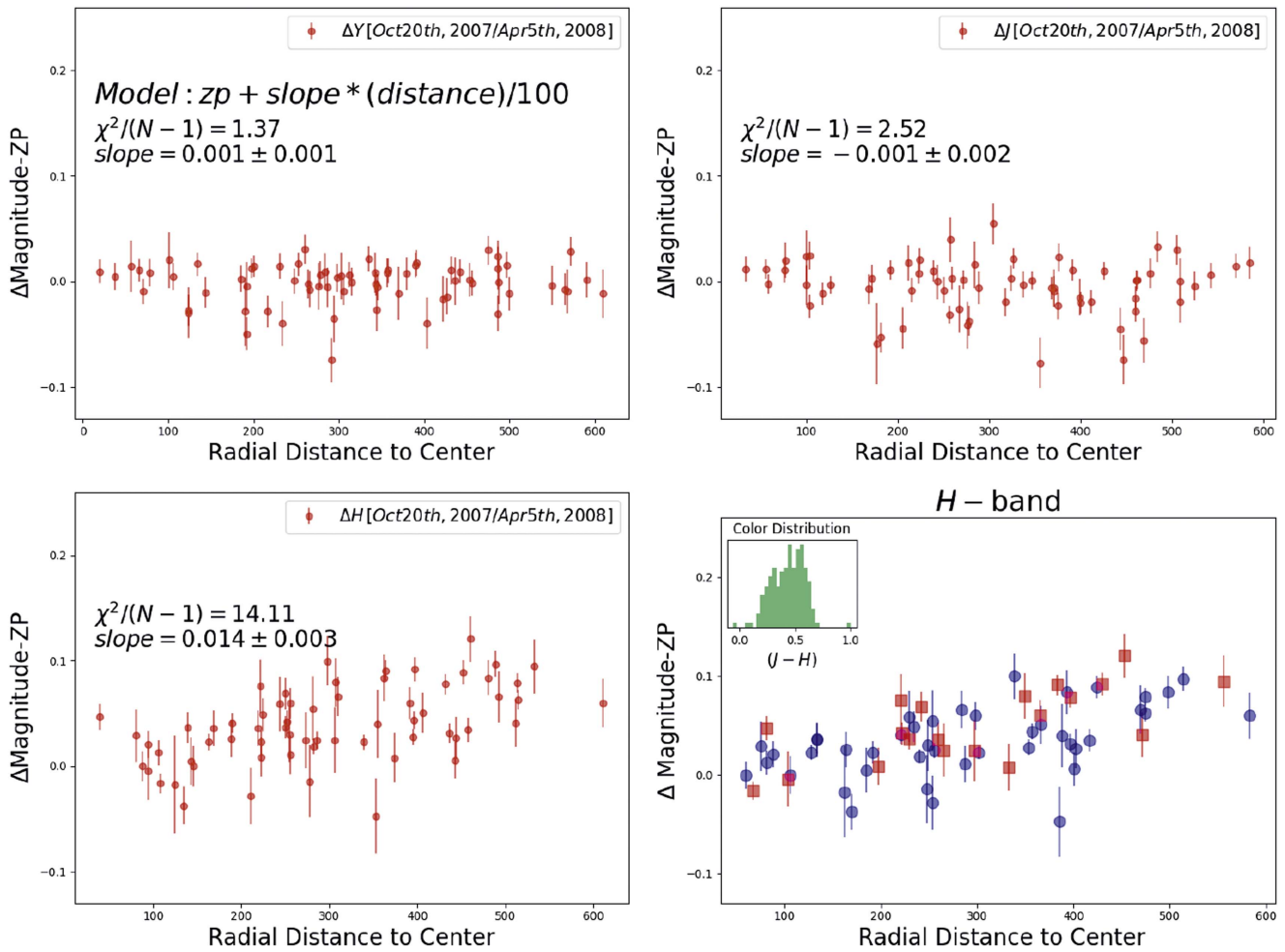


Figure 11. Magnitude differences in the Y (top left), J (top right), and H (bottom left) bands shown as a function of radial distance in pixels from the detector center of field stars in RetroCam images obtained on 2007 October 20 and 2008 April 5. The “magnitude difference” is the arithmetic difference of the instrumental magnitudes of a given star observed on two different nights. The bottom right plot shows the H -band magnitude differences dividing the field stars by color into two subsamples, with the inset plot showing the $(J - H)$ color distribution. The blue symbols correspond to stars with $(J - H) \leq 0.45$ mag, and the red symbols are stars with $(J - H) > 0.45$ mag.

Unfortunately, these contamination problems were not recognized during the course of the CSP-I campaigns. For most SNe, the error in the photometry due to the contamination is relatively small (0.02–0.03 mag) but systematic; we must therefore correct for the effect. Fortunately, the growth of the contamination was nearly linear in time. This is illustrated in Figure 12, where magnitude differences in H -band photometry of stars in the field of SN 2008ag are plotted at five epochs between 2008 February 20 and 2008 June 20 with respect to observations made on 2008 February 16. Fitting these trends with straight lines provides a recipe for correcting the SN and tertiary standard photometry, with the correction being a function of both time and the (x, y) coordinates of the SN or standard on the RetroCam detector. Specifically, we fit the slope measurements as a function of time by the relation

$$p(\text{JD}) = p(\text{JD}_{\text{end}}) \times (\text{JD} - \text{JD}_{\text{start}})/365.25, \quad (41)$$

where JD is the Julian date of the observation and $p(\text{JD}_{\text{end}})$ is the slope (measured in units of mag per 100 pixels) on the Julian date at the end of the period of contamination, JD_{end} . The formula for calculating the correction to the photometry of the tertiary standards and SN in an image taken on any Julian

date during the period of contamination is then

$$\Delta m_{\text{corr}}(\text{JD}) = p(\text{JD}) \times (d_{\text{radial}}/100 - 256/100), \quad (42)$$

where d_{radial} is the radial distance in pixels from of the star or SN from the center of the image, and the constant 256/100 makes the average of the magnitude corrections for each image approximately zero.

These corrections were applied to photometry obtained with the Swope+RetroCam as follows:

1. Campaign 3, Y band: $\text{JD}_{\text{start}} = 2,453,980.0$, $\text{JD}_{\text{end}} = 2,454,260.0$, $p(\text{JD}_{\text{end}}) = 0.027$.
2. Campaign 3, H band: $\text{JD}_{\text{start}} = 2,453,980.0$, $\text{JD}_{\text{end}} = 2,454,260.0$, $p(\text{JD}_{\text{end}}) = 0.021$.
3. Campaign 4, H band: $\text{JD}_{\text{start}} = 2,454,509.3$, $\text{JD}_{\text{end}} = 2,454,646.0$, $p(\text{JD}_{\text{end}}) = 0.110$.

6.2.5. Final Photometry

Final YJH magnitudes of the tertiary standards for all 134 SNe are listed in Table 6. Note that the J and H magnitudes are given in the *standard* P98 system, whereas the Y magnitudes are in the *natural* system of the Swope

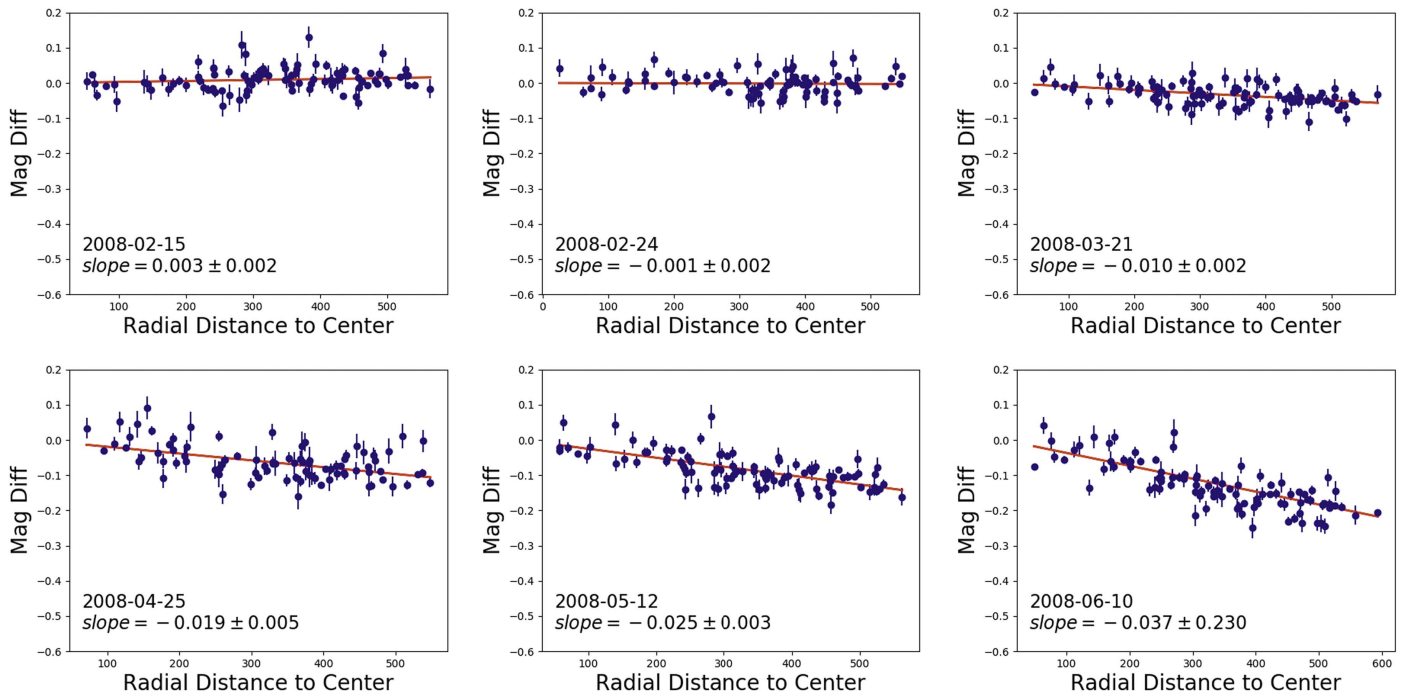


Figure 12. Magnitude differences in the *H* band plotted as a function of radial distance in pixels from the detector center of field stars in RetroCam images obtained on five different epochs during campaign 4. The slope of each fit is given in the panels. The dates shown in the individual panels are the dates of sunset, not the UT date at midnight.

Table 6
Infrared Photometry of Secondary Standards^a

ID	α (2000)	δ (2000)	<i>Y</i>	<i>J</i>	<i>H</i>
			SN 2004ef		
101	22:42:11.38	+20:00:57.6	14.690(046)	14.382(052)	14.008(069)
102	22:42:12.06	+20:00:25.1	15.262(066)	14.940(049)	14.414(067)
103	22:42:11.13	+19:58:37.6	15.698(050)	15.326(057)	14.698(051)
104	22:42:13.33	+19:58:32.7	16.539(044)	16.072(081)	15.396(094)
106	22:42:17.65	+19:59:44.9	15.933(035)	15.573(040)	14.994(068)
108	22:42:12.82	+20:00:02.8	16.496(083)	16.121(056)	15.452(038)
109	22:42:12.90	+19:59:18.3	16.869(049)	16.552(096)	16.248(057)
110	22:42:15.27	+19:59:16.0	13.114(042)	0.000(000)	0.000(000)
111	22:42:13.70	+19:59:30.1	0.000(000)	16.894(075)	0.000(000)
112	22:42:10.76	+19:59:03.3	17.381(119)	16.997(095)	0.000(000)

Note.

^a All photometry is measured in magnitudes. Values in parentheses are 1σ uncertainties. The *JH* photometry presented here is in the P98 system. The *Y*-band photometry is in the natural system.

(This table is available in its entirety in machine-readable form.)

+RetroCam (which we have adopted as the “standard” system). The accompanying uncertainties are the dispersions of the multiple measurements of each sequence star.

7. Final Light Curves

Final optical and NIR photometry of the 134 SNe in the CSP-I sample is given in Tables 7–12. Tables 7 and 8 give the *ugriBV* photometry in the natural systems of the Swope+SITE3 and du Pont+Tek5, respectively, and Table 9 gives the small amount of *V*-band photometry obtained in the natural system of the LC-3009 filter at the Swope. NIR photometry of 120 SNe in the natural systems of the Swope+RetroCam and du Pont +WIRC is found in Tables 10–12. On those occasions when

more than one NIR measurement is given for an object on a given night, it is because the WIRC used on the du Pont telescope images the SN location on more than one chip. Rather than averaging the measurements, we give the individual values.

7.1. Type Ia SNe

Plots of the individual light curves of the Type Ia SNe²¹ in the CSP-I sample are displayed in Figure 13 along with fits (solid red lines) using SNooPy (Burns et al. 2011). Photometric

²¹ By “Type Ia SNe,” we mean those classified as “normal,” “SN 1991T-like,” “SN 1986G-like,” and “SN 1991bg-like” in Table 2.

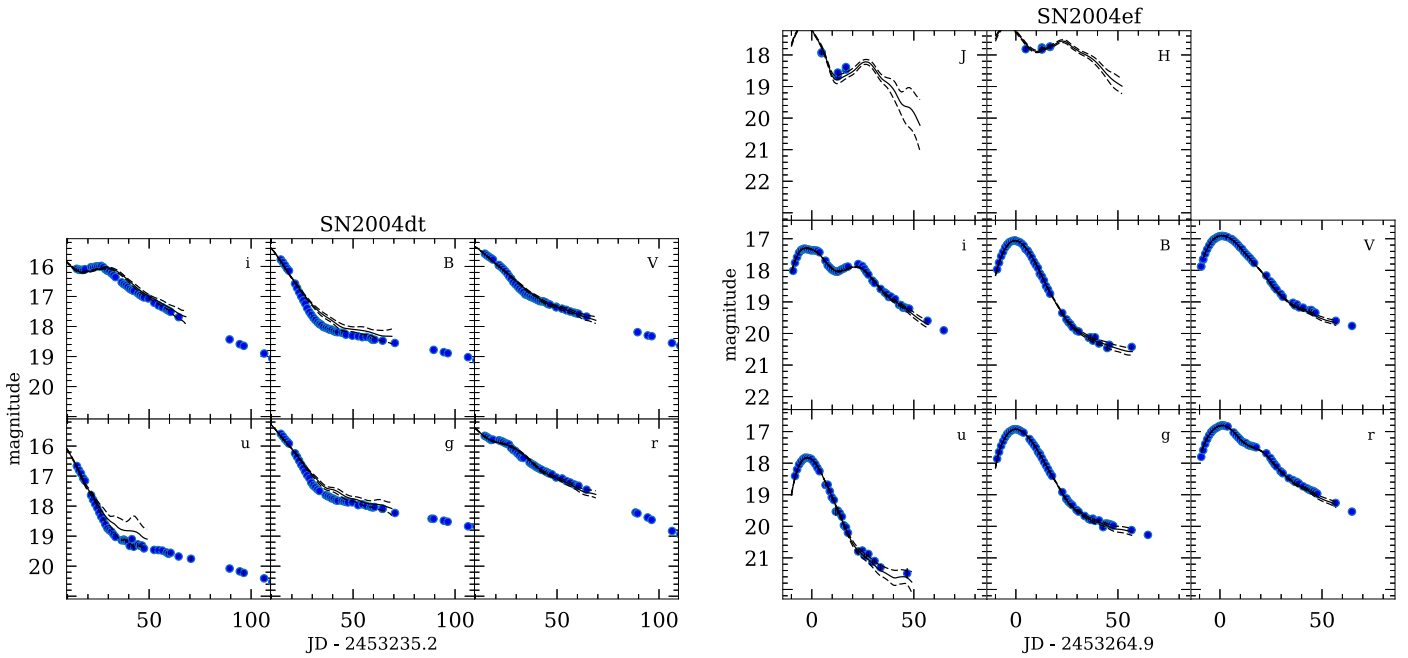


Figure 13. Multiband light curves of the Type Ia SNe observed by CSP-I. For better intercomparison each subplot has an abscissa (x -axis) range of 100 *observer-frame* days and an ordinate (y -axis) range of 6 mag. Note that $x = 0$ corresponds to the time of B -band maximum. Best-fitting SNooPy fits using the “max model” mode are shown for each SN. As the Y -band photometry obtained with two different cameras has different color terms, we color-code the Y -band photometry obtained with the du Pont telescope and WIRC with orange points. Starting 2009 January 15 the J -band photometry was obtained with the Swope telescope and RetroCam using the J_{RC2} filter. Those data points are color-coded orange. All 123 light curves are in the Figure Set.

(The complete figure set (123 images) is available.)

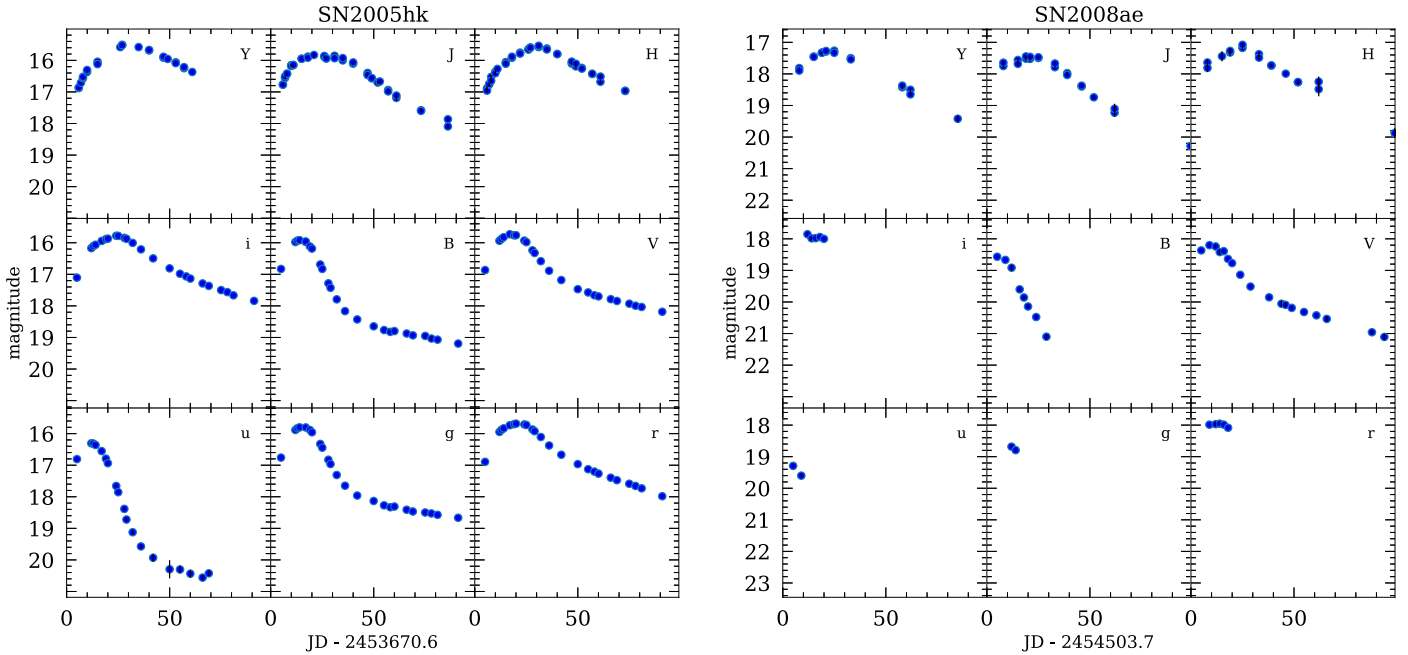


Figure 14. Same as Figure 13, except for Type Iax SNe. All five Type Iax SNe are in the Figure Set.

(The complete figure set (5 images) is available.)

parameters derived from the SNooPy fits are provided in Table 3. In some cases we can directly measure the epoch of B -band maximum, $T_{\max}(B)$, and the B -band decline rate,

$\Delta m_{15}(B)$. The latter is defined as the number of magnitudes the object faded in the first 15 days since the time of B -band maximum and has long been known to correlate with the

Table 7
Optical Photometry of SNe in Natural System of Swope (+SITE3)^a

JD	<i>u</i>	<i>g</i>	<i>r</i>	<i>i</i>	<i>B</i>	<i>V</i>
SN 2004dt						
2,453,249.79	16.665(017)	15.593(006)	15.659(006)	16.079(008)	15.769(006)	15.575(006)
2,453,250.81	16.804(012)	15.675(009)	15.695(008)	16.112(010)	15.859(008)	15.630(009)
2,453,251.83	16.912(012)	15.769(009)	15.745(010)	16.111(009)	15.961(009)	15.677(008)
2,453,252.86	17.069(014)	15.846(006)	15.796(006)	16.117(007)	16.069(007)	15.723(006)
2,453,253.78	17.158(012)	15.915(006)	15.785(006)	16.091(005)	16.142(014)	15.770(006)
2,453,256.75	17.637(010)	16.241(006)	15.807(006)	16.024(007)	16.573(007)	15.950(006)
2,453,257.73	17.787(013)	16.357(008)	15.833(012)	16.029(009)	16.715(008)	16.012(008)
2,453,258.76	17.929(012)	16.484(006)	15.857(006)	16.007(005)	16.858(008)	16.078(008)
2,453,259.78	18.060(013)	16.618(006)	15.899(006)	15.993(005)	16.995(007)	16.151(006)
2,453,260.80	18.215(012)	16.724(008)	15.926(009)	15.995(009)	17.126(008)	16.227(008)
2,453,261.71	18.349(014)	16.844(008)	15.950(009)	15.981(010)	17.239(011)	16.325(010)
2,453,262.70	18.461(014)	16.970(010)	16.058(010)	16.021(010)	17.388(009)	16.402(009)
2,453,263.76	18.611(017)	17.068(013)	16.130(013)	16.093(016)	17.515(014)	16.518(013)
2,453,264.75	18.736(020)	17.219(011)	16.160(011)	16.143(016)	17.612(014)	16.589(013)
2,453,265.79	18.807(015)	17.312(010)	16.239(008)	16.163(009)	17.712(013)	16.660(009)
2,453,266.73	18.848(016)	17.372(006)	16.299(006)	16.227(005)	17.783(009)	16.735(007)
2,453,267.74	18.943(023)	17.441(008)	16.381(006)	16.290(009)	17.856(011)	16.796(008)
2,453,268.74	19.027(019)	17.495(009)	16.396(009)	16.356(011)	17.921(009)	16.853(007)
2,453,269.68	0.000(000)	0.000(000)	0.000(000)	0.000(000)	17.947(017)	16.931(008)
2,453,270.68	0.000(000)	0.000(000)	0.000(000)	0.000(000)	18.016(011)	16.951(006)

Note.

^a All photometry is measured in magnitudes. Values in parentheses are 1σ uncertainties.

(This table is available in its entirety in machine-readable form.)

absolute magnitudes of SNe Ia at maximum light (Phillips 1993). Often, however, photometric coverage is not optimal for direct measurements, and it is more robust to estimate $T_{\max}(B)$ and the decline rate using a family of light-curve templates. Hence, for each object in Table 3, we have used the “max model” method of SNooPy to calculate template-derived estimates of the epoch of B -band maximum and the decline-rate parameter, $\Delta m_{15}(B)$, which we denote as $T_{\max}(\text{template})$ and $\Delta m_{15}(\text{template})$, respectively. We also give the dimensionless “stretch BV parameter,” s_{BV} , which is equal to $\Delta T_{BV}/(30 \text{ days})$, where ΔT_{BV} is the number of days since $T(B_{\max})$ that a supernova’s $(B - V)$ color reaches its maximum value (Burns et al. 2014). Burns et al. discuss the advantages of this new parameter over the usual decline-rate parameter, especially for rapidly declining light curves. In particular, plots of reddening-corrected colors versus s_{BV} show low rms scatter, allowing a more definitive characterization of the photometric properties of SNe Ia.

One “normal” SN Ia listed in Table 3 that we cannot fit using just CSP-I photometry is SN 2006dd, because the CSP-I data cover only the post-maximum linear decline. We refer the reader to Stritzinger et al. (2010), which contains pre-maximum, maximum-light, and post-maximum photometry of this SN obtained with the CTIO 1.3 m telescope using its dual optical/NIR imager ANDICAM.

The middle panel of Figure 2 shows a histogram of the values of the B -band decline rate, $\Delta m_{15}(B)$, as obtained from the template fits. The bottom panel of this figure shows a histogram of “stretch BV ” values.

7.2. Type Iax SNe

Type Iax SNe are spectroscopically similar to Type Ia SNe that are more luminous than average because they show

high-ionization lines such as Fe III but have lower maximum-light velocities and fainter absolute magnitudes for their light-curve decline rates (Foley et al. 2013). The prototype of this subclass is SN 2002cx (Filippenko 2003; Li et al. 2003). Plots of the individual light curves of the five Type Iax SNe in the CSP-I sample (SN 2005hk, SN 2008ae, SN 2008ha, SN 2009J, and SN 2010ae) are displayed in Figure 14. Preliminary photometry of SN 2005hk was published by Phillips et al. (2007). Stritzinger et al. (2014, 2015) have published updated photometry of SNe 2005hk, 2008ha, and 2010ae.

7.3. Other Subtypes

Two objects observed by the CSP-I, SN 2007if and SN 2009dc, are candidates for the super-Chandrasekhar (“SC”) subtype (Howell et al. 2006). SN 2006bt and SN 2006ot are members of the SN 2006bt-like subclass (Foley et al. 2010b, Paper II). Two other events (SN 2005gj and SN 2008J) belong to the rare Type Ia-CSM subtype (Silverman et al. 2013). The light curves of these six SNe are shown in Figure 15.

8. Conclusions

In this paper we have presented the third and final data release of optical and NIR photometry of the 134 nearby ($0.004 \lesssim z \lesssim 0.08$) white dwarf SNe observed during the CSP-I. This sample consists of 123 Type Ia SNe, 5 Type Iax SNe, 2 super-Chandrasekhar candidates, 2 Type Ia-CSM SNe, and 2 SN 2006bt-like events. NIR photometry was obtained for 90% of these SNe. Optical spectroscopy has already been published for approximately two-thirds of the SNe Ia in the sample, and the remaining spectra are currently being prepared for publication. In addition to providing a new set of light curves of low-redshift SNe Ia in a stable,

Table 8
Optical Photometry of SNe in Natural System of du Pont (+Tek5)^a

JD	<i>u</i>	<i>g</i>	<i>r</i>	<i>i</i>	<i>B</i>	<i>V</i>
			SN 2005hj			
2,453,678.68	18.592(033)	17.848(006)	17.748(009)	18.354(012)	17.927(009)	17.820(009)
			SN 2005ke			
2,453,967.85	0.000(000)	20.720(149)	0.000(000)	0.000(000)	20.661(143)	20.867(167)
			SN 2006bh			
2,453,828.88	0.000(000)	14.636(007)	14.672(024)	15.004(021)	14.724(006)	14.748(007)
2,453,829.88	14.924(011)	14.523(009)	0.000(000)	0.000(000)	14.618(006)	14.663(009)
2,453,830.89	14.880(011)	14.422(011)	14.519(014)	15.030(051)	14.544(006)	14.550(008)
2,453,886.79	19.033(020)	17.543(043)	16.890(041)	17.064(041)	17.919(010)	17.139(050)
2,453,892.78	19.236(036)	17.651(023)	17.209(030)	17.449(018)	18.001(008)	17.293(009)
2,453,893.79	19.271(031)	17.657(011)	17.188(020)	17.490(016)	18.030(008)	17.320(009)
			SN 2006D			
2,453,828.83	0.000(000)	0.000(000)	17.471(005)	17.684(006)	0.000(000)	0.000(000)
			SN 2006eq			
2,454,022.50	0.000(000)	0.000(000)	0.000(000)	0.000(000)	0.000(000)	20.942(049)
2,454,023.48	0.000(000)	0.000(000)	20.297(045)	0.000(000)	21.770(056)	0.000(000)
2,454,024.46	0.000(000)	0.000(000)	20.294(069)	0.000(000)	21.672(093)	20.900(054)
			SN 2006et			
2,454,023.71	19.758(035)	17.918(009)	16.814(012)	0.000(000)	18.329(011)	0.000(000)
2,454,024.59	19.893(032)	17.913(009)	16.754(017)	16.860(008)	18.371(008)	17.225(006)
			SN 2006ev			
2,454,023.50	0.000(000)	19.966(013)	18.669(009)	18.696(015)	20.307(025)	19.202(012)
2,454,024.50	0.000(000)	0.000(000)	18.727(012)	18.850(027)	20.408(029)	19.288(016)
			SN 2006gt			
2,454,024.63	0.000(000)	20.317(013)	19.136(008)	19.039(011)	20.829(020)	19.621(012)
			SN 2006hx			
2,454,024.67	18.478(024)	17.516(022)	0.000(000)	0.000(000)	17.746(009)	17.584(020)
			SN 2007hx			
2,454,386.79	0.000(000)	21.427(046)	20.354(026)	19.936(035)	21.935(115)	21.048(056)
			SN 2007if			
2,454,386.67	0.000(000)	19.714(009)	18.635(005)	18.474(007)	20.277(021)	19.140(009)
			SN 2008C			
2,454,539.51	0.000(000)	18.907(016)	0.000(000)	18.664(018)	19.474(033)	18.620(016)
			SN 2008ia			
2,454,889.63	0.000(000)	20.031(022)	0.000(000)	0.000(000)	20.450(044)	19.791(028)
2,454,890.75	0.000(000)	0.000(000)	0.000(000)	0.000(000)	0.000(000)	19.779(036)
2,454,894.61	0.000(000)	20.096(021)	0.000(000)	0.000(000)	20.643(044)	19.937(027)
			SN 2008O			
2,454,531.55	0.000(000)	21.172(028)	19.927(017)	19.982(023)	21.438(073)	20.652(039)
2,454,538.56	0.000(000)	21.401(073)	20.118(043)	20.277(068)	21.717(163)	20.772(067)
2,454,539.65	0.000(000)	21.219(059)	20.158(031)	20.249(050)	0.000(000)	20.727(055)
2,454,540.52	0.000(000)	21.220(053)	20.191(033)	20.240(048)	0.000(000)	20.827(079)
			SN 2009ag			
2,454,894.58	16.752(012)	15.365(015)	15.041(005)	15.535(005)	15.605(006)	15.200(005)
			SN 2009al			
2,454,894.67	16.544(042)	16.306(061)	16.351(066)	16.562(052)	16.360(033)	16.223(061)
			SN 2009cz			
2,454,951.46	0.000(000)	0.000(000)	0.000(000)	0.000(000)	0.000(000)	15.908(006)
2,454,952.47	16.970(021)	15.932(006)	15.918(006)	16.661(006)	16.121(007)	0.000(000)
2,454,954.47	17.225(024)	16.011(009)	15.979(006)	16.727(009)	16.242(007)	15.989(006)
			SN 2009ds			
2,454,952.46	16.682(014)	16.133(006)	16.063(008)	16.304(010)	16.228(007)	16.160(006)
2,454,953.50	16.432(016)	15.909(008)	15.968(009)	16.262(012)	16.072(009)	0.000(000)
2,454,954.46	0.000(000)	0.000(000)	0.000(000)	0.000(000)	0.000(000)	15.993(009)

Note.

^a All photometry is measured in magnitudes. Values in parentheses are 1σ uncertainties.

well-characterized photometric system for cosmological studies, the combined CSP-I data set is allowing us to improve dust extinction corrections for SNe Ia (Burns et al. 2014). The excellent precision and high cadence of

the CSP-I observations also facilitate detailed analysis of the light curves, leading to a deeper understanding of the physics of thermonuclear events (e.g., Höflich et al. 2010, 2017).

Table 9
V-band Photometry of SNe in Natural System of Swope (+SITe3)^a

UT Date	JD	Object	<i>V</i>	σ_V
2006 Jan 16	2,453,751.65	SN 2005eq	19.654	0.071
2006 Jan 19	2,453,754.60	SN 2005gj	18.319	0.018
2006 Jan 16	2,453,751.60	SN 2005hc	20.392	0.095
2006 Jan 20	2,453,755.61	SN 2005hc	20.534	0.065
2006 Jan 17	2,453,752.54	SN 2005hj	20.505	0.077
2006 Jan 16	2,453,751.53	SN 2005hk	18.023	0.017
2006 Jan 15	2,453,750.54	SN 2005iq	19.640	0.090
2006 Jan 20	2,453,755.55	SN 2005iq	19.884	0.052
2006 Jan 15	2,453,750.60	SN 2005ke	16.967	0.010
2006 Jan 20	2,453,755.64	SN 2005ke	17.111	0.009
2006 Jan 16	2,453,751.79	SN 2005ki	18.164	0.024
2006 Jan 17	2,453,752.78	SN 2005ki	18.120	0.025
2006 Jan 17	2,453,752.61	SN 2005lu	19.058	0.028
2006 Jan 17	2,453,752.74	SN 2005mc	18.198	0.022
2006 Jan 20	2,453,755.74	SN 2005mc	18.473	0.019
2006 Jan 16	2,453,751.68	SN 2005na	16.570	0.007
2006 Jan 19	2,453,754.69	SN 2005na	16.787	0.007
2006 Jan 20	2,453,755.68	SN 2005na	16.851	0.008
2006 Jan 16	2,453,751.83	SN 2006D	14.693	0.006
2006 Jan 17	2,453,752.86	SN 2006D	14.538	0.006
2006 Jan 19	2,453,754.77	SN 2006D	14.331	0.007

Note.^a All photometry is measured in magnitudes. Data taken using LC-3009 filter.**Table 10**Infrared Photometry of SNe in Natural System of Swope (+RetroCam)^a

JD	<i>Y</i>	<i>J</i>	<i>H</i>
SN 2005el			
2,453,640.80	15.652(012)	15.650(014)	15.707(022)
2,453,640.81	15.647(011)	15.617(013)	15.730(021)
2,453,643.79	15.561(010)	15.513(013)	15.733(026)
2,453,643.80	15.542(010)	15.521(015)	15.739(027)
2,453,648.79	16.051(030)	15.858(021)	16.044(048)
2,453,648.80	16.047(017)	15.905(029)	15.928(058)
2,453,656.83	16.608(018)	17.426(065)	0.000(000)
2,453,656.83	16.603(020)	0.000(000)	0.000(000)
2,453,657.76	16.600(017)	17.364(040)	16.442(039)
2,453,657.77	16.585(020)	17.266(038)	16.371(034)
2,453,660.83	16.484(017)	17.409(058)	16.277(039)
2,453,660.84	16.460(018)	17.320(044)	16.401(062)
2,453,664.82	16.151(017)	17.151(041)	0.000(000)
2,453,664.84	16.183(020)	17.304(058)	0.000(000)
2,453,668.80	15.800(012)	16.798(040)	15.936(029)
2,453,668.81	15.765(012)	16.873(034)	15.916(034)

Note.^a The photometry presented here was obtained with the *J*-band filter RC1, which was used prior to 2009 January 15. All photometry is measured in magnitudes. Values in parentheses are 1σ uncertainties.

(This table is available in its entirety in machine-readable form.)

Over the course of the CSP-I, more than 100 core-collapse SNe were observed. Photometry of seven SNe II_n has already been presented by Stritzinger et al. (2012) and Taddia et al. (2013). In an accompanying paper to this one (Stritzinger et al. 2017), the final data release of optical and NIR photometry of

Table 11Infrared Photometry of SNe in Natural System of Swope (+RetroCam)^a

JD	<i>Y</i>	<i>J</i>	<i>H</i>
SN 2008hv			
2,454,849.78	15.764(012)	16.960(024)	16.332(036)
2,454,849.79	15.769(016)	16.988(025)	16.336(033)
2,454,854.78	16.090(013)	17.521(036)	16.634(044)
2,454,854.79	16.088(013)	17.462(036)	16.700(046)
2,454,868.66	16.971(020)	18.370(100)	17.252(047)
2,454,868.67	16.985(021)	18.560(100)	17.283(048)
2,454,875.65	17.339(018)	18.867(112)	17.549(065)
2,454,875.66	17.333(026)	19.074(112)	17.584(074)
2,454,887.66	17.970(036)	0.000(000)	0.000(000)
2,454,887.66	17.996(037)	0.000(000)	0.000(000)
2,454,889.66	18.131(052)	0.000(000)	0.000(000)
2,454,889.67	18.046(047)	0.000(000)	0.000(000)
2,454,895.58	18.212(051)	0.000(000)	0.000(000)
2,454,895.59	18.283(051)	0.000(000)	0.000(000)
2,454,899.62	18.339(069)	0.000(000)	0.000(000)
2,454,912.69	18.774(067)	0.000(000)	0.000(000)
2,454,912.70	18.710(068)	0.000(000)	0.000(000)
2,454,912.70	18.710(068)	0.000(000)	0.000(000)

Note.^a The photometry presented here was obtained with the *J*-band filter RC2, which was used after 2009 January 15. All photometry is measured in magnitudes. Values in parentheses are 1σ uncertainties.

(This table is available in its entirety in machine-readable form.)

Table 12Infrared Photometry of SNe in Natural System of du Pont (+WIRC)^a

JD	<i>Y</i>	<i>J</i>	<i>H</i>
SN 2004ef			
2,453,269.70	17.897(042)	17.946(056)	17.817(096)
2,453,269.68	0.000(000)	17.919(068)	0.000(000)
2,453,277.63	17.835(025)	18.679(049)	17.764(050)
2,453,277.64	0.000(000)	18.559(047)	17.829(052)
2,453,281.59	17.590(021)	18.463(036)	17.747(037)
2,453,281.60	17.574(021)	18.384(036)	17.732(039)
2,453,328.58	19.161(051)	0.000(000)	0.000(000)
2,453,328.59	19.211(061)	0.000(000)	0.000(000)

Note.^a All photometry is measured in magnitudes. Values in parentheses are 1σ uncertainties.

(This table is available in its entirety in machine-readable form.)

34 stripped-envelope core-collapse SNe is presented. Publication of optical and NIR photometry of 83 SNe II observed during the course of the CSP-I is also in preparation. Preliminary *V*-band light curves for this sample have already been published by Anderson et al. (2014), and CSP-I observations of two SN 1987A-like events were presented by Taddia et al. (2012). Extensive optical spectroscopy of many of these core-collapse SNe was also obtained and is currently being prepared for publication.

In 2011, we began a second phase of the CSP to obtain optical and NIR observations of SNe Ia in the smooth Hubble

flow. Over a 4 yr period, light curves were obtained for nearly 200 SNe Ia, ~ 100 of which were at $0.03 \lesssim z \lesssim 0.10$. NIR spectra were also obtained of more than 150 SNe Ia. This data set, which we plan to publish over the next 3 yr, in combination with the CSP-I light curves published in the present paper, should provide a definitive test of the ultimate precision of SNe Ia as cosmological standard candles.

9. Electronic Access

To obtain an electronic copy of the photometry of any of the SNe included in this paper, the reader is directed to the CSP website at <http://csp.obs.carnegiescience.edu/>. Also available at this website are the optical spectra of CSP-I SNe Ia published by Folatelli et al. (2013).

This paper is dedicated to the memory of our dear colleague, Wojtek Krzeminski (1933–2017), who played an important role in the early history of Las Campanas Observatory and who, during his retirement, obtained many of the observations presented in this paper.

The CSP particularly thanks the mountain staff of the Las Campanas Observatory for their assistance throughout the duration of our observational program, and Jim Hughes and Skip Schaller for computer support. Special thanks are due to Allyn Smith and Douglas Tucker for allowing us to publish their $u'g'r'i'$ magnitudes of P177D and P330E (and to Dan Scolnic for leading us to Allyn and Douglas). This project was supported by NSF under grants AST-0306969, AST-0908886, AST-0607438, and AST-1008343. M.D.S., C.C., and E.H. acknowledge generous support from the Danish Agency for Science and Technology and Innovation through a Sapere Aude Level 2 grant. M.D.S. is supported by a research grant (13261) from VILLUM FONDEN. M.H. acknowledges support by CONICYT through grants FONDECYT Regular 1060808, Centro de Astrofísica FONDAP 15010003, Centro BASAL CATA (PFB-06), and by the Millennium Center for Supernova Science (P06-045-F). A.V.F. is grateful for the financial support of the NSF, the Richard and Rhoda Goldman Fund, the TABASGO Foundation, the Christopher R. Redlich Fund, and the Miller Institute for Basic Research in Science (University of California, Berkeley). This research has made use of the NASA/IPAC Extragalactic Database (NED), which is operated by the Jet Propulsion Laboratory, California Institute of Technology, under contract with the National Aeronautics and Space Administration. N.S. is grateful for the support provided by the Mitchell/Heep/Munnerlyn Chair in Observational Astronomy at Texas A&M University. The CSP thanks the Mitchell Foundation and Sheridan Lorenz for sponsoring our group meetings at Cook's Branch Nature Conservancy.

We thank the Lick Observatory staff for their assistance with the operation of KAIT. LOSS, which discovered many of the SNe studied here, has been supported by many grants from the NSF (most recently AST-0908886 and AST-1211916), the TABASGO Foundation, U.S. Department of Energy SciDAC grant DE-FC02-06ER41453, and U.S. Department of Energy grant DE-FG02-08ER41563. KAIT and its ongoing operation were made possible by donations from Sun Microsystems, Inc., the Hewlett-Packard Company, AutoScope Corporation, Lick Observatory, the NSF, the University of California, the Sylvia & Jim Katzman Foundation, and the TABASGO Foundation.

We give particular thanks to Russ Genet, who made KAIT possible with his initial special gift, and the TABASGO Foundation, without which this work would not have been completed.

Appendix A CSP-I NIR Bandpasses

Paper II provided a detailed description of the calibration of the CSP-I optical bandpasses. The setup consisted of a monochromator that allowed the throughput of the entire telescope plus detector system to be measured in situ without having to rely on multiple calibrations (filters, windows, aluminum reflections, detector quantum efficiency) multiplied together. Here we provide a summary of the calibration of the NIR bandpasses using the same monochromator.

The calibration of the two NIR cameras used for CSP-I was carried out in late July of 2010 (Swope+RetroCam) and early August of 2010 (du Pont+WIRC). The measurements were made on at least two different nights for each filter to ensure that the method was repeatable. The monochromator system uses a fiber that splits, sending 90% of the power to the dome-flat screen and 10% to a “witness screen.” The witness screen was placed in a dark box to prevent ambient light from reaching it.

Two germanium detectors were used, each 10 mm in diameter, which were calibrated in the lab at Texas A&M University using an NIST traceable Gentec calibrated photodiode. The Ge detectors are sensitive from 900 to 1600 nm and were used only for the calibration of the Y -band filter (900 to 1100 nm). To calibrate the three longer-wavelength CSP-I bandpasses (J , H , and K_s), a 2 mm diameter InGaAs detector was purchased and shipped to the National Research Council of Canada for calibration prior to its use in Chile.

Due to the lower light levels produced by this system in the NIR and because of the smaller area of the InGaAs detector, all of the actual calibrations were done using the 35 cm \times 35 cm witness screen made of the same material as the dome-flat screen. When taking Y -band data, one Ge detector detected photons from the dome-flat screen while the other Ge detector simultaneously detected photons from the witness screen in the dark box. The two detectors in the box were placed about 10 cm from the witness screen.

The Y -band signal at the witness screen was about 50 times stronger than the signal from the dome-flat screen. The voltage of the Ge photodiode (as a function of wavelength) measured from the dome-flat screen and scaled by a factor of ~ 50 matches, within the errors of measurement, the voltage of the other Ge photodiode used to measure the witness screen. Thus, we are confident that the witness screen can give reliable results for the longer-wavelength bandpasses.

A challenge inherent to IR measurements is the presence of background thermal drifts occurring on timescales of seconds. Also, during the day and on nights with moonlight, even with the dome closed there is some ambient light in the dome, which is relevant to the Y -band calibration described here.

To minimize the problem of thermal drifts and residual light in the dome, we took data using the following method. For each wavelength we obtained two 30 s “Dark” images and two 30 s “Light” images. A “Dark” image is taken with the light off

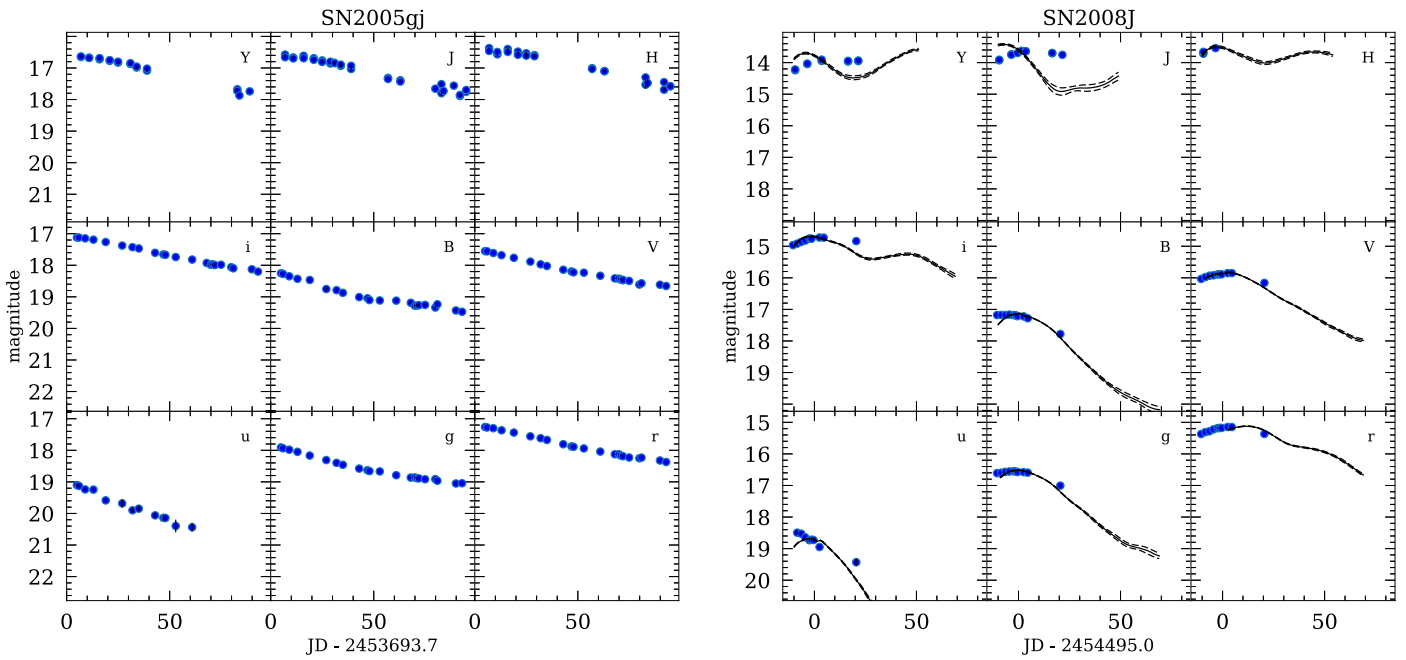


Figure 15. Multiband light curves of the Type Ia-CSM object SN 2005gj, SN 2008J, two SN 2006bt-like objects, and two super-Chandrasekhar candidates observed by CSP-I in the Figure Set. The axes are laid out as in Figures 13 and 14.

(The complete figure set (6 images) is available.)

and a “Light” image is taken with the light on. We subtract one “Dark” image from one “Light” and average the two net values to get a single measurement. Additionally, RetroCam on the Swope telescope exhibited severe image persistence, so we took a short (6 s) “Dark” exposure after each “Light” one to clear the camera detector.

The photodiode detectors are not temperature stabilized, so the amplifier offsets and the background drift significantly during the 30 s required for an exposure. They are relatively stable on a 1 s timescale. The error caused by the drift is much more important than the noise in the detector. It is then better to take shorter integration times (~ 1 s) to avoid drift problems even if we sacrifice a bit of averaging of the noise.

Since the output of the lamp is very stable ($<1\%$) over a period of hours, we assumed that the output was constant over the 30 s exposure time and only measured the amplitude just before opening the shutter to take a camera image. Before each exposure, we cycled the light on and off five times for a 10 s period to obtain five values of the amplitude, which we averaged to calculate the power at the detector.

The normalized transmission curves for each filter were obtained using a subsection (x and y from 60 to 964 pixels) of chip 2 in WIRC on the du Pont telescope. For RetroCam on the Swope telescope we used the same subsection of its chip. In general, we are confident that the measured transmission is accurate to 2%–3% of the peak transmission.

We have normalized each filter for each camera separately. We estimate that the transfer from the dome-flat screen to the witness screen and the relative photodiode calibration uncertainties are 1% and 2%, respectively, for the Swope and du Pont cameras. For the Swope+RetroCam, the relative photodiode noise level is 0.5% for the YJH filters, as is the

relative noise level of the camera. The total uncertainty in each filter is obtained from the square root of the sum of the individual components added in quadrature, or 2.3%. For the du Pont+WIRC, the relative photodiode noise level and the relative noise level of the camera are 1%–2% for YJH . For these filters the total uncertainty is 2.6% in Y and J and 3.2% in H .

We have also investigated the focal-plane uniformity of the filters in the Swope and du Pont cameras. Each filter was scanned twice on at least two separate nights. The scans were performed with a wavelength step of 5 or 10 nm. The analysis involved dividing each chip into four quadrants and comparing the relative response curves for each quadrant. At worst there is a 1.5 nm shift in the filter cutons and cutoffs as a function of quadrant and chip. This effect would be negligible unless a very narrow emission line happens to fall at that exact wavelength.

Appendix B Optical Color Terms

To test the accuracy of the response functions of the CSP-I optical bandpasses shown in Figure 3, we computed color terms using a subset of the stars from the spectrophotometric atlas of Landolt standards published by Stritzinger et al. (2005). Eighteen of the stars in this atlas are in the list of Smith et al. (2002) $u'g'r'i'$ standards. Of these, one star (SA 98-653) does not have sufficient wavelength coverage to include the u and g bands, and we suspect that another (SA 104-598) is variable. The results of synthetic photometry of the 16 remaining stars are shown in Figure 16. In each plot, the abscissa is the color from the published standard-star magnitudes, and the ordinate is the difference of the magnitude calculated via synthetic photometry using the bandpasses in Figure 3 and the published

standard-star magnitude. The red triangles correspond to the 16 stars in the Stritzinger et al. (2005) atlas, and the dashed lines are the best fits to these points. The slopes of these fits correspond to the color terms, and the values are indicated in red. The slopes of the observed color terms are indicated by the solid black lines, with the values shown in black. The histograms in each plot correspond to the colors of the Smith et al. (2002) and Landolt (1992) standard stars observed routinely by CSP-I.

In general, the agreement between the measured and computed color terms is good. For the u , r , i , B , and V bands, the color terms agree to better than 1σ . For the g band, the agreement is within 2σ . Considering the relatively small number of stars used for this test and the fact that these cover a somewhat smaller range of color than the actual standards used routinely by CSP-I, we consider the results of this test to be consistent with the observations.

Appendix C NIR Color Terms

In principle, we can check the color terms derived in Section 6.2.1 for the J_{RC2} and H filters of the Swope+RetroCam through observations of the red stars listed in Table 3 of P98. Unfortunately, although some of the red stars were observed on a few nights during the CSP-I campaigns, these data were not reduced at the time they were taken, and a subsequent disk crash made it impossible to recover them. However, since mid-2011, RetroCam has been in use on the du Pont telescope, and observations of several of the P98 red stars were made in late December of 2015.

Figure 17 shows synthetic photometry in J_{RC2} and H of the Castelli & Kurucz (2003) atmosphere models for a range of stellar parameters and reddenings ($E(B - V) = 0.0$ to 2.5 mag). Here the differences between the P98 magnitudes and the RetroCam magnitudes are plotted as a function of the $(J - H)_{P98}$ color. The filter response functions used for these calculations were measured in 2013 November for RetroCam on the du Pont telescope using the same monochromator and setup described in Appendix A. The predicted color terms of RetroCam on the du Pont telescope and on the Swope telescope are very similar, as might be expected. The black symbols in Figure 17 are our observations of several P98 standards, along with three stars with $(J - H)_{P98} > 1.5$ mag taken from the P98 red-star list that correspond to reddened M giants (typically M3 III) in Bok globules in the Coal Sack. The three red stars plotted with red symbols are young stellar objects (YSOs) from the P98 list. The latter stars are not representative of the Castelli & Kurucz (2003) models used for calculating the synthetic photometry and are also often variable.²² Hence, we do not include these stars in the fits shown in Figure 17.

Comparing the synthetic photometry of the models with the observations (excluding the YSOs), we find excellent agreement between the predicted and observed color terms in J and H . This gives us confidence in the reliability of the color terms calculated for the Swope+RetroCam in Equations (27) and (28) of Section 6.2.1.

²² Our observations of the YSO IRAS-537-S, which is included in the P98 list of red stars, showed a brightness change of ~ 0.2 mag in a space of two nights.

Appendix D Y-band Photometric Standards

Hamuy et al. (2006, Appendix C) describe how we derived Y-band magnitudes for the NIR standards of P98. In brief, we used Kurucz (1991) model atmospheres, the P98 filter functions, J_{P98} and K_{P98} , and our best estimate of our Y filter transmission to compute synthetic $(Y - K_{s,P98})$ colors as a function of synthetic $(J_{P98} - K_{s,P98})$ colors. Since then, we have scanned our NIR filters (see Appendix A) and improved stellar atmosphere models (Castelli & Kurucz 2003) have become available. Hence, in this appendix we rederive Y-band magnitudes for the NIR standards of P98. Note that the photometric zero-points for the NIR filters are computed assuming that Vega colors are all zero.

Figure 18 shows the results for the Swope+RetroCam Y band. The gray circles correspond to synthetic photometry of model dwarf star atmospheres with nearly solar metallicity ($\log(g) > 4.0$, $-0.1 < \log(Z/Z_{\odot}) < 0.1$, where g is the local acceleration of gravity in cm s^{-2} and Z is the abundance of elements heavier than helium). The gray region indicates the color range spanned by the P98 standards used by the CSP-I. The green solid line is a fifth-order polynomial fit to the data,

$$\begin{aligned} Y - K_{s,P98} = & 2.393(J_{P98} - K_{s,P98}) \\ & - 4.473(J_{P98} - K_{s,P98})^2 + 10.715(J_{P98} - K_{s,P98})^3 \\ & - 13.011(J_{P98} - K_{s,P98})^4 + 6.232(J_{P98} - K_{s,P98})^5. \end{aligned} \quad (43)$$

The blue dashed line is the fit from Hamuy et al. (2006). As with Hamuy et al. (2006), we do not allow a constant offset, forcing the polynomial through $Y - K_{s,P98} = J_{P98} - K_{s,P98} = 0$ mag. However, we note that the synthetic colors of the Castelli & Kurucz (2003) model atmospheres do not have zero NIR colors for an A0 V star. This can be seen in the bottom panel of Figure 18, where we have subtracted a linear fit (solid red line) to the points in order to better visualize the difference between the old and new fits. We could adjust the NIR zero-points to make all synthetic NIR colors zero at the expense of Vega acquiring nonzero colors, but we choose not to do this in order to be more consistent with our previous natural system.

In Table 13 we give the final Y-band photometric values of most of the P98 standard stars. We include values for stars considerably farther north than we can observe at LCO, in case Northern Hemisphere observers require them.

Appendix E Photometric Zero-points

The zero-points of a photometric system are necessary for computing transformations to other photometric systems (commonly referred to as S -corrections), as well as computing cross-band K -corrections within the same photometric system. The definition of the magnitude of a source with SED f_{λ} measured by an instrument with response F_{λ} is given by

$$m = m^* - 2.5 \log_{10} \left(\frac{\frac{1}{\text{ch}} \int F_{\lambda} f_{\lambda} \lambda d\lambda}{\frac{1}{\text{ch}} \int F_{\lambda} f_{\lambda}^* \lambda d\lambda} \right), \quad (44)$$

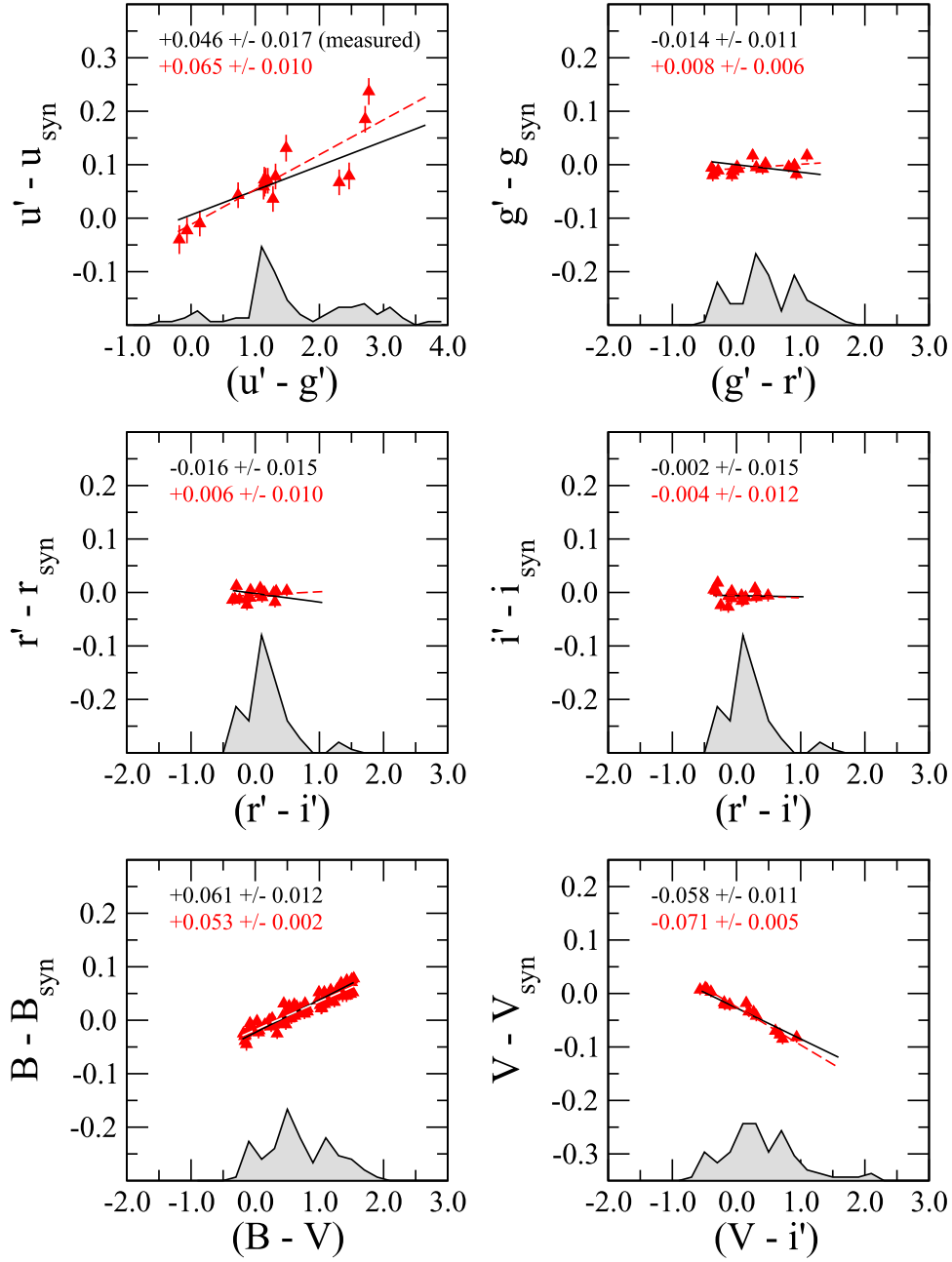


Figure 16. Magnitude differences vs. colors for *ugriBV*, derived synthetically from the scanned CSP-I bandpasses and the Stritzinger et al. (2005) spectrophotometric atlas of Landolt standards. The dashed lines are the best fits to the red triangles; the slope of each fit is listed numerically in the panels using a red font. The slopes corresponding to the measured mean color terms (see Table 4) are indicated by the solid black lines; the numerical values of these are reproduced in the panels using a black font. The histograms in each panel correspond to the colors of the standard stars observed routinely by the CSP-I.

where f_{λ}^* is some standard SED (e.g., Vega) and m^* is its magnitude through the instrument defined by F_{λ} . Here and in Equation (45) below c and h are the speed of light and Planck's constant, respectively. The numerator within the log function is the observed photon flux detected by the CCD, while the denominator is the photon flux of the standard SED through the same instrument and is generally not observed. Defining the zero-point as

$$\zeta = m^* + 2.5 \log_{10} \left(\frac{1}{ch} \int F_{\lambda} f_{\lambda}^* \lambda d\lambda \right), \quad (45)$$

we clearly need three pieces of information to compute the zero-point: the total instrument response, the standard SED, and the magnitude m^* . As mentioned previously, the CSP-I has directly measured all components of F_{λ} except the atmosphere. This leaves the standard SED and value of m^* .

The CSP-I used three sets of secondary standards to calibrate our photometry: Landolt (1992) for *BV*, Smith et al. (2002) for *ugri*, and P98 for *YJH*. These standards, more than anything else, define our photometric zero-point. However, we also require a high-fidelity SED that covers the wavelength range of our filters, and such SEDs generally do not exist for these standards. Stritzinger et al. (2005) give SEDs at optical

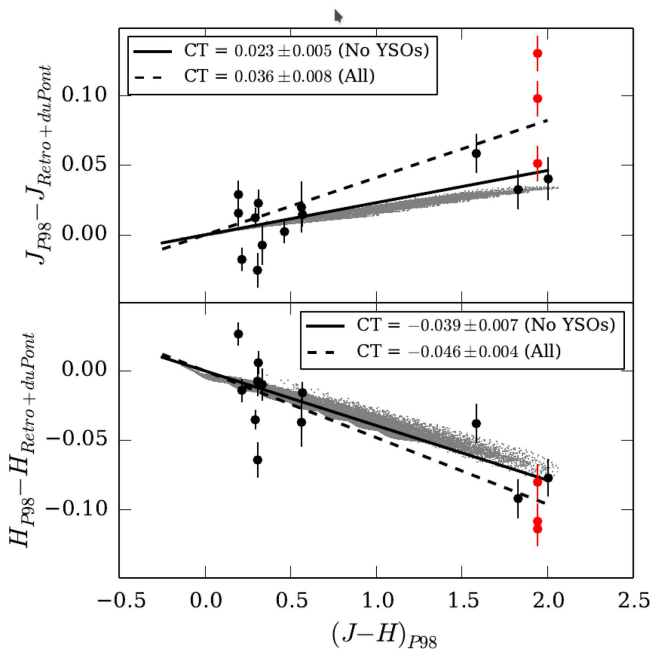


Figure 17. Observations of P98 standards and six red stars with $(J - H)_{P98} > 1.5$ mag from Table 3 of P98 obtained with RetroCam on the du Pont telescope. The differences between the P98 and observed magnitudes are plotted vs. the $(J - H)_{P98}$ color. The red stars plotted with black symbols correspond to reddened M giants in the Coal Sack, while those plotted with red symbols are YSOs. The solid and dashed lines are fits to the observations excluding and including the YSOs, respectively. Top: the swath of gray points shows the differences between synthetic photometry in the natural system of the Swope+RetroCam J_{RC2} bandpass and the P98 J filter for Castelli & Kurucz (2003) atmosphere models covering a range of stellar parameters and reddenings ($E(B - V) = 0.0$ to 2.5 mag), plotted vs. the $(J - H)_{P98}$ color. Bottom: same as the top panel, but for the H band.

wavelengths for 18 Landolt (1992) and Smith et al. (2002) standards. Ultimately, the Landolt (1992) and P98 standards are tied to α Lyr, while the Smith et al. 2002 standards are tied to BD +17°4708, both of which have accurate SEDs (Bohlin & Gilliland 2004a, 2004b), so we use these to compute our zero-points.

Lastly, we need the value of m^* for each instrument and SED combination. We begin with the standard magnitudes of each star in the system for which it was defined and use our color terms (see Table 4) to compute the magnitudes that would have been observed through *our* instrument. The adopted standard magnitudes and transformed natural-system magnitudes are listed in Table 14. For B and V , we adopt the standard magnitudes for α Lyr from Fukugita et al. (1996). For YJH , we adopt zero magnitudes for α Lyr to be consistent with Elias et al. (1982). For $ugri$, we adopt the standard magnitudes of BD +17°4708 from Smith et al. (2002).

The reader should note that Bohlin & Landolt (2015) present evidence that BD +17°4708 is slightly variable. From 1986 to 1991 this star brightened by ~ 0.04 mag in multiple optical bands. Following the suggestion of Bohlin & Landolt (2015), we have also calculated zero-points in $ugriBV$ using the standard and natural-system magnitudes of the CALSPEC standards P177D and P330E. For B and V we use the values measured by Bohlin & Landolt (2015), while for $ugri$ we adopt

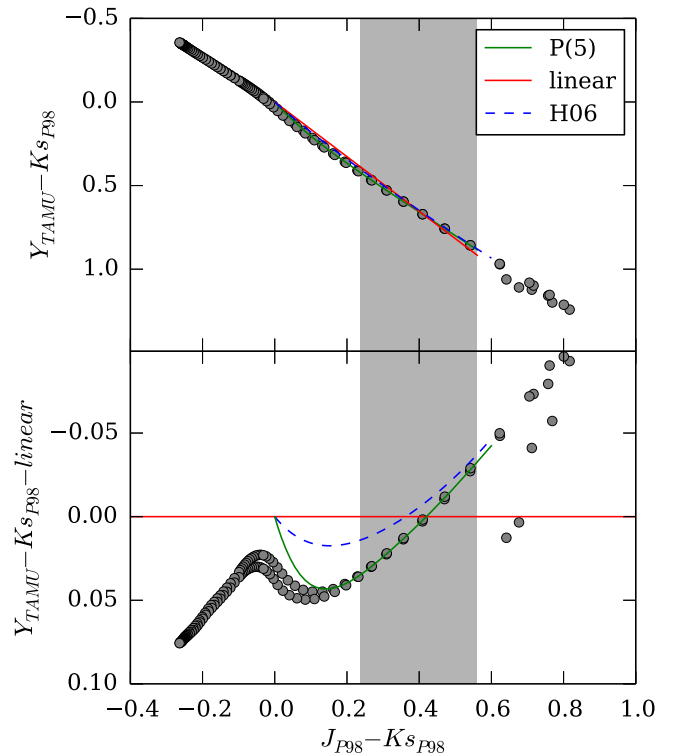


Figure 18. Synthetic $(Y - K_{s,P98})$ colors plotted as a function of synthetic $(J_{P98} - K_{s,P98})$ colors. The gray circles correspond to model dwarf star atmospheres with nearly solar metallicity. The red and green solid lines are linear and fifth-order polynomial fits to these data, respectively, while the blue dashed line is the relation given by Hamuy et al. (2006). The gray shaded region indicates the color range of the P98 standards used by the CSP-I.

unpublished measurements made by Allyn Smith in the USNO $u'g'r'i'z'$ standard system of Smith et al. (2002).

In Table 15 we give corresponding zero-points calculated with the SEDs of the four primary calibration standards. The agreement in zero-points between P177D, P330E, and α Lyr for B and V is excellent, as is also the case between P177D, P330E, and BD +17°4708 for $ugri$.

It is worth pointing out that we have two different networks of standard stars in the optical. As such, there is no guarantee that the BV zero-points will be consistent with the $ugri$ zero-points in an absolute sense. To investigate this, we compute synthetic photometry of the Pickles (1998) stellar library and compare the $(B - g)$ and $(V - g)$ colors with the observed colors of stars common to Landolt (1992) and Smith et al. (2002). The results, shown in Figure 19, indicate a systematic offset between the synthetic and observed $(B - g)$ and $(V - g)$ colors of ~ 0.03 mag. This could easily be fixed by adding the appropriate offsets to the zero-points of the B and V filters, thereby bringing both systems into alignment. However, this introduces a reliance on the Pickles (1998) spectra and presupposes that it is the B and V magnitudes that should be adjusted, when the problem could just as easily be with the $ugri$ zero-points. Hence, we prefer not to apply a zero-point correction to either system. Nevertheless, users of the CSP-I photometry should be aware of this inconsistency.

Table 13
Y-band Photometric Standards

ID ^a	HST	α (2000)	δ (2000)	Y^b
9101	P525-E	00:24:28.3	+07:49:02	11.880(011)
9103	S294-D	00:33:15.2	-39:24:10	11.163(011)
9104	S754-C	01:03:15.8	-04:20:44	11.282(011)
9105	P530-D	02:33:32.1	+06:25:38	11.567(017)
9106	S301-D	03:26:53.9	-39:50:38	12.396(015)
9107	P247-U	03:32:03.0	+37:20:40	12.205(011)
9108	P533-D	03:41:02.4	+06:56:13	11.995(016)
9109	S055-D	04:18:18.9	-69:27:35	11.759(005)
9111	S361-D	04:49:54.6	-35:11:17	11.445(014)
9113	S252-D	05:10:25.6	-44:52:46	11.294(011)
9115	S363-D	05:36:44.8	-34:46:39	12.255(014)
9116	S840-F	05:42:32.1	+00:09:04	11.670(019)
9118	S842-E	06:22:43.7	-00:36:30	12.007(023)
9119	S121-E	06:29:29.4	-59:39:31	12.343(012)
9121	S255-S	06:42:36.5	-45:09:12	11.954(009)
9122	P161-D	07:00:52.0	+48:29:24	11.907(014)
9123	S427-D	06:59:45.6	-30:13:44	11.087(019)
9125	S005-D	07:19:38.6	-84:35:06	11.127(017)
9126	P309-U	07:30:34.5	+29:51:12	12.145(042)
9129	S209-D	08:01:15.4	-50:19:33	11.180(019)
9131	P035-R	08:25:43.8	+73:01:18	11.035(018)
9132	S312-T	08:25:36.1	-39:05:59	12.181(011)
9133	S495-E	08:27:12.5	-25:08:01	11.844(020)
9134	P545-C	08:29:25.1	+05:56:08	12.089(015)
9135	S705-D	08:36:12.5	-10:13:39	12.586(029)
9136	S165-E	08:54:21.7	-54:48:08	12.724(022)
9137	S372-S	09:15:50.5	-36:32:34	11.375(020)
9138	S852-C	09:41:35.8	+00:33:12	11.600(016)
9139	P091-D	09:42:58.7	+59:03:43	11.941(021)
9140	S262-E	09:45:42.8	-45:49:40	11.661(026)
9141	S708-D	09:48:56.4	-10:30:32	11.323(021)
9142	P212-C	10:06:29.0	+41:01:26	12.206(015)
9143	P550-C	10:33:51.8	+04:49:05	12.542(014)
9144	S264-D	10:47:24.1	-44:34:05	11.884(022)
9145	P064-D	12:13:12.0	+64:28:56	12.165(021)
9146	S217-D	12:01:45.2	-50:03:10	11.575(012)
9147	S064-F	12:03:30.2	-69:04:56	12.363(016)
9148	P266-C	12:14:25.4	+35:35:55	11.856(019)
9149	S860-D	12:21:39.3	-00:07:13	12.449(013)
9150	S791-C	13:17:29.6	-05:32:37	11.916(018)
9152	P133-C	13:58:40.2	+52:06:24	11.368(022)
9153	P499-E	14:07:33.9	+12:23:51	12.208(018)
9154	S008-D	14:23:45.5	-84:09:58	11.454(017)
9155	S867-V	14:40:58.0	-00:27:47	12.308(014)
9156	P041-C	14:51:57.9	+71:43:13	11.106(017)
9157	S273-E	14:56:51.9	-44:49:14	11.637(012)
9158	P272-D	14:58:33.1	+37:08:33	11.905(017)
9160	S870-T	15:39:03.5	+00:14:54	11.108(020)
9162	P177-D	15:59:13.6	+47:36:40	12.512(027)
9164	P565-C	16:26:42.7	+05:52:20	12.410(015)
9166	P330-E	16:31:33.6	+30:08:48	12.068(015)
9169	P138-C	17:13:44.5	+54:33:21	11.558(016)
9170	S875-C	17:27:22.2	-00:19:25	11.385(011)
9172	S279-F	17:48:22.6	-45:25:45	12.754(016)
9173	S024-D	18:18:46.2	-80:06:58	11.266(017)
9175	S071-D	18:28:08.9	-69:26:03	12.516(015)
9177	P182-E	18:39:33.7	+49:05:38	12.365(011)
9178	S808-C	19:01:55.4	-04:29:12	11.220(017)
9181	S234-E	20:31:20.4	-49:38:58	12.719(020)
9182	S813-D	20:41:05.1	-05:03:43	11.734(011)
9183	P576-F	20:52:47.3	+06:40:05	12.491(010)
9185	S889-E	22:02:05.7	-01:06:02	12.294(011)
9186	S893-D	23:18:10.0	+00:32:56	11.639(017)
9187	S677-D	23:23:34.4	-15:21:07	12.078(007)

Table 13
(Continued)

ID ^a	HST	α (2000)	δ (2000)	Y^b
9101	P525-E	00:24:28.3	+07:49:02	11.880(011)
9188	P290-D	23:30:33.4	+38:18:57	11.880(013)

Notes.^a Star ID in Persson et al. (1998).^b All photometry is measured in magnitudes. Values in parentheses are 1σ uncertainties.**Appendix F**
AB Magnitude Offsets

According to Equation (7) of Fukugita et al. (1996), a broadband AB magnitude is defined as

$$m_{\text{AB}} = -2.5 \log_{10} \left[\frac{\int d(\log_{10} \nu) f_{\nu} F_{\nu}}{\int d(\log_{10} \nu) F_{\nu}} \right] - 48.6, \quad (46)$$

where f_{ν} is the flux per unit frequency of the object, expressed in units of $\text{ergs s}^{-1} \text{cm}^{-2} \text{Hz}^{-1}$, and F_{ν} is the response function of the filter. Since AB magnitudes are directly related to physical units (Oke & Gunn 1983), they offer a straightforward way of transforming magnitudes to flux densities.

To convert from natural magnitudes to AB magnitudes, we need to solve for an offset for each filter such that

$$m_{\text{AB}} = m_{\text{natural}} + \text{offset}. \quad (47)$$

Combining Equations (46) and (47) with the definition of our CSP natural magnitudes,

$$m_{\text{natural}} = -2.5 \log_{10} \left[\frac{1}{\text{ch}} \int F_{\lambda} f_{\lambda} \lambda d\lambda \right] + \zeta, \quad (48)$$

it can be shown that

$$\text{offset} = 16.847 - \zeta + 2.5 \log_{10} \left[\int \frac{F_{\lambda} d\lambda}{\lambda} \right], \quad (49)$$

where ζ is the zero-point of the filter. The zero-points of the CSP natural magnitudes are derived in Appendix E and are listed in Table 15.

Table 16 shows offsets calculated with Equation (49) for all of the CSP-I filters. Once the offsets have been applied, the flux in each band is given by

$$\langle f_{\nu} \rangle_{\nu} = 10^{-0.4(m_{\text{AB}} + 48.6)} \text{ erg s}^{-1} \text{cm}^{-2} \text{Hz}^{-1}, \quad (50)$$

where $\langle f_{\nu} \rangle_{\nu}$ is the weighted average of f_{ν} with weight function $F(\nu) \cdot \nu^{-1}$. Note that Equation (50) is not the proper inverse of Equation (46). One cannot derive a precise monochromatic flux from an AB magnitude, especially for objects such as

Table 14
Standard- and Natural-system Magnitudes of Fundamental Standards

Filter	Vega std	Vega nat	BD +17°4708 std	BD +17°4708 nat	P177D std	P177D nat	P330E std	P330E nat
<i>u</i>	10.560	10.518	15.128	15.066	14.539	14.481
<i>g</i>	9.640	9.644	13.771	13.777	13.287	13.293
<i>r</i>	9.350	9.352	13.316	13.318	12.848	12.850
<i>i</i>	0.382	...	9.250	9.250	13.170	13.170	12.701	12.701
<i>B</i>	0.030	0.030	14.138	14.099	13.658	13.620
V(LC-3014)	0.030	0.010	13.492	13.511	13.028	13.047
V(LC-3009)	0.030	0.015	13.492	13.506	13.028	13.042
V(LC-9844)	0.030	0.010	13.492	13.511	13.028	13.047
<i>Y</i>	0.000	0.000
<i>J</i>	0.000	0.000
<i>H</i>	0.000	0.000

Note. The V(LC-3014) filter was in use until JD 2,453,749 (2006 January 14 UT). The V(LC-3009) filter was employed from JD 2,453,750 to 2,453,759 (2006 January 15–24 UT). From JD 2,453,760 (2006 January 25 UT) onward, the V(LC-9844) filter was used.

Table 15
Photometric Zero-points Derived via Fundamental Standards^a

Filter	Vega	BD +17°			Average with BD +17° 4708	Average without BD +17° 4708
		4708	P177D	P330E		
<i>u</i>	...	12.98	12.98	12.98	12.98	12.98
<i>g</i>	...	15.11	15.12	15.12	15.12	15.12
<i>r</i>	...	14.90	14.90	14.90	14.90	14.90
<i>i</i>	...	14.54	14.53	14.52	14.53	14.53
<hr/>						
		Average with Vega			Average without Vega	
<i>B</i>	14.33	...	14.32	14.32	14.32	14.32
V(LC-3014)	14.44	...	14.43	14.44	14.44	14.44
V(LC-3009)	14.39	...	14.39	14.40	14.39	14.40
V(LC-9844)	14.44	...	14.43	14.44	14.44	14.44
<hr/>						
<i>Y</i> _{RC}	13.92
<i>J</i> _{RC1}	13.83
<i>J</i> _{RC2}	13.80
<i>H</i> _{RC}	13.51
<hr/>						
<i>Y</i> _{WIRC}	13.77
<i>J</i> _{WIRC}	13.86
<i>H</i> _{WIRC}	13.50

Note. The V(LC-3014) filter was in use until JD 2,453,749 (2006 January 14 UT). The V(LC-3009) filter was employed from JD 2,453,750 to 2,453,759 (2006 January 15–24 UT). From JD 2,453,760 (2006 January 25 UT) onward, the V(LC-9844) filter was used. The *J*_{RC1} filter was in use through 2009 January 2 (JD 2,454,833) and was not used thereafter. All observations obtained from 2009 January 15 (JD 2,454,846) onward were obtained with the *J*_{RC2} filter.

^a See Equation (45).

supernovae that have SEDs very different from the stars used in the fundamental spectrophotometric system. This is discussed in detail by Brown et al. (2016).

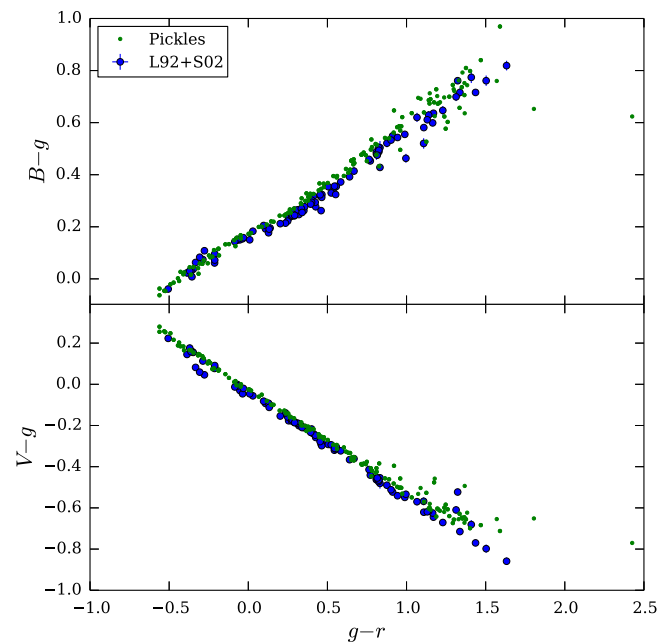












Figure 19. Comparison of synthetic photometry of the Pickles (1998) stellar library with the $(B - g)$ and $(V - g)$ colors of stars common to Landolt (1992) and Smith et al. (2002).

Table 16
AB Magnitude Offsets for CSP-I Filters

Filter	AB Offset	Filter	AB Offset
<i>u</i>	-0.06	<i>Y</i> _{RC}	+0.63
<i>g</i>	-0.02	<i>J</i> _{RC1}	+0.91
<i>r</i>	-0.01	<i>J</i> _{RC2}	+0.90
<i>i</i>	0.00	<i>H</i> _{RC}	+1.34
<i>B</i>	-0.13		
V(LC-3014)	-0.02	<i>Y</i> _{WIRC}	+0.64
V(LC-3009)	-0.02	<i>J</i> _{WIRC}	+0.90
V(LC-9844)	-0.02	<i>H</i> _{WIRC}	+1.34

ORCID iDs

Kevin Krisciunas <https://orcid.org/0000-0002-6650-694X>
Christopher R. Burns <https://orcid.org/0000-0003-4625-6629>

M. M. Phillips  <https://orcid.org/0000-0003-2734-0796>
 Maximilian D. Stritzinger  <https://orcid.org/0000-0002-5571-1833>
 Nidia Morrell  <https://orcid.org/0000-0003-2535-3091>
 Luis Busta  <https://orcid.org/0000-0001-9952-0652>
 Eric Y. Hsiao  <https://orcid.org/0000-0003-1039-2928>
 Sven Eric Persson  <https://orcid.org/0000-0003-0554-7083>
 Francisco Salgado  <https://orcid.org/0000-0002-2162-7641>
 Alexei V. Filippenko  <https://orcid.org/0000-0003-3460-0103>
 Barry F. Madore  <https://orcid.org/0000-0002-1576-1676>
 Jennifer L. Marshall  <https://orcid.org/0000-0003-0710-9474>

References

- Akerlof, C. W., Kehoe, R. L., McKay, T. A., et al. 2003, *PASP*, 115, 132
 Aldering, G., Antilogus, P., Bailey, S., et al. 2006, *ApJ*, 650, 510
 Anderson, J. P., González-Gaitán, S., Hamuy, M., et al. 2014, *ApJ*, 786, 67
 Bessell, M. S. 1990, *PASP*, 102, 1181
 Betoule, M., Kessler, R., Guy, J., et al. 2014, *A&A*, 568, A22
 Blondin, S., & Tonry, J. L. 2007, *ApJ*, 666, 1024
 Bohlin, R. C., & Gilliland, R. L. 2004a, *AJ*, 127, 3508
 Bohlin, R. C., & Gilliland, R. L. 2004b, *AJ*, 128, 3053
 Bohlin, R. C., Gordon, K. D., & Tremblay, P.-E. 2014, *PASP*, 126, 711
 Bohlin, R. C., & Landolt, A. U. 2015, *AJ*, 149, 122
 Branch, D., Dang, L. C., Hall, N., et al. 2006, *PASP*, 118, 560
 Brown, P. J., Breeveld, A., Roming, P. W. A., & Siegel, M. 2016, *AJ*, 152, 102
 Burki, G., Rufener, F., Burnet, M., et al. 1995, *A&A*, 112, 383
 Burns, C. R., Stritzinger, M., Phillips, M. M., et al. 2011, *AJ*, 141, 19
 Burns, C. R., Stritzinger, M., Phillips, M. M., et al. 2014, *ApJ*, 789, 32
 Castelli, F., & Kurucz, R. L. 2003, in Proc. 210th Symp. Int. Astronomical Union, Modelling of Stellar Atmospheres, ed. N. Piskunov, W. W. Weiss, & D. F. Gray (San Francisco, CA: ASP), A20
 Conley, A., Guy, J., Sullivan, M., et al. 2011, *ApJS*, 192, 1
 Contreras, C., Hamuy, M., Phillips, M. M., et al. 2010, *AJ*, 139, 519 (Paper I)
 Dilday, B., Howell, D. A., Cenko, S. B., et al. 2012, *Sci*, 337, 942
 Elias, J. H., Frogel, J. A., Matthews, K., & Neugebauer, G. 1982, *AJ*, 87, 1029
 Filippenko, A. V. 2003, in From Twilight to Highlight: The Physics of Supernovae, ed. W. Hillebrandt & B. Leibundgut (Berlin: Springer), 171
 Filippenko, A. V. 2005, in ASP Conf. Ser. 332, The Fate of the Most Massive Stars, ed. R. Humphreys & K. Stanek (San Francisco, CA: ASP), 33
 Filippenko, A. V., Li, W. D., Treffers, R. R., & Modjaz, M. 2001, in ASP Conf. Ser. 246, Small-Telescope Astronomy on Global Scales, IAU Coll. 183, ed. W. P. Chen, C. Lemme, & B. Paczyński (San Francisco, CA: ASP), 121
 Folatelli, G., Morrell, N., Phillips, M. M., et al. 2013, *ApJ*, 773, 53
 Folatelli, G., Phillips, M. M., Burns, C. R., et al. 2010, *AJ*, 139, 120
 Foley, R. J., Challis, P. J., Chornock, R., et al. 2013, *ApJ*, 767, 57
 Foley, R. J., Narayan, G., Challis, P. J., et al. 2010, *ApJ*, 708, 1748
 Freedman, W. L., Burns, C. R., Phillips, M. M., et al. 2009, *ApJ*, 704, 1036
 Freedman, W. L., Madore, B. F., Gibson, B. K., et al. 2001, *ApJ*, 553, 47
 Friedman, A. S., Wood-Vasey, W. M., Marion, G. H., et al. 2015, *ApJS*, 220, 9
 Frieman, J. A., Bassett, B., Becker, A., et al. 2008, *AJ*, 135, 338
 Fukugita, M., Ichikawa, T., Gunn, J. E., et al. 1996, *AJ*, 111, 1748
 Gall, C., Stritzinger, M. D., Ashall, C., et al. 2017, arXiv:1707.03823
 Hamuy, M., Folatelli, G., Morrell, N. I., et al. 2006, *PASP*, 118, 2
 Hamuy, M., Phillips, M. M., Suntzeff, N. B., et al. 1996, *AJ*, 112, 2391
 Hamuy, M., Phillips, M. M., Suntzeff, N. B., et al. 2003, *Natur*, 424, 651
 Harris, W. E., Fitzgerald, M. P., & Reed, B. C. 1981, *PASP*, 93, 507
 Hicken, M., Challis, P., Jha, S., et al. 2009, *ApJ*, 700, 331
 Hicken, M., Challis, P., Kirshner, R. P., et al. 2012, *ApJS*, 200, 12
 Hillenbrand, L. A., Foster, J. B., Persson, S. E., & Matthews, K. 2002, *PASP*, 114, 708
 Höflich, P., Hsiao, E. Y., Ashall, C., et al. 2017, *ApJ*, 846, 58
 Höflich, P., Krisciunas, K., Khokhlov, A. M., et al. 2010, *ApJ*, 710, 444
 Hogg, D. W., Bovy, J., & Lang, D. 2010, arXiv:1008.4686
 Hosseinzadeh, G., Sand, D. J., Valenti, S., et al. 2017, arXiv:1706.08990
 Howell, D. A., Sullivan, M., Nugent, P. E., et al. 2006, *Natur*, 443, 308
 Hoyle, F., & Fowler, W. A. 1960, *ApJ*, 132, 565
 Iben, I., Jr., & Tutukov, A. V. 1984, *ApJ*, 284, 719
 Kasen, D. 2006, *ApJ*, 649, 939
 Kattner, S., Leonard, D. C., Burns, C. R., et al. 2012, *PASP*, 124, 114
 Krisciunas, K. 2012, *JAVSO*, 40, 334
 Krisciunas, K., Hastings, N. C., Loomis, K., et al. 2000, *ApJ*, 539, 658
 Krisciunas, K., Phillips, M. M., & Suntzeff, N. B. 2004, *ApJL*, 602, L81
 Krisciunas, K., Suntzeff, N. B., Candia, P., et al. 2003, *AJ*, 125, 166
 Kurucz, R. L. 1991, in Stellar Atmospheres: Beyond Classical Models, ed. L. Crivellari et al. (Dordrecht: Reidel), 441
 Kushnir, D., Katz, B., Dong, S., Livne, E., & Fernández, R. 2013, *ApJ*, 778, 37
 Landolt, A. U. 1992, *AJ*, 104, 340
 Leaman, J., Li, W., Chornock, R., & Filippenko, A. V. 2011, *MNRAS*, 412, 1419
 Li, W., Bloom, J. S., Podsiadlowski, P., et al. 2011, *Natur*, 480, 348
 Li, W., Filippenko, A. V., Chornock, R., et al. 2003, *PASP*, 115, 453
 Li, W., Leaman, J., Chornock, R., et al. 2011, *MNRAS*, 412, 1441
 Mandel, K. S., Narayan, G., & Kirshner, K. P. 2011, *ApJ*, 731, 120
 Mandel, K. S., Wood-Vasey, W. M., Friedman, A. S., & Kirshner, R. P. 2009, *ApJ*, 704, 629
 Maoz, D., Sharon, K., & Gal-Yam, A. 2010, *ApJ*, 772, 1879
 Marion, G. H., Brown, P. J., Vinkó, J., et al. 2016, *ApJ*, 820, 92
 Nomoto, K. 1982, *ApJ*, 257, 780
 Nomoto, K., Kobayashi, C., & Tominaga, N. 2013, *ARA&A*, 51, 457
 Oke, J. B., & Gunn, J. E. 1983, *ApJ*, 266, 713
 Olling, R. P., Mushotzky, R., Shaya, E. J., et al. 2015, *Natur*, 521, 332
 Perlmutter, S., Aldering, G., Goldhaber, G., et al. 1999, *ApJ*, 517, 565
 Persson, S. E., Murphy, D. C., Gunnels, S. M., et al. 2002, *AJ*, 124, 619
 Persson, S. E., Murphy, D. C., Krzemiński, W., Roth, M., & Rieke, M. J. 1998, *AJ*, 116, 2475 (P98)
 Phillips, M. M. 1993, *ApJL*, 413, L105
 Phillips, M. M. 2012, *PASA*, 29, 434
 Phillips, M. M., Li, W., Frieman, J. A., et al. 2007, *PASP*, 119, 360
 Phillips, M. M., Phillips, M. M., Lira, P., et al. 1999, *AJ*, 118, 1766
 Pickles, A. J. 1998, *PASP*, 110, 863
 Pignata, G., Maza, J., Hamuy, M., Antezana, R., & Gonzales, L. 2009, *RMxAC*, 35, 317
 Prieto, J. L., Garnavich, P. M., Phillips, M. M., et al. 2007, arXiv:0706.4088
 Quimby, R. M. 2006, PhD thesis, Univ. Texas
 Rhaeult, J.-P., Mondrik, N. P., DePoy, D. L., Marshall, J. L., & Suntzeff, N. B. 2014, *Proc. SPIE*, 9147, 91475L
 Riess, A. G., Filippenko, A. V., Challis, P., et al. 1998, *AJ*, 116, 1009
 Riess, A. G., Macri, L. M., Hoffmann, S. L., et al. 2016, *ApJ*, 826, 56
 Riess, A. G., Press, W. H., & Kirshner, R. P. 1996, *ApJ*, 473, 88
 Schaefer, B. E., & Pagnotta, A. 2012, *Natur*, 481, 164
 Schweizer, F., Burns, C. R., Madore, B. F., et al. 2008, *AJ*, 136, 1482
 Silverman, J. M., Nugent, P. E., Gal-Yam, A., et al. 2013, *ApJS*, 207, 3
 Smith, J. A., Tucker, D. L., Kent, S., et al. 2002, *AJ*, 123, 2121
 Stetson, P. B. 1987, *PASP*, 99, 191
 Stritzinger, M., Burns, C. R., Phillips, M. M., et al. 2010, *AJ*, 140, 2036
 Stritzinger, M., Hamuy, M., Suntzeff, N. B., et al. 2002, *AJ*, 124, 2100
 Stritzinger, M., Suntzeff, N. B., Hamuy, M., et al. 2005, *PASP*, 117, 810
 Stritzinger, M., Taddia, F., Fransson, C., et al. 2012, *ApJ*, 756, 173
 Stritzinger, M. D., Anderson, J. P., Contreras, C., et al. 2017, *A&A*, in press (arXiv:1707.07616)
 Stritzinger, M. D., Hsiao, E., Valenti, S., et al. 2014, *A&A*, 561, A146
 Stritzinger, M. D., Phillips, M. M., Boldt, L. N., et al. 2011, *AJ*, 142, 156 (Paper II)
 Stritzinger, M. D., Valenti, S., Höflich, P., et al. 2015, *A&A*, 573, A2
 Stubbs, C. W., & Tonry, J. L. 2006, *ApJ*, 646, 1436
 Sullivan, M., Guy, J., Conley, A., et al. 2011, *ApJ*, 737, 102
 Taddia, F., Stritzinger, M. D., Phillips, M. M., et al. 2012, *A&A*, 545, L7
 Taddia, F., Stritzinger, M. D., Sollerman, J., et al. 2012, *A&A*, 537, A140
 Taddia, F., Stritzinger, M. D., Sollerman, J., et al. 2013, *A&A*, 555, 10
 Wang, X., Filippenko, A. V., Ganeshalingam, M., et al. 2009, *ApJL*, 699, L139
 Webbink, R. F. 1984, *ApJ*, 277, 355
 Wheeler, J. C., & Hansen, C. J. 1971, *Ap&SS*, 11, 373
 Whelan, J., & Iben, I. 1973, *ApJ*, 186, 1007
 Williams, A. J. 1997, *PASA*, 14, 208
 Wood-Vasey, W. M., Miknaitis, G., Stubbs, C. W., et al. 2007, *ApJ*, 666, 694



Erratum: “The Carnegie Supernova Project. I. Third Photometry Data Release of Low-redshift Type Ia Supernovae and Other White Dwarf Explosions” (2017, AJ, 154, 211)

Kevin Krisciunas¹ , Carlos Contreras^{2,3}, Christopher R. Burns⁴, M. M. Phillips², Mario Hamuy⁵, Maximilian D. Stritzinger^{2,3} , Jorge Anais², Luis Boldt², Luis Busta² , Abdo Campillay², Sergio Castellón², Gastón Folatelli^{2,6}, Wendy L. Freedman^{4,7}, Consuelo González², Eric Y. Hsiao^{2,3,8} , Wojtek Krzeminski^{2,16}, Nidia Morrell², Sven Eric Persson⁴, Miguel Roth^{2,9}, Francisco Salgado^{2,10} , Jacqueline Serón^{2,11}, Nicholas B. Suntzeff¹, Simón Torres^{2,12}, Alexei V. Filippenko¹³ , Weidong Li^{13,16}, Barry F. Madore^{4,14}, D. L. Depoy¹, Jennifer L. Marshall¹, Jean-Philippe Rheault¹, and Steven Villanueva^{1,15}

¹George P. and Cynthia Woods Mitchell Institute for Fundamental Physics and Astronomy, Department of Physics and Astronomy, Texas A&M University, College Station, TX 77843, USA; krisciunas@physics.tamu.edu

²Carnegie Observatories, Las Campanas Observatory, Casilla 601, La Serena, Chile

³Department of Physics and Astronomy, Aarhus University, Ny Munkegade 120, DK-8000 Aarhus C, Denmark

⁴Observatories of the Carnegie Institution for Science, 813 Santa Barbara Street, Pasadena, CA 91101, USA

⁵Departamento de Astronomía, Universidad de Chile, Casilla 36-D, Santiago, Chile

⁶Facultad de Ciencias Astronómicas y Geofísicas, Universidad Nacional de La Plata, Instituto de Astrofísica de La Plata (IALP), CONICET, Paseo del Bosque S/N, B1900FWA La Plata, Argentina

⁷Department of Astronomy and Astrophysics, University of Chicago, 5640 South Ellis Avenue, Chicago, IL 60637, USA

⁸Department of Physics, Florida State University, Tallahassee, FL 32306, USA

⁹GMTO Corporation, Avenida Presidente Riesco 5335, Suite 501 Las Condes, Santiago, Chile

¹⁰Leiden Observatory, Leiden University, PO Box 9513, NL-2300 RA Leiden, The Netherlands

¹¹Cerro Tololo Inter-American Observatory, Casilla 603, La Serena, Chile

¹²SOAR Telescope, Casilla 603, La Serena, Chile

¹³Department of Astronomy, University of California, Berkeley, CA 94720-3411, USA

¹⁴Infrared Processing and Analysis Center, Caltech/Jet Propulsion Laboratory, Pasadena, CA 91125, USA

¹⁵Department of Astronomy, Ohio State University, Columbus, OH 43210, USA

Received 2017 November 9; published 2017 December 5

In Table 4, the J -band color term for photometry with the Swope telescope and RetroCam is given as 0.016. This is correct for observations starting on 2009 January 15, which used the “RC2” J -band filter. Prior to that date, J -band photometry with RetroCam used a different filter, which we designate “RC1”. The corresponding color term is +0.039. See Equations (26) and (27).

ORCID iDs

Kevin Krisciunas <https://orcid.org/0000-0002-6650-694X>

Maximilian D. Stritzinger <https://orcid.org/0000-0002-5571-1833>

Luis Busta <https://orcid.org/0000-0001-9952-0652>

Eric Y. Hsiao <https://orcid.org/0000-0003-1039-2928>

Francisco Salgado <https://orcid.org/0000-0002-2162-7641>

Alexei V. Filippenko <https://orcid.org/0000-0003-3460-0103>

¹⁶ Deceased.

